Search for new phenomena in events with an energetic jet and missing transverse momentum in *pp* collisions at $\sqrt{s} = 13$ TeV with the ATLAS detector

G. Aad *et al.*[*]
(ATLAS Collaboration)

(Received 23 February 2021; accepted 6 May 2021; published 10 June 2021)

Results of a search for new physics in final states with an energetic jet and large missing transverse momentum are reported. The search uses proton-proton collision data corresponding to an integrated luminosity of 139 fb^{-1} at a center-of-mass energy of 13 TeV collected in the period 2015–2018 with the ATLAS detector at the Large Hadron Collider. Compared to previous publications, in addition to an increase of almost a factor of four in the data size, the analysis implements a number of improvements in the signal selection and the background determination leading to enhanced sensitivity. Events are required to have at least one jet with transverse momentum above 150 GeV and no reconstructed leptons (e, μ or τ) or photons. Several signal regions are considered with increasing requirements on the missing transverse momentum starting at 200 GeV. Overall agreement is observed between the number of events in data and the Standard Model predictions. Model-independent 95% confidence-level limits on visible cross sections for new processes are obtained in the range between 736 fb and 0.3 fb. Results are also translated into improved exclusion limits in models with pair-produced weakly interacting dark-matter candidates, large extra spatial dimensions, supersymmetric particles in several compressed scenarios, axionlike particles, and new scalar particles in dark-energy-inspired models. In addition, the data are translated into bounds on the invisible branching ratio of the Higgs boson.

DOI: 10.1103/PhysRevD.103.112006

I. INTRODUCTION

This paper presents the results of a new search for new phenomena in events containing an energetic jet and large missing transverse momentum $\mathbf{p}_{\mathrm{T}}^{\mathrm{miss}}$ (with magnitude $E_{\mathrm{T}}^{\mathrm{miss}}$) in proton-proton collisions at a center-of-mass energy $\sqrt{s} = 13$ TeV recorded by the ATLAS detector at the Large Hadron Collider (LHC). The final-state monojet signature of at least one energetic jet, large $E_{\mathrm{T}}^{\mathrm{miss}}$ and no leptons constitutes a distinctive signature for new physics beyond the Standard Model (SM) at colliders. This signature has been extensively studied at the LHC in the context of searches for large extra spatial dimensions (LED), supersymmetry (SUSY), weakly interacting massive particles (WIMPs) as candidates for dark matter (DM) [1–5], and signals from models inspired by dark energy (DE) with new scalar particles in the final state [6]. In addition, experimental results have been reinterpreted in terms of new theoretical scenarios with axionlike particles [7]. Finally, the monojet final-state results have been used to constrain the invisible branching fraction of the Higgs boson [8,9]. In the following, the different models are discussed briefly. Figure 1 shows diagrams for some of the models.

The existence of a nonbaryonic form of matter is well established from a number of astronomical observations [10–12]. The existence of a new, weakly interacting massive particle is often hypothesized [13], as it can lead to the correct relic density for nonrelativistic matter in the early universe [14] as measured from data from the Planck [15] and WMAP [16] Collaborations. For WIMP masses below 1 TeV, WIMPs may be pair-produced at the LHC. Traditionally, a monojet final state has been considered a golden channel for the discovery of WIMPs at colliders. In this case, the WIMP pair is produced in association with a jet of particles from initial-state radiation, leading to the signature of a jet and missing transverse momentum [see Fig. 1(a)]. Results are presented for simplified DM models [17–19] where Dirac fermion WIMPs (χ) are pair-produced from quarks via s-channel exchange of a spin-1 mediator particle (Z_A) or a spin-0 mediator particle (Z_P) with axial-vector or pseudoscalar couplings, respectively. In the case of the axial-vector mediator model with couplings of the

[*]Full author list given at the end of the article.

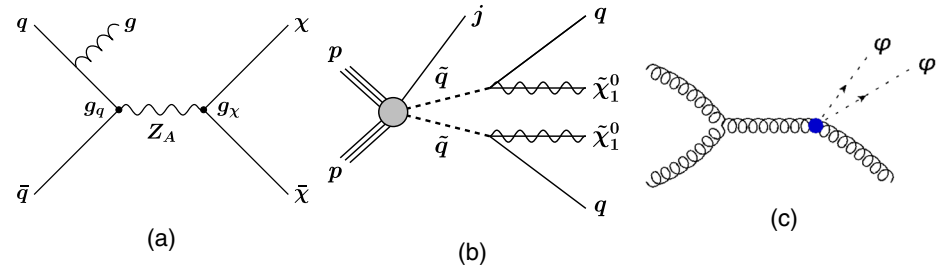

FIG. 1. (a) Diagram for the pair production of weakly interacting massive particles χ, with a mediator Z_A with axial-vector couplings exchanged in the s-channel. (b) A generic diagram for the pair production of squarks with the decay mode $\tilde{q} \to q + \tilde{\chi}_1^0$. The presence of a jet from initial-state radiation is indicated for illustration purposes. (c) Diagram for the pair production of dark-energy scalar fields φ in association with an energetic jet in the final state.

mediator to WIMPs and SM quarks set to $g_\chi = 1$ and $g_q = 1/4$, respectively, mediator masses below 1.55 TeV have been already excluded at 95% confidence level (CL) for very light WIMPs in previous analyses [4].

Supersymmetry is a theory of physics beyond the SM which can solve the hierarchy problem in a natural way and can provide candidates for dark matter [20–25]. SUSY introduces a new supersymmetric partner (sparticle) for each particle in the SM. Specifically, a new scalar field is associated with each quark chirality state. Two squark mass eigenstates $\tilde{q}_1$ and $\tilde{q}_2$ result from the mixing of the scalar fields for a particular flavor. In supersymmetric extensions of the SM that assume R-parity conservation [26–28], sparticles are produced in pairs and the lightest supersymmetric particle (LSP) is stable. The LSP is assumed to be the lightest neutralino $\tilde{\chi}_1^0$. The results are interpreted in terms of searches for squark production using simplified models in scenarios for which the mass difference $\Delta m \equiv m_{\tilde{q}} - m_{\tilde{\chi}_1^0}$ is small (compressed-mass scenario). In this case, the p_{T} of the resulting quark jets and the $E_{\mathrm{T}}^{\mathrm{miss}}$ in the final state are both small, making it difficult to reconstruct the SUSY signal. The monojet signature provides unique access to this parameter space, for which the presence of jets from initial-state radiation is used to identify signal events, leading to larger $E_{\mathrm{T}}^{\mathrm{miss}}$ [see Fig. 1(b)]. In the case of bottom-squark (sbottom) and top-squark (stop) pair production in a compressed-mass supersymmetric scenario, squark masses below about 430 GeV have been already excluded at 95% CL [4].

The origin of the accelerating expansion of the universe [29,30] is, together with the nature of the dark matter, a major open question in cosmology. The theoretical understanding of the accelerating expansion of the universe in terms of fundamental physics, beyond the *ad hoc* adoption of a cosmological constant in general relativity, often involves the introduction of additional scalars interacting with both the gravity and matter fields [31]. Here an effective field theory implementation of the Horndeski theories [32] is considered [33], introducing a new dark-energy scalar field φ, governed by an effective mass M_2 and a coupling g_* to matter, which is considered universal. For the model relevant for this case, the new scalar particle is stable and is produced in pairs, leaving the experiment undetected. When they are produced in association with an energetic gluon, it leads to a monojet final-state topology [see Fig. 1(c)]. Previous results [6] indicate no sensitivity for $g_* \leq 1.8$, and values of M_2 below 1.2 TeV have been excluded at 95% CL for $g_* \geq 3.5$.

Large extra spatial dimensions have been postulated to explain the large difference between the electroweak unification scale at $O(10^2)$ GeV and the Planck scale M_{Pl} at $O(10^{19})$ GeV. In the Arkani-Hamed, Dimopoulos, and Dvali (ADD) model of LED [34], the presence of n extra spatial dimensions of size R leads to a fundamental Planck scale in $4+n$ dimensions given by ${M_{\mathrm{Pl}}}^2 \sim {M_D}^{2+n} R^n$, where M_D is the fundamental scale of the $4+n$-dimensional theory. The extra spatial dimensions are compactified, resulting in a Kaluza-Klein tower of massive graviton modes (KK graviton). If produced in high-energy proton-proton collisions in association with a jet of hadrons, a KK graviton escaping into the extra dimensions can be inferred from $E_{\mathrm{T}}^{\mathrm{miss}}$, and can lead to a monojet event signature. Values of M_D below 7.7 TeV at $n = 2$ and below 4.8 TeV at $n = 6$ have been already excluded at 95% CL [4].

New pseudoscalar bosons, referred to as axionlike particles (ALPs), are introduced in different models involving the breaking of additional U(1) symmetries. The existence of axions was postulated [35] in order to address the strong CP problem for which an anomalous global U(1) symmetry is spontaneously broken. Axions are candidates for explaining the dark-matter content of the universe. The strength of the coupling between the axions and the ordinary matter is governed by the electroweak symmetry breaking scale, leading to rather strong constraints. Other models with ALPs, going beyond the minimal QCD axion realization, consider much weaker interactions suppressed

by a much higher scale [7,36]. In this paper, an effective implementation of an ALP model (with an effective scale f_a) is considered, in which ALPs are produced in association with a gluon in a final state governed by an ALP-gluon coupling $c_{\tilde{G}}$. By construction, ALP decays are suppressed and the ALP leaves the detector undetected, leading to a monojet final-state topology.

A variety of models of WIMP dark matter at the LHC involve the Higgs boson acting as a portal between the dark sector and the SM sector, either via direct Yukawa couplings to fermionic dark-matter candidates or via other mechanisms. The decay of the Higgs boson into dark-matter particles translates into a signature of $E_{\mathrm{T}}^{\mathrm{miss}}$ in the final state. Searches for invisible Higgs boson decays have been carried out at ATLAS and CMS, considering different SM Higgs production processes and different center-of-mass energies, leading to a 95% CL upper limit on the invisible Higgs boson branching ratio of 0.26 [37] and 0.19 [38], respectively.

In this publication, a data sample corresponding to a total integrated luminosity of 139 fb^{-1} is used, and the analysis strategy closely follows that of the previous publication based on 36.1 fb^{-1} [4]. In addition, a number of improvements are implemented leading to enhanced sensitivity to new phenomena. The p_{T} requirements for identifying electrons and muons in the final state are lowered, translating into tighter lepton vetoes and a larger background reduction, which is also complemented with the inclusion of τ-lepton and photon vetoes. The kinematic range covered by the analysis is extended towards lower values of $E_{\mathrm{T}}^{\mathrm{miss}}$ and leading-jet p_{T}, and new control regions are defined for a better determination of backgrounds related to top-quark and Z-boson production processes. Finally, the analysis profits from improved theoretical predictions for $W+\mathrm{jets}$ and $Z+\mathrm{jets}$ production, including higher-order corrections at next-to-next-to-leading order in QCD and next-to-leading order in electroweak couplings supplemented by Sudakov logarithms at two loops.

The paper is organized as follows. The ATLAS detector is described in the next section. Section III provides details of the Monte Carlo simulations used in the analysis for background and signal processes. Section IV discusses the reconstruction and identification of jets, leptons, and missing transverse momentum, while Sec. V describes the event selection. The estimation of background contributions and the study of systematic uncertainties are discussed in Secs. VI and VII. The results are presented in Sec. VIII and are interpreted in terms of limits in models of WIMP-pair production, ADD, SUSY in compressed scenarios, axionlike particles, new bosons in DE-inspired models, and limits on the Higgs boson invisible branching fraction. Finally, Sec. IX is devoted to the conclusions.

II. ATLAS DETECTOR

The ATLAS detector [39] at the LHC covers nearly the entire solid angle around the collision point.[1] It consists of an inner tracking detector surrounded by a thin superconducting solenoid, electromagnetic and hadronic calorimeters, and a muon spectrometer incorporating three large superconducting toroidal magnets.

The inner-detector system is immersed in a 2 T axial magnetic field and provides charged-particle tracking in the range $|\eta| < 2.5$. The high-granularity silicon pixel detector covers the vertex region and typically provides four measurements per track, the first hit normally being in the insertable B-layer installed before Run 2 [40,41]. It is followed by the silicon microstrip tracker, which usually provides eight measurements per track. These silicon detectors are complemented by the transition radiation tracker (TRT), which enables radially extended track reconstruction up to $|\eta| = 2.0$. The TRT also provides electron identification information based on the fraction of hits (typically 30 in total) above a higher energy-deposit threshold corresponding to transition radiation.

The calorimeter system covers the pseudorapidity range $|\eta| < 4.9$. Within the region $|\eta| < 3.2$, electromagnetic calorimetry is provided by barrel and end cap high-granularity lead/liquid-argon (LAr) calorimeters, with an additional thin LAr presampler covering $|\eta| < 1.8$ to correct for energy loss in material upstream of the calorimeters. Hadronic calorimetry is provided by the steel/scintillator-tile calorimeter, segmented into three barrel structures within $|\eta| < 1.7$, and two copper/LAr hadronic end cap calorimeters. The solid angle coverage is completed with forward copper/LAr and tungsten/LAr calorimeter modules optimized for electromagnetic and hadronic measurements respectively.

The muon spectrometer comprises separate trigger and high-precision tracking chambers measuring the deflection of muons in a magnetic field generated by the superconducting air-core toroids. The field integral of the toroids ranges between 2.0 and 6.0 Tm across most of the detector. A set of precision chambers covers the region $|\eta| < 2.7$ with three layers of monitored drift tubes, complemented by cathode-strip chambers in the forward region, where the background is highest. The muon trigger system covers the range $|\eta| < 2.4$ with resistive-plate chambers in the barrel, and thin-gap chambers in the end cap regions.

[1]ATLAS uses a right-handed coordinate system with its origin at the nominal interaction point (IP) in the center of the detector and the z-axis along the beam pipe. The x-axis points from the IP to the center of the LHC ring, and the y-axis points upwards. Cylindrical coordinates (r, ϕ) are used in the transverse plane, ϕ being the azimuthal angle around the z-axis. The pseudorapidity is defined in terms of the polar angle θ as $\eta = -\ln\tan(\theta/2)$. Angular distance is measured in units of $\Delta R \equiv \sqrt{(\Delta\eta)^2 + (\Delta\phi)^2}$.

Events of interest are selected to be recorded by the first-level trigger system implemented in custom hardware, followed by selections made by algorithms implemented in software in the high-level trigger [42]. The first-level trigger accepts events from the 40 MHz bunch crossings at a rate below 100 kHz, which the high-level trigger reduces in order to record events to disk at about 1 kHz.

III. MONTE CARLO SIMULATION

Monte Carlo (MC) simulated event samples are used to compute detector acceptance and reconstruction efficiencies, determine signal and background contributions, and estimate systematic uncertainties in the final results. The SM background samples were processed with the full ATLAS detector simulation [43] based on GEANT4 [44]. Signal simulated samples, with the exception of those for Higgs production for which full simulation is used, were processed with a fast simulation using a parameterization of the calorimeter response and GEANT4 for the other parts of the detector. Simulated events are then reconstructed and analyzed with the same analysis chain as for the data, using the same trigger and event selection criteria. The effects of multiple proton-proton interactions in the same or neighboring bunch-crossings (pileup) were taken into account by overlaying the hard-scattering process with simulated minimum-bias events, distributed according to the frequency in data and generated by PYTHIA 8.186 [45] with the A3 set of tuned parameters (tune) [46] and the NNPDF2.3LO parton distribution function (PDF) set [47]. Correction factors are applied to the Monte Carlo simulation to account for differences between simulation and the data in pileup, the energy and momentum scales, and reconstruction and identification efficiencies of physics objects.

A. Signal simulation

WIMP s-channel signal samples were simulated in POWHEG-BOX v2 [48–50] (revision 3049) using two implementations of simplified models, introduced in Ref. [51]. The DMV model of WIMP-pair production was used for s-channel spin-1 axial-vector mediator exchange at NLO in the strong coupling constant, and the DMS_tloop model was used for WIMP-pair production with s-channel spin-0 pseudoscalar mediator exchange with the full quark-loop calculation at leading order (LO) [52]. Renormalization and factorization scales were set to $H_{\mathrm{T}}/2$ on an event-by-event basis, where $H_{\mathrm{T}} = \sqrt{m_{\chi\chi}^2 + p_{\mathrm{T},j1}^2} + p_{\mathrm{T},j1}$ is defined by the invariant mass of the WIMP pair ($m_{\chi\chi}$) and the transverse momentum of the highest-p_{T} parton-level jet ($p_{\mathrm{T},j1}$). The mediator propagator is described by a Breit–Wigner distribution. Events were generated using the NNPDF30 [47] PDFs and interfaced to PYTHIA 8.205 with the A14 tune [53] for parton showering, hadronization and the underlying event. Couplings of the mediator to WIMP particles and those of the SM quarks were set to $g_\chi = 1$ and $g_q = 1/4$, respectively, for the axial-vector mediator model whereas both couplings were set to one in the case of the pseudoscalar mediator model, following the conventions of the LHC DM Working Group [17,18]. Each model was simulated for a range of possible WIMP and mediator masses, with WIMP masses ranging from 1 GeV to 1 TeV and mediator masses between 10 GeV and 10 TeV.

SUSY signals for squark-pair production were generated with MadGraph5_aMC@NLO v2.2.3 [54] and interfaced to PYTHIA 8.186 with the A14 tune for modeling of the squark decay, parton showering, hadronization, and the underlying event. The PDF set used for the generation was NNPDF23LO, and the renormalization and factorization scales were set to $\mu = \sum_i \sqrt{m_i^2 + p_{\mathrm{T},i}^2}$, where the sum runs over all final-state particles from the hard-scatter process. The matrix-element calculation was performed at tree level, and includes the emission of up to two additional partons. Matching to parton-shower calculations was accomplished by using the CKKW-L prescription [55], with a matching scale set to one quarter of the pair-produced superpartner mass. All signal cross sections were calculated to approximate next-to-next-to-leading order (NNLO) in the strong coupling constant, adding the resummation of soft gluon emission at next-to-next-to-leading-logarithm accuracy (approximate NNLO + NNLL) [56–59]. The nominal cross section and its uncertainty were taken from an envelope of cross-section predictions using different PDF sets and factorization and renormalization scales, as discussed in Ref. [60]. Simulated samples were produced with squark masses in the range between 250 GeV and 1.2 TeV, and squark–neutralino mass differences Δm varying between 5 GeV and 50 GeV.

Simulated events for the dark-energy model were generated using an effective field theory implementation [31] in MadGraph5_aMC@NLO v2.6.1 at LO accuracy in the strong coupling constant. Following the work in Ref. [6], only terms corresponding to the $\mathcal{L}_2$ operator, relevant for the monojet final-state topology, were considered, with the Wilson coefficient $c_2 = 1$ and the rest of the Wilson coefficients (c_i) set to zero. Electroweak terms were vetoed and only one insertion of a $\mathcal{L}_2$ operator in each diagram was allowed. The generated events were interfaced to PYTHIA 8.240 with the A14 tune for modeling of parton showering, hadronization, and the underlying event. The PDF set used for the generation was NNPDF23LO, and the renormalization and factorization scales were set to $0.5 \times H_{\mathrm{T}} = \sqrt{m_{\varphi\varphi}^2 + p_{\mathrm{T},j1}^2} + p_{\mathrm{T},j1}$, where $m_{\varphi\varphi}$ is the invariant mass of the two scalar particles in the final state. The dark-energy field mass and the coupling to gluons were set to $m_\varphi = 100$ MeV and $g_* = 4\pi$, respectively. Effective scales M_2 up to 3 TeV are explored.

Simulated samples for the ADD LED model with different numbers of extra dimensions in the range $n =$ 2–6 and a fundamental scale M_D in the range 3–12 TeV

were generated using PYTHIA 8.205 with the A14 tune and NNPDF2.3LO PDFs. The cross section is computed at next-to-leading order (NLO) accuracy in the strong coupling constant. The renormalization scale was set to the geometric mean of the squared transverse masses of the two produced particles, $\sqrt{(p_{\mathrm{T},G}^2+m_G^2)(p_{\mathrm{T},p}^2+m_p^2)}$, where $p_{\mathrm{T},G}$ and m_G ($p_{\mathrm{T},p}$ and m_p) denote, respectively, the transverse momentum and the mass of the KK graviton (parton) in the final state. The factorization scale was set to the smaller of the transverse masses, $\sqrt{p_{\mathrm{T}}^2+m^2}$, of the KK graviton and the parton.

Samples of simulated events for ALP production in association with a jet [36] were generated at leading-order (LO) accuracy in the strong coupling constant with MadGraph5_aMC@NLO v2.6.2 and interfaced to PYTHIA 8.240 with the A14 tune for modeling of parton showering, hadronization, and the underlying event. The PDF set used for the generation was NNPDF23LO, and the renormalization and factorization scales were set to half of the transverse mass, $0.5\times\sqrt{p_{\mathrm{T}}^2+m^2}$, of the ALP and the parton. Other processes related to the coupling of the ALP to photons, vector bosons or the Higgs boson are suppressed. Values for the ALP mass up to $m_a=1$ GeV and values for the coupling to gluons up to $c_{\tilde{G}}=1$ were considered. Effective scales f_a in the range between 1 TeV and 10 TeV are explored.

Simulated samples for the production of a 125 GeV Higgs boson were generated, with NLO accuracy in QCD emissions, using the POWHEG-BOX v2 [61] event generator. The samples include gluon-gluon fusion processes ($gg\to H$ and $gg\to ZH$), vector-boson fusion (VBF) processes ($VV\to H$), the associated production with a W/Z boson in the final state (VH), and the associated production with a $t\bar{t}$ pair in the final state ($t\bar{t}+H$). The simulated events were interfaced with PYTHIA 8.212 for parton shower, hadronization and underlying-event modeling using the AZNLO tune [62] with the NNPDF30+CTEQ6L1 PDF in the case of $gg\to H$ and $gg\to ZH$, CT10 in the case of VH, and NNPDF30 PDFs in the case of $VV\to H$ and $t\bar{t}+H$ processes. The $gg\to H$ sample was normalized such that it reproduces the total cross section predicted by a next-to-next-to-next-to-leading-order (NNNLO) QCD calculation with NLO electroweak (EW) corrections applied, and $VV\to H$ and VH processes were normalized to cross sections calculated at NNLO in QCD with NLO EW corrections. The $gg\to ZH$ sample was normalized to cross sections calculated at NLO in QCD, and the $t\bar{t}+H$ sample was normalized to cross sections calculated at NLO in QCD with NLO EW corrections [63]. In all cases, the Higgs boson invisible decay $H\to Z^*Z\to 4\nu$ is considered because it provides final-state topologies consistent with those from models of new phenomena with invisibly decaying Higgs bosons.

B. Background simulation

After applying the final-state selection as described in Sec. V, the primary SM background contributing to monojet event signatures is $Z\to\nu\nu+$ jets. There are also significant contributions from $W+$ jets events, primarily from $W\to\tau\nu+$ jets, with unidentified leptons in the final state. Small contributions are expected from $Z\to\ell\ell+$ jets ($\ell=e,\ \mu,\ \tau$), multijet, $t\bar{t}$, single-top, and diboson (WW, WZ, ZZ) processes. Contributions from top-quark production associated with additional vector bosons ($t\bar{t}+W$, $t\bar{t}+Z$, or $t+Z+q/b$ processes) are negligible and not considered in this analysis. As discussed in detail in Sec. VI, the contribution from SM background processes in the signal regions are determined using simulated samples constrained with data in control regions. In the following, the generation of the different simulation samples is described.

Events containing W or Z bosons with associated jets were simulated using the SHERPA 2.2.1 [64] event generator. Matrix elements (ME) were calculated for up to two partons at NLO and four partons at LO using OPENLOOPS [65] and COMIX [66], and merged with the SHERPA parton shower (PS) [67] using the ME+PS@NLO prescription [68]. The NNPDF3.0NNLO [47] PDF set was used in conjunction with a dedicated parton-shower tuning developed by the authors of SHERPA. The MC predictions were initially normalized to NNLO perturbative QCD (pQCD) predictions according to DYNNLO [69,70] using the MSTW2008 90% CL NNLO PDF set [71].

In order to improve the description of $W+$ jets and $Z+$ jets processes, their MC predictions were reweighted to account for higher-order QCD and electroweak corrections. The reweighting procedure is based on parton-level predictions for $W/Z+$ jets production from Ref. [72], which include NNLO QCD corrections [73–76] and NLO electroweak corrections [77–80] supplemented by Sudakov logarithms at two loops [81–84]. These corrections are provided separately for $W+$ jets, $Z\to\ell^+\ell^-+$ jets and $Z\to\nu\nu+$ jets processes, as a function of the vector-boson p_{T}, in order to improve the description of the measured Z-boson p_{T} distribution [85]. The reweighting procedure takes into account the difference between the QCD NLO predictions as included already in SHERPA and as provided by the parton-level calculations. Uncertainties in these higher-order corrections and their correlations across processes are described in Sec. VII.

Separate nonoverlapping samples for $W/Z+$ jets production via VBF-driven processes were generated using Herwig++ (v7.1.3 for electron and τ-lepton decays and v7.2 for muon decays) [86]. The samples were produced at NLO accuracy in pQCD using VBFNLO v3.0.0 [87]. The NNPDF30 PDF set was used along with the default set of tuned parameters for parton showering, hadronization and the underlying event. The EvtGen v1.2.0 program [88] was used to model the decays of the bottom and charm hadrons.

For the generation of $t\bar{t}$ and single-top-quark events in the Wt-channel and s-channel, the POWHEG-BOX v2 [61] event generator was used with CT10 [89] PDFs. Electroweak t-channel single-top-quark events were generated using the POWHEG-BOX v1 event generator. This event generator uses the four-flavor scheme to calculate NLO matrix elements, with the CT10 four-flavor PDF set. Interference occurring beyond tree level between Wt and $t\bar{t}$ processes was studied, considering both the diagram subtraction (DS) and diagram removal (DR) production schemes [90]; DR was used for the nominal background prediction, DS for the evaluation of systematic uncertainties as described in Sec. VII. The samples were normalized to NNLO pQCD predictions. The parton shower, hadronization, and underlying event were simulated using PYTHIA 8.205 with the A14 tune. The top-quark mass was set to 172.5 GeV. The EvtGen v1.2.0 program was used to model the decays of the bottom and charm hadrons. Alternative samples were generated using MadGraph5_aMC@NLO (v2.2.1) and POWHEG-BOX interfaced to Herwig++ (v7.1.3) [86] in order to estimate the effects of the choice of matrix-element event generator and parton-shower algorithms, and fragmentation and hadronization effects. The EvtGen v1.2.0 program was used to model the decays of the bottom and charm hadrons.

Diboson samples (WW, WZ, and ZZ production) were generated using SHERPA 2.2.1 or SHERPA 2.2.2 with NNPDF3.0NNLO, and were normalized to NLO pQCD predictions [91]. The EvtGen v1.2.0 program was used to model the decays of the bottom and charm hadrons.

IV. EVENT RECONSTRUCTION

Jets are reconstructed from energy deposits in the calorimeters[92] using the anti-k_t jet algorithm [93] as provided by the FastJet [94] toolkit, with the radius parameter $R = 0.4$. The measured jet four-momentum is calibrated using information from both simulation and data [95]. In addition, jets are corrected for contributions from pileup. Jets with $p_{\mathrm{T}} > 20$ GeV and $|\eta| < 2.8$ are considered in the analysis. A combination of track-based variables developed to suppress pileup jets, called the jet-vertex tagger (JVT) [96], is constructed. In order to remove jets originating from pileup collisions, for central jets ($|\eta| < 2.5$) with $p_{\mathrm{T}} < 120$ GeV a significant fraction of the tracks associated with each jet must have an origin compatible with the primary vertex, as defined by the jet-vertex tagger.

Jets with $p_{\mathrm{T}} > 30$ GeV and $|\eta| < 2.5$ are identified as jets containing b-hadrons (b-jets) if tagged by a multivariate algorithm which uses information about the impact parameters of inner-detector tracks matched to the jet, the presence of displaced secondary vertices, and the reconstructed flight paths of b- and c-hadrons inside the jet [97,98]. A 60% efficient b-tagging working point, as determined in a simulated sample of $t\bar{t}$ events, is chosen. This corresponds to rejection factors of approximately 1500, 35 and 180 for light-quark and gluon jets, c-jets, and τ-leptons decaying hadronically, respectively.

Electrons are found by combining energy deposits in the calorimeter with tracks found in the inner detector. They are initially required to have $p_{\mathrm{T}} > 7$ GeV and $|\eta| < 2.47$, and to satisfy the "loose" electron shower shape and track selection criteria described in Ref. [99], including a requirement on the match between the track and the primary vertex, which requires the longitudinal impact parameter $|z_0| \sin\theta$ to be less than 0.5 mm. Overlaps between identified electrons and jets with $p_{\mathrm{T}} > 30$ GeV in the final state are resolved. Jets are discarded if they are not b-tagged and their separation $\Delta R = \sqrt{(\Delta\eta)^2 + (\Delta\phi)^2}$ from an identified electron is less than 0.2. Otherwise, the electron is removed as it most likely originates from a semileptonic b-hadron decay. The electrons separated by ΔR between 0.2 and 0.4 from any remaining jet are removed.

Muon candidates are formed by combining information from the muon spectrometer and inner tracking detectors. They are required to pass "medium" identification requirements [100], and to have $p_{\mathrm{T}} > 7$ GeV and $|\eta| < 2.5$. As in the case of electrons, the muon track is required to have $|z_0| \sin\theta < 0.5$ mm. Jets with $p_{\mathrm{T}} > 30$ GeV and fewer than three tracks with $p_{\mathrm{T}} > 500$ MeV associated with them are discarded if their separation ΔR from an identified muon is less than 0.4. The muon is discarded if it is matched to a jet with $p_{\mathrm{T}} > 30$ GeV that has at least three tracks associated with it. If an electron and a muon share the same inner-detector track, the muon is retained and the electron is discarded in order to remove electron candidates originating from muon bremsstrahlung followed by photon conversion.

Hadronically decaying τ-lepton candidates are formed by combining information from the calorimeters and inner tracking detectors. The τ-lepton reconstruction algorithm [101] is seeded by reconstructed jets with $p_{\mathrm{T}} > 10$ GeV and $|\eta| < 2.5$, and the reconstructed energies of the τ-lepton candidates are corrected to the τ-lepton energy scale [102]. They are required to pass loose identification requirements [103], to have $p_{\mathrm{T}} > 20$ GeV and $|\eta| < 2.5$, excluding the transition region between the electromagnetic barrel and end cap calorimeters ($1.37 < |\eta| < 1.52$), and to have one or three associated charged tracks. The τ-leptons close to electrons or muons ($\Delta R < 0.2$) are removed. Any jet within $\Delta R = 0.2$ of a τ-lepton is removed.

Photons are reconstructed from clusters of energy deposited in the electromagnetic calorimeter. They are required to pass "tight" identification requirements [99], and to have $p_{\mathrm{T}} > 10$ GeV and $|\eta| < 2.37$. Photons are discarded if their separation ΔR from an identified muon or electron is less than 0.4. Jets are instead discarded if their separation ΔR from an identified photon is less than 0.4.

The vector missing transverse momentum $\mathbf{p}_{\mathrm{T}}^{\mathrm{miss}}$ is reconstructed from the negative vectorial sum of the transverse momenta of electrons, muons, τ-leptons,

TABLE I. Intervals and labels of the $E_{\mathrm{T}}^{\mathrm{miss}}$ bins used for the signal region. Details are given in the text.

Exclusive (EM)	EM0	EM1	EM2	EM3	EM4	EM5	EM6
$E_{\mathrm{T}}^{\mathrm{miss}}$ [GeV]	200–250	250–300	300–350	350–400	400–500	500–600	600–700
	EM7	EM8	EM9	EM10	EM11	EM12	
	700–800	800–900	900–1000	1000–1100	1100–1200	>1200	
Inclusive (IM)	IM0	IM1	IM2	IM3	IM4	IM5	IM6
$E_{\mathrm{T}}^{\mathrm{miss}}$ [GeV]	>200	>250	>300	>350	>400	>500	>600
	IM7	IM8	IM9	IM10	IM11	IM12	
	>700	>800	>900	>1000	>1100	>1200	

photons, and jets with $p_{\mathrm{T}} > 20$ GeV and $|\eta| < 4.5$. Tracks compatible with the primary vertex but not associated with any of those objects are also included in the vectorial sum, as described in Sec. 3.4.2 of Ref. [104].

V. EVENT SELECTION

This analysis is based on data collected by ATLAS during Run 2 of the LHC, corresponding to a total integrated luminosity of 139 fb^{-1}. The data were collected using a trigger based on a requirement on $E_{\mathrm{T}}^{\mathrm{miss}}$ as computed from calorimetry information at the final stage of the two-level trigger system [105]. After analysis selections, the trigger was measured to be fully efficient for events with $E_{\mathrm{T}}^{\mathrm{miss}} > 200$ GeV, as determined using a data sample with muons in the final state.

Events are required to have at least one reconstructed primary vertex consistent with the beamspot envelope and containing at least two associated tracks of $p_{\mathrm{T}} > 500$ MeV. When more than one such vertex is found, the vertex with the largest summed p_{T}^2 of the associated tracks is chosen. Events having identified muons, electrons, photons or τ-leptons in the final state are vetoed. Selected events have $E_{\mathrm{T}}^{\mathrm{miss}} > 200$ GeV, a leading jet with $p_{\mathrm{T}} > 150$ GeV and $|\eta| < 2.4$, and up to three additional jets with $p_{\mathrm{T}} > 30$ GeV and $|\eta| < 2.8$. Separation in the azimuthal angle of $\Delta\phi(\mathrm{jet}, \mathbf{p}_{\mathrm{T}}^{\mathrm{miss}}) > 0.4(0.6)$ between the missing transverse momentum direction and each selected jet is required for events with $E_{\mathrm{T}}^{\mathrm{miss}} > 250$ GeV (200 GeV $< E_{\mathrm{T}}^{\mathrm{miss}} \leq$ 250 GeV) to reduce the multijet background contribution, since large $E_{\mathrm{T}}^{\mathrm{miss}}$ can originate from jet energy mismeasurement. Jet quality criteria [106] are imposed, which involve selections based on quantities such as the pulse shape of the energy depositions measured in the cells of the calorimeters, electromagnetic energy fraction in the calorimeter, maximum fraction of the jet energy collected by a single calorimeter layer, and the charged-particle fraction.[2] Loose selection criteria are applied to all jets with $p_{\mathrm{T}} > 30$ GeV and $|\eta| < 2.8$, which remove anomalous energy depositions due to coherent noise and electronic noise bursts in the calorimeter [107]. Events with any jet not satisfying the loose criteria [106] are discarded.

Noncollision backgrounds, for example energy depositions in the calorimeters due to muons of beam-induced or cosmic-ray origin, are suppressed by imposing tight selection criteria on the leading jet: the ratio of the jet charged-particle fraction to the maximum fraction of the jet energy collected by a single calorimeter layer, $f_{\mathrm{ch}}/f_{\mathrm{max}}$, is required to be larger than 0.1. Jet quality requirements altogether have a negligible effect on the signal efficiency.

The signal region (SR) is divided into different bins of $E_{\mathrm{T}}^{\mathrm{miss}}$, which are listed in Table I. Inclusive bins are used for a model-independent interpretation of search results, while the full set of exclusive bins are used for the interpretation within different models of new physics.

VI. BACKGROUND ESTIMATION

A semidata-driven technique, supported by statistically independent control regions, is used to constrain the normalization of Standard Model backgrounds. The approach followed is similar to the one used in previous versions of the analysis [4].

A. Control regions

The estimation of the Z + jets, W + jets, $t\bar{t}$, and single-t backgrounds is performed using five control regions, as described below. These regions are defined in a way similar to the SR: events are selected in terms of a quantity which is—similarly to $\mathbf{p}_{\mathrm{T}}^{\mathrm{miss}}$ in the SR—a proxy for the transverse momentum of the system which recoils against the hadronic activity in the event. This quantity is denoted in the following by $\mathbf{p}_{\mathrm{T}}^{\mathrm{recoil}}$, and its magnitude by $p_{\mathrm{T}}^{\mathrm{recoil}}$. The same selection criteria for jet multiplicity and leading jet p_{T} as in the SR are applied in the control regions, with the same requirements on the azimuthal separation of jets from $\mathbf{p}_{\mathrm{T}}^{\mathrm{recoil}}$. Control regions are binned in terms of $p_{\mathrm{T}}^{\mathrm{recoil}}$, using the same binning as in the signal region (see Table I). In the signal region, $p_{\mathrm{T}}^{\mathrm{recoil}}$ is equivalent to $E_{\mathrm{T}}^{\mathrm{miss}}$.

[2]The charged-particle fraction is defined as $f_{\mathrm{ch}} = \sum p_{\mathrm{T}}^{\mathrm{track,jet}} / p_{\mathrm{T}}^{\mathrm{jet}}$, where $\sum p_{\mathrm{T}}^{\mathrm{track,jet}}$ is the scalar sum of the transverse momenta of tracks associated with the primary vertex within a cone of size $\Delta R = 0.4$ around the jet axis, and $p_{\mathrm{T}}^{\mathrm{jet}}$ is the transverse momentum of the jet as determined from calorimetric measurements.

A control region enriched in $W \to \mu\nu$ events is defined by selecting events that pass the same trigger requirements as in the signal region, if they have exactly one reconstructed muon and this muon has $p_{\mathrm{T}} > 10$ GeV and passes the requirement on the transverse impact parameter significance, $d_0/\sigma(d_0)$, to be less than 3, and if no electrons, τ-leptons, photons or b-jets are reconstructed. In this region, $p_{\mathrm{T}}^{\mathrm{recoil}}$ is defined as the magnitude of the vector sum of the missing transverse momentum and the muon transverse momentum, $|\mathbf{p}_{\mathrm{T}}^{\mathrm{miss}} + \mathbf{p}_{\mathrm{T}}(\mu)|$, and is required to be higher than 200 GeV. An additional requirement on the transverse mass is applied, 30 GeV $< m_{\mathrm{T}} <$ 100 GeV, where $m_{\mathrm{T}} = \sqrt{2p_{\mathrm{T}}(\mu)p_{\mathrm{T}}(\nu)[1-\cos(\Delta\phi(\mu,\nu))]}$ and the neutrino transverse momentum, $\mathbf{p}_{\mathrm{T}}(\nu)$, is taken to be the same as $\mathbf{p}_{\mathrm{T}}^{\mathrm{miss}}$.

Similarly, a control region enriched in $Z \to \mu\mu$ events is defined by selecting events that pass the same trigger requirements but have exactly two reconstructed muons, where these muons have $p_{\mathrm{T}} > 10$ GeV and $d_0/\sigma(d_0) < 3$, and the invariant mass of the dimuon system is between 66 and 116 GeV. In this region, $p_{\mathrm{T}}^{\mathrm{recoil}}$ is defined as the magnitude of the vector sum of the missing transverse momentum and the transverse momentum of the dimuon system, $|\mathbf{p}_{\mathrm{T}}^{\mathrm{miss}} + \mathbf{p}_{\mathrm{T}}(\mu\mu)|$, and is required to be higher than 200 GeV. The trigger requirements used for these two regions do not include muon information in the calculation of $E_{\mathrm{T}}^{\mathrm{miss}}$, and are fully efficient for events satisfying the selection criteria.

A control region enriched in $W \to e\nu$ events is defined by selecting events that pass single-electron triggers, if they have exactly one reconstructed electron and this electron satisfies tight identification criteria described in Ref. [103], is reconstructed outside the transition region between the electromagnetic barrel and end cap calorimeters, has $p_{\mathrm{T}} > 30$ GeV and $d_0/\sigma(d_0) < 5$, and passes the tight isolation requirements based on information from the electromagnetic calorimeter and from tracking detectors, described in Ref. [99]. In this region, $p_{\mathrm{T}}^{\mathrm{recoil}}$ is defined as the magnitude of the vector sum of the missing transverse momentum and the electron transverse momentum, $|\mathbf{p}_{\mathrm{T}}^{\mathrm{miss}} + \mathbf{p}_{\mathrm{T}}(e)|$, and is required to be higher than 200 GeV. The transverse mass is required to be 30 GeV $< m_{\mathrm{T}} <$ 100 GeV. In order to further suppress backgrounds from multijet processes with jets misidentified as high-p_{T} electrons, the events are required to have $E_{\mathrm{T}}^{\mathrm{miss}} > 70$ GeV and $E_{\mathrm{T}}^{\mathrm{miss}}/\sqrt{H_{\mathrm{T}}} > 5$ GeV$^{1/2}$, where H_{T} denotes the scalar sum of the p_{T} of the identified jets in the final state.

Similarly, a control region enriched in $Z \to ee$ events is defined by selecting events with exactly two reconstructed electrons, where these electrons have $p_{\mathrm{T}} > 30$ GeV and $d_0/\sigma(d_0) < 5$, and the invariant mass of the dielectron system is between 66 and 116 GeV. In this region, $p_{\mathrm{T}}^{\mathrm{recoil}}$ is defined as the magnitude of the vector sum of the missing transverse momentum and the transverse momentum of the dielectron system, $|\mathbf{p}_{\mathrm{T}}^{\mathrm{miss}} + \mathbf{p}_{\mathrm{T}}(ee)|$, and is required to be higher than 200 GeV. The single-electron trigger requirements are fully efficient for events satisfying the selection criteria for these two regions.

A control region enriched in $t\bar{t}$ and single-t events is defined by selecting events which pass the same cuts as for the $W \to \mu\nu$ and $W \to e\nu$ regions, but which have at least one identified b-jet.

Table II shows a summary of the selection criteria for all regions.

B. Multijet background

The multijet background with large $E_{\mathrm{T}}^{\mathrm{miss}}$ originates mainly from the misreconstruction of the energy of a jet in the calorimeter and, to a lesser extent, is due to the presence of neutrinos in the final state from heavy-flavor hadron decays. In this analysis, the multijet background is determined from data, using the jet smearing method as described in Ref. [108]. It relies on the assumption that the $E_{\mathrm{T}}^{\mathrm{miss}}$ value of multijet events is dominated by fluctuations in the jet response in the detector, which can be measured in the data. The method was checked using a validation region where events were selected as in the signal region, except for a modified requirement that the minimum azimuthal distance between a jet and $\mathbf{p}_{\mathrm{T}}^{\mathrm{miss}}$ is between 0.3 and 0.4. After event selection, the multijet background is estimated to be about 1.2%, 0.8%, 0.4% and 0.3% of the total background in the exclusive signal region bins EM0, EM1, EM2 and EM3, respectively, and it is less than 0.1% for the other signal region bins. A conservative 100% uncertainty is assigned to the normalization of this background.

C. Noncollision background

After event selections are applied, the signal region may contain residual contributions from noncollision backgrounds. These backgrounds, which are not included in simulation, mainly arise when beam-halo protons intercept the LHC collimators, leading to particle cascades which produce muons. The remaining contributions are estimated following the methods set out in Ref. [107]. In particular, the jet timing, t_j, calculated from the energy-weighted average of the time of the jet energy deposits, defined relative to the event time in nominal collisions, is used. A dedicated region enhanced in beam-induced background, defined by inverting the tight jet-quality selection imposed on the leading jet, is used to estimate the amount of noncollision background from the fraction of events with a leading-jet timing $|t_j| > 5$ ns. The results indicate a contribution at the per-mille level from noncollision backgrounds in the signal region. A conservative 100% uncertainty is assigned to the normalization of this background.

TABLE II. Event selection criteria for the signal and control regions. Reconstructed objects are defined as explained in Sec. IV.

Requirement	SR	$W \to \mu\nu$	$Z \to \mu\mu$	$W \to e\nu$	$Z \to ee$	Top
Primary vertex	at least one with ≥ 2 Associated tracks with $p_T > 500$ MeV					
Trigger	E_T^{miss}		Single-electron			E_T^{miss}, single-electron
p_T^{recoil} cut	$E_T^{miss} > 200$ GeV	$\lvert\mathbf{p}_T^{miss} + \mathbf{p}_T(\mu)\rvert > 200$ GeV	$\lvert\mathbf{p}_T^{miss} + \mathbf{p}_T(\mu\mu)\rvert > 200$ GeV	$\lvert\mathbf{p}_T^{miss} + \mathbf{p}_T(e)\rvert > 200$ GeV	$\lvert\mathbf{p}_T^{miss} + \mathbf{p}_T(ee)\rvert > 200$ GeV	$\lvert\mathbf{p}_T^{miss} + \mathbf{p}_T(\mu)\rvert > 200$ GeV or $\lvert\mathbf{p}_T^{miss} + \mathbf{p}_T(e)\rvert > 200$ GeV
Jets	Up to 4 with $p_T > 30$ GeV, $\lvert\eta\rvert < 2.8$					
$\lvert\Delta\phi(\text{jets}, \mathbf{p}_T^{recoil})\rvert$	> 0.4 (> 0.6 if 200 GeV $< E_T^{miss} \leq 250$ GeV)					
Leading jet	$p_T > 150$ GeV, $\lvert\eta\rvert < 2.4$, $f_{ch}/f_{max} > 0.1$					
b-jets	Any	None	Any	None	Any	At least one
Electrons or muons	None	Exactly one muon, with $p_T > 10$ GeV, $30 < m_T < 100$ GeV; no electron	Exactly two muons, with $p_T > 10$ GeV, $66 < m_{\mu\mu} < 116$ GeV; no electron	Exactly one electron, tight, with $p_T > 30$ GeV, $\lvert\eta\rvert \notin (1.37, 1.52)$, tight isolation, $30 < m_T < 100$ GeV; no muon	Exactly two electrons, with $p_T > 30$ GeV, $66 < m_{ee} < 116$ GeV; no muon	Same as for $W \to \mu\nu$ or same as for $W \to e\nu$
τ-leptons	None					
Photons	None					

D. Standard Model background fit

The estimation of backgrounds in the SR is based on a simultaneous, binned likelihood fit to the $p_{\mathrm{T}}^{\mathrm{recoil}}$ distribution of the five control regions described in Sec. VI A. The number of events in each region and in each bin is treated as a random variable with a Poisson distribution function, with an expectation value given by the sum of the SM predictions for each background in that bin. The likelihood fit is based on the profile likelihood method [109]. Systematic uncertainties are represented by Gaussian-distributed nuisance parameters, and take into account the correlation among systematic variations and across $p_{\mathrm{T}}^{\mathrm{recoil}}$ bins.

The normalization of all $W+$jets and $Z+$jets processes, excluding those initiated by VBF, is multiplied by a common single floating normalization factor, which is the same across all $p_{\mathrm{T}}^{\mathrm{recoil}}$ bins. As a result, data from both W and Z control regions are used simultaneously to constrain the $Z \to \nu\nu$ background in the signal region. Systematic uncertainties in $W+$jets and $Z+$jets event yields, as described in Sec. VII, cover the residual bin-by-bin differences among processes when higher-order calculations are included, taking into account the correlation of theoretical uncertainties across different processes with the calculation provided in Ref. [72]. Similarly, one floating normalization factor is used for each of the $t\bar{t}$ and single-t backgrounds, resulting in a total of three floating background normalization factors in the fit. Compared to the previous version of the analysis, the usage of two independent normalization factors for the two main sources of top-quark backgrounds is introduced to better take into account their different expected contribution as a function of $p_{\mathrm{T}}^{\mathrm{recoil}}$.

Table III shows the results of the background-only fit to the control regions, when all exclusive bins are fitted simultaneously. As determined in the signal region, the normalizations of the $W+$jets and $Z+$jets backgrounds get corrected by a multiplicative factor of 1.13 ± 0.01, while the normalization of the $t\bar{t}$ and single-t backgrounds

TABLE III. Data and expected events with $p_{\mathrm{T}}^{\mathrm{recoil}} > 200$ GeV in the five control regions (Top: post-fit, Bottom: pre-fit). The post-fit predictions for the SM backgrounds are obtained after the simultaneous binned likelihood fit to the five control regions, performed in the exclusive bins of $p_{\mathrm{T}}^{\mathrm{recoil}}$ (EM0–EM12). The background predictions include both the statistical and systematic uncertainties. The individual uncertainties are correlated, and do not necessarily add in quadrature to equal the total background uncertainty. The … denotes contributions of less than 0.01% to the total background.

$p_{\mathrm{T}}^{\mathrm{recoil}} > 200$ GeV	$W \to \mu\nu$	$W \to e\nu$	Top	$Z \to \mu\mu$	$Z \to ee$
Data events (139 fb^{-1})	1 364 958	699 674	225 606	196 800	145 531
SM prediction (post-fit)	1 364 800 ± 3300	699 700 ± 1800	225 600 ± 1100	197 000 ± 600	145 500 ± 500
Fitted $W \to e\nu$	…	578 800 ± 3400	16 100 ± 900	…	…
Fitted $W \to \mu\nu$	1 149 000 ± 6000	…	31 600 ± 1700	…	…
Fitted $W \to \tau\nu$	71 500 ± 800	45 200 ± 500	3380 ± 180	…	…
Fitted VBF $W+$jets	26 200 ± 3100	14 300 ± 1700	2020 ± 340	…	…
Fitted $Z \to ee$	…	…	…	…	138 100 ± 700
Fitted $Z \to \mu\mu$	21 500 ± 500	…	778 ± 20	185 200 ± 900	…
Fitted $Z \to \tau\tau$	…	1900 ± 50	…	…	…
Fitted $Z \to \nu\nu$	…	…	…	…	…
Fitted VBF $Z+$jets	…	…	…	3300 ± 400	2530 ± 320
Fitted single-t	22 000 ± 6000	13 200 ± 3500	33 000 ± 10 000	350 ± 170	110 ± 60
Fitted $t\bar{t}$	52 000 ± 4000	34 000 ± 2800	137 000 ± 9000	4000 ± 400	1790 ± 180
Expected dibosons	23 000 ± 4000	12 400 ± 1900	1880 ± 340	4000 ± 700	2900 ± 500
MC exp. SM events	1 220 000 ± 60 000	623 000 ± 32 000	233 000 ± 31 000	175 000 ± 9000	127 000 ± 7000
Fit input $W \to e\nu$	…	509 000 ± 27 000	14 200 ± 1200	…	…
Fit input $W \to \mu\nu$	1 010 000 ± 50 000	…	28 000 ± 2300	…	…
Fit input $W \to \tau\nu$	63 000 ± 3400	39 800 ± 2100	2970 ± 250	…	…
Fit input VBF $W+$jets	22 000 ± 4000	11 700 ± 2300	1500 ± 500	…	…
Fit input $Z \to ee$	…	…	…	…	120 000 ± 7000
Fit input $Z \to \mu\mu$	18 900 ± 1100	…	689 ± 23	163 000 ± 9000	…
Fit input $Z \to \tau\tau$	…	1680 ± 60	…	…	…
Fit input $Z \to \nu\nu$	…	…	…	…	…
Fit input VBF $Z+$jets	…	…	…	2700 ± 500	2000 ± 400
Fit input single-t	16 000 ± 6000	10 000 ± 4000	28 000 ± 13 000	700 ± 500	280 ± 210
Fit input $t\bar{t}$	60 000 ± 7000	39 000 ± 5000	155 000 ± 27 000	4600 ± 1300	2000 ± 700
Fit input dibosons	23 000 ± 4000	12 600 ± 2300	1900 ± 400	4100 ± 800	3000 ± 600

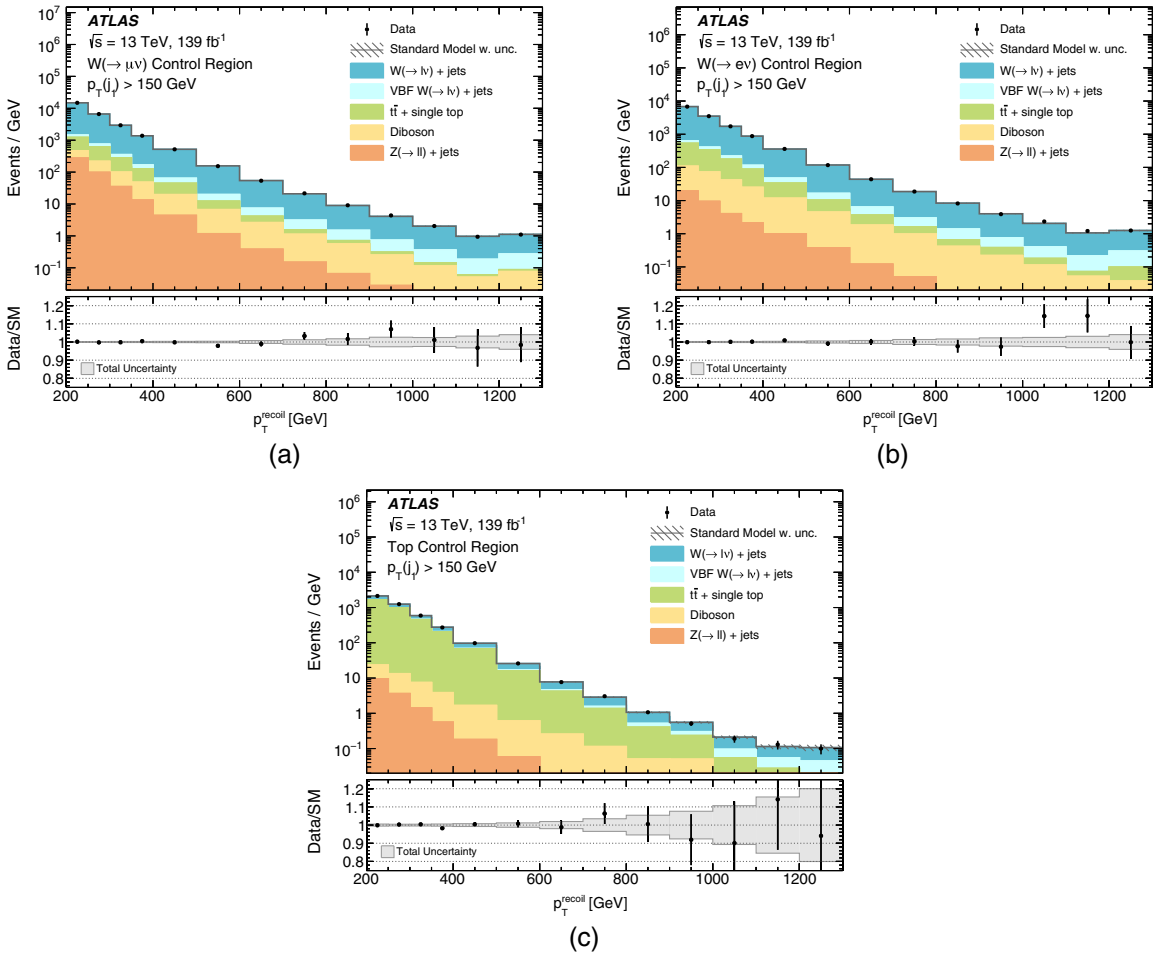

FIG. 2. The measured $p_{\mathrm{T}}^{\mathrm{recoil}}$ distributions in the (a) $W \to \mu\nu$, (b) $W \to e\nu$ and (c) top control regions, compared with the background predictions as estimated after the simultaneous, binned background-only fit to the data in the control regions. The ratios of data to SM predictions after the CR fit are shown in the lower panels (black dots). The error bands in the ratios include the statistical and systematic uncertainties in the background predictions. Events with values beyond the range of the histogram are included in the last bin.

gets corrected by a multiplicative factor of 0.9 ± 0.1 and 1.6 ± 0.4, respectively.

Figures 2 and 3 show the expected and observed distributions of the $p_{\mathrm{T}}^{\mathrm{recoil}}$ in the control regions. The shown expected distributions include the data-driven normalization factors as extracted from the binned likelihood fit to the different exclusive $p_{\mathrm{T}}^{\mathrm{recoil}}$ bins in the control regions. Good agreement is observed, within statistical and systematic uncertainties, with data. As an illustration, χ^2-statistical tests, using the binned profile likelihood fit described above, probing potential shape discrepancies between the observed and predicted $p_{\mathrm{T}}^{\mathrm{recoil}}$ distributions, give p-values in a range from 0.49 (in the $W \to \mu\nu$ control region) to 0.96 (in the top-quark control region).

In order to perform model-independent tests for new physics processes, discussed in Sec. VIII A, the same fit procedure is repeated in each of the inclusive bins of $p_{\mathrm{T}}^{\mathrm{recoil}}$ for signal and control regions, denoted in Table I by IM0–IM12. Since in this case no shape information is available to constrain the separate contributions of $t\bar{t}$ and single-t, a single normalization factor is used for all top-quark-related processes, along with the normalization factor for W/Z + jets, resulting in two free background normalization factors in the fit. Additionally, the nuisance parameters related to systematic uncertainties refer to the given $E_{\mathrm{T}}^{\mathrm{miss}}$ inclusive region. A total of 13 separate fits are therefore performed, based on five control regions each and including two free background normalization factors. The results are expected to differ from those of the simultaneous fit to exclusive bins, due to the lack of $p_{\mathrm{T}}^{\mathrm{recoil}}$ shape information to constrain uncertainties and the normalization of backgrounds.

VII. SYSTEMATIC UNCERTAINTIES

The impact of systematic uncertainties is estimated after performing a background-only fit to data from the exclusive CRs, and evaluating the impact of the uncertainty in the total background yield in each bin of $p_{\mathrm{T}}^{\mathrm{recoil}}$ in the SR. The dominant sources of experimental uncertainty are those

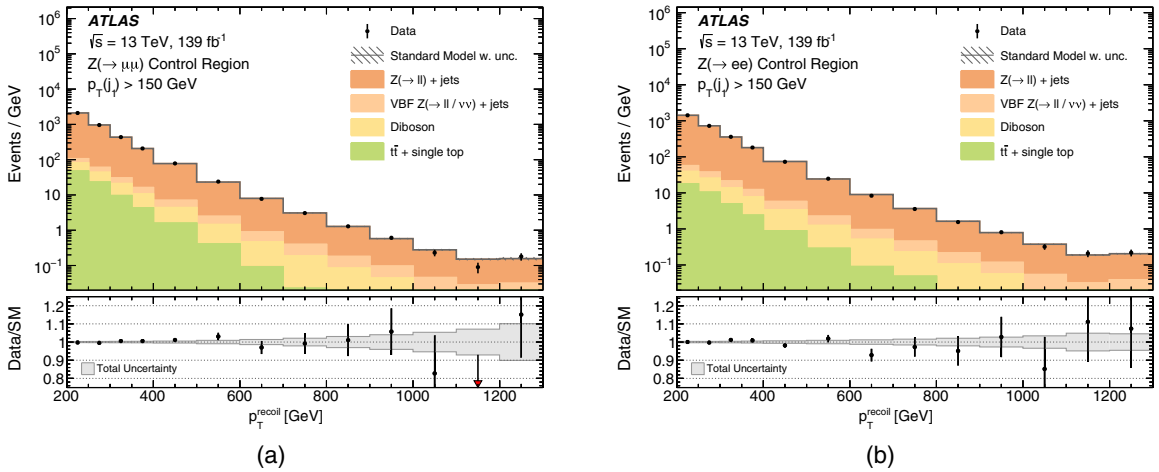

FIG. 3. The measured $p_{\mathrm{T}}^{\mathrm{recoil}}$ distributions in the (a) $Z \to \mu\mu$ and (b) $Z \to ee$ control regions, compared with the background predictions as estimated after the simultaneous, binned background-only fit to the data in the control regions. The ratios of data to SM predictions after the CR fit are shown in the lower panels (black dots). The error bands in the ratios include the statistical and systematic uncertainties in the background predictions. Events with values beyond the range of the histogram are included in the last bin. The red arrow marker in the ratio panel indicates the point falls beyond the vertical axis range of the plot.

related to the electron, muon and jet identification and reconstruction efficiencies, while uncertainties in the $V+$jets predictions give the leading contribution to theory uncertainties. More details are provided in the following sections.

A. Background uncertainties

The uncertainty in the combined 2015–2018 integrated luminosity is 1.7%. It is derived from the calibration of the luminosity scale using x–y beam-separation scans, following a methodology similar to that described in Ref. [110], and using the LUCID-2 detector for the baseline luminosity measurements [111]. This uncertainty nearly cancels out in the semidata-driven background estimation procedure, and translates into a residual uncertainty in the total background in the SR of less than 0.01% (0.05%) for $p_{\mathrm{T}}^{\mathrm{recoil}} = 200$ GeV (1200 GeV). The uncertainty in the pileup reweighting procedure translates into a residual uncertainty in the total background in the SR of less than 0.4% (0.24%) for $p_{\mathrm{T}}^{\mathrm{recoil}} = 200$ GeV (1200 GeV).

Systematic uncertainties in the jet energy scale (resolution) [95] translate into uncertainties in the total background in the SR which vary between 0.17% (0.15%) and 1.0% (1.3%) for $p_{\mathrm{T}}^{\mathrm{recoil}}$ between 200 GeV and 1200 GeV. The uncertainty in the modeling of the JVT requirement used to reject jets coming from pileup [112] is below 0.03% across the $p_{\mathrm{T}}^{\mathrm{recoil}}$ spectrum. Uncertainties in the flavor-tagging efficiency [113] translate into uncertainties in the total background in the SR between 0.1% and 0.9% for $p_{\mathrm{T}}^{\mathrm{recoil}}$ between 200 GeV and 1200 GeV.

Uncertainties in the $E_{\mathrm{T}}^{\mathrm{miss}}$ scale (resolution) due to soft contributions to the $E_{\mathrm{T}}^{\mathrm{miss}}$ calculation translate into uncertainties in the total background in the SR between 0.5% (0.34%) and 0.25% (0.04%) for $p_{\mathrm{T}}^{\mathrm{recoil}}$ between 200 GeV and 1200 GeV.

Uncertainties in the electron reconstruction and identification efficiencies are computed following the method described in Ref. [99]; the latter are treated as uncorrelated between selected and vetoed electrons, since different working points are used for their identification, as described in Sec. V. Uncertainties in the electron and photon energy scale and resolution are computed following the method described in Ref. [114]. Overall, they translate into uncertainties in the total background in the SR between 0.7% and 1.3% for $p_{\mathrm{T}}^{\mathrm{recoil}}$ between 200 GeV and 1200 GeV. Uncertainties due to the electron isolation efficiency give a contribution of less than 0.2% across the $p_{\mathrm{T}}^{\mathrm{recoil}}$ spectrum. Negligible contributions are given by the electron trigger efficiency and by the photon identification efficiency. Uncertainties in the muon reconstruction and identification efficiencies and in their momentum measurement are computed following the method described in Ref. [100]. In order to take into account the difference between the simulated and measured identification efficiencies for muons with p_{T} above 300 GeV, an additional uncertainty is included, conservatively taken as uncorrelated in muon p_{T} and η. Overall, these translate into uncertainties in the total background in the SR between 0.4% and 1.9% for $p_{\mathrm{T}}^{\mathrm{recoil}}$ between 200 GeV and 1200 GeV. Uncertainties in the τ-lepton reconstruction and identification efficiencies translate into uncertainties in the total background in the SR of 0.1% (0.07%) for $p_{\mathrm{T}}^{\mathrm{recoil}} = 200$ GeV (> 1200 GeV).

Uncertainties in the higher-order QCD and electroweak parton-level calculations used to correct the MC prediction for $V+$jets processes not initiated by VBF are calculated following the procedure described in Ref. [72]. They are provided in the form of event weights parametrized as a

function of vector-boson p_{T}, which are applied to derive shape and normalization uncertainties for simulated $V+$jets processes in signal and control regions. The correlations across $p_{\mathrm{T}}^{\mathrm{recoil}}$ bins are implemented as recommended in Ref. [72]. The correlations across processes are implemented as follows.

Three sources of pure QCD uncertainties are considered. The uncertainty associated with the truncation of the perturbative expansion in the strong coupling constant is estimated by varying the QCD renormalization and factorization scales both individually and simultaneously by factors 2 and 0.5, and evaluating the change in differential cross section in bins of the vector-boson p_{T} for these seven combinations. The center of the resulting band is taken as the nominal estimate, and its half width is taken as its systematic uncertainty. Uncertainties in the shape of the vector-boson p_{T} distribution, which are relevant for the extrapolation of low-p_{T} measurements to high p_{T}, are taken into account by applying an additional uncertainty estimated from a conservative shape distortion of the aforementioned scale uncertainty.[3] These two uncertainties are represented by two nuisance parameters, $\delta^{(1)}K_{\mathrm{NNLO}}$ and $\delta^{(2)}K_{\mathrm{NNLO}}$, which are taken as correlated across $V+$jets processes, assuming that for $p_{\mathrm{T}}^{\mathrm{recoil}} \gg m_{W,Z}$ the QCD effects on the $W+$jets and $Z+$jets predictions are very similar. Residual differences in QCD corrections between $W+$jets and $Z+$jets processes are estimated from the difference in QCD NNLO k-factors with respect to $Z+$jets production, and taken into account as an additional nuisance parameter, $\delta^{(3)}K_{\mathrm{NNLO}}$.

Three sources of pure EW uncertainties and one source of mixed QCD–EW uncertainties are considered. Unknown Sudakov logarithms beyond NNLO are considered as the dominant source of uncertainty at high p_{T}, and are treated as correlated across $V+$jets processes and represented by one nuisance parameter, $\delta^{(1)}\kappa_{\mathrm{nNLO\,EW}}$. An additional source of uncertainty is considered to cover possible NNLO effects not included in the calculation, conservatively defined as 5% of the absolute full NLO EW correction, and is treated as uncorrelated across $V+$jets processes and hence represented by the three nuisance parameters $\delta^{(2)}\kappa_{\mathrm{nNLO\,EW}}^{(W)}$, $\delta^{(2)}\kappa_{\mathrm{nNLO\,EW}}^{(Z\to\ell^+\ell^-)}$, and $\delta^{(2)}\kappa_{\mathrm{nNLO\,EW}}^{(Z\to\nu\nu)}$. The uncertainty in the limitations of the Sudakov approximation at two loops is estimated as the difference between the NLL Sudakov approximation and the exponentiation of the full NLO EW correction, and is treated as uncorrelated between $W+$jets and $Z+$jets processes, resulting in two nuisance parameters, $\delta^{(3)}\kappa_{\mathrm{nNLO\,EW}}^{(W)}$ and $\delta^{(3)}\kappa_{\mathrm{nNLO\,EW}}^{(Z)}$. Uncertainties due to the approximation of mixed QCD–EW corrections via a factorized combination of QCD and EW corrections are assumed to be proportional to the difference between the additive and multiplicative combination of QCD and EW corrections, and are treated as correlated across $V+$jets processes, resulting in a single nuisance parameter, $\delta K_{\mathrm{NNLO\,mix}}$.

Uncertainties in the parton distribution functions are treated as correlated across $V+$jets processes, following the prescription of Ref. [72]. They are estimated by the sum in quadrature over the 107 independent Hessian PDF replicas provided by the PDF set `LUXqed_plus_PDF4LHC15_nnlo`, following Eq. (20) of Ref. [115]. The resulting nuisance parameter is denoted by δK_{PDF}.

Table IV summarizes the considered nuisance parameters and their assumed correlations. Before the CR-only fit, the leading impacts on the signal region background prediction for the EM0 selection come from $\delta^{(1)}K_{\mathrm{NNLO}}$ (1.8%), $\delta^{(2)}K_{\mathrm{NNLO}}$ (1.5%) and δK_{PDF} (0.7%), while the largest contributions for the EM12 selection come from δK_{PDF} (2.9%), $\delta^{(1)}K_{\mathrm{NNLO}}$ (2.8%), $\delta^{(3)}\kappa_{\mathrm{nNLO\,EW}}^{(Z)}$ (1.6%) and $\delta^{(2)}K_{\mathrm{NNLO}}$ (1.5%). After the CR-only fit, these uncertainties translate into uncertainties in the total background in the SR between 0.4% and 2% for $p_{\mathrm{T}}^{\mathrm{recoil}}$ between 200 GeV and 1200 GeV, dominated by QCD uncertainties at low $p_{\mathrm{T}}^{\mathrm{recoil}}$ and by EW uncertainties at high $p_{\mathrm{T}}^{\mathrm{recoil}}$. The leading contributions for the EM0 selection are given by $\delta^{(1)}K_{\mathrm{NNLO}}$ (0.20%), $\delta^{(3)}K_{\mathrm{NNLO}}$ (0.12%) and $\delta^{(2)}\kappa_{\mathrm{nNLO\,EW}}^{(Z\to\nu\nu)}$ (0.11%), while the largest contributions for the EM12 selection come from $\delta^{(3)}\kappa_{\mathrm{nNLO\,EW}}^{(Z)}$ (1.3%), $\delta^{(2)}\kappa_{\mathrm{nNLO\,EW}}^{(Z\to\nu\nu)}$ (1.2%) and $\delta^{(2)}\kappa_{\mathrm{nNLO\,EW}}^{(W)}$ (1.0%). An additional systematic uncertainty is included to cover possible differences between the definition of τ-leptons at Monte Carlo generator level and the one used in the theoretical calculation from Ref. [72], which translates into uncertainties in the total background in the SR between 0.05% and 0.1% for $p_{\mathrm{T}}^{\mathrm{recoil}}$ between 200 GeV and 1200 GeV.

Uncertainties in the $V+$jets processes initiated by VBF include scale and PDF uncertainties and the comparison with SHERPA as an alternative MC generator. They translate into uncertainties in the total background in the SR between 0.024% and 0.1% for $p_{\mathrm{T}}^{\mathrm{recoil}}$ between 200 GeV and 900 GeV, and between 0.2% and 1.1% for $p_{\mathrm{T}}^{\mathrm{recoil}}$ between 1000 GeV and 1200 GeV.

Uncertainties in the theoretical predictions of the $t\bar{t}$ and single-t backgrounds are estimated for the two processes separately by varying parton-shower parameters and the amount of initial- and final-state soft gluon radiation, by comparing predictions from different MC event generators [116] and by comparing the degree of interference between single-t in the Wt-channel and $t\bar{t}$ when using the DR and DS schemes described in Ref. [117]. In the case of $t\bar{t}$ (single-t), they translate into uncertainties in the total background in the SR between 0.06% (0.13%) and 0.7% (0.28%) for $p_{\mathrm{T}}^{\mathrm{recoil}}$ between 200 GeV and 1200 GeV.

[3]This distortion is parameterized as a function of the vector-boson p_{T} between 200 GeV and 2 TeV and has the form $(p_{\mathrm{T}}^2 - p_{\mathrm{T},0}^2)/(p_{\mathrm{T}}^2 + p_{\mathrm{T},0}^2)$, where $p_{\mathrm{T},0} = 650$ GeV.

TABLE IV. Uncertainties considered in the reweighting of $V+$jets samples to higher-order QCD and EW parton-level calculations. For reference, the correspondence with the nuisance parameters included in Table 3 from Ref. [72] is also indicated.

Source of uncertainty	Correlation	Nuisance parameter name(s) in Ref. [72]
Truncation of perturbative expansion in α_s	Correlated across p_T^{recoil} bins and $V+$jets processes	$\delta^{(1)}K_{NNLO}$
Shape of the vector-boson distribution and extrapolation from low p_T to high p_T	Correlated across p_T^{recoil} bins and $V+$jets processes	$\delta^{(2)}K_{NNLO}$
Difference in QCD corrections between $W+$jets and $Z+$jets	Correlated across p_T^{recoil} bins and $V+$jets processes	$\delta^{(3)}K_{NNLO}$
Unknown Sudakov logarithms beyond NNLO	Correlated across p_T^{recoil} bins and $V+$jets processes	$\delta^{(1)}\kappa_{nNLO\,EW}$
Additional possible NNLO effects	Correlated across p_T^{recoil} bins, uncorrelated between $V+$jets processes	$\delta^{(2)}\kappa_{nNLO\,EW}^{(W)}$, $\delta^{(2)}\kappa_{nNLO\,EW}^{(Z\to\ell^+\ell^-)}$, $\delta^{(2)}\kappa_{nNLO\,EW}^{(Z\to\nu\nu)}$
Limitations of the Sudakov approximation at two loops	Correlated across p_T^{recoil} bins, uncorrelated between $W+$jets and $Z+$jets processes	$\delta^{(3)}\kappa_{nNLO\,EW}^{(W)}$, $\delta^{(3)}\kappa_{nNLO\,EW}^{(Z)}$
Interference terms between QCD and EW corrections	Correlated across p_T^{recoil} bins and $V+$jets processes	$\delta K_{NNLO\,mix}$
PDF uncertainties	Correlated across p_T^{recoil} bins and $V+$jets processes	Sum in quadrature of $\delta K_{PDF}^{(i)}$
Different definition of τ-leptons between parton-level calculation and simulation	Correlated across p_T^{recoil} bins and $V+$jets processes	…

Uncertainties in the theoretical predictions of diboson backgrounds include uncertainties in the QCD renormalization, factorization and resummation scales, uncertainties due to the choice of parton distribution functions and uncertainties in the modeling of the parton showers. They translate into uncertainties in the total background in the SR between 0.01% and 0.22% for p_T^{recoil} between 200 GeV and 1200 GeV.

Uncertainties in the multijet and noncollision backgrounds translate into uncertainties in the total background in the SR for $p_T^{recoil} = 200$ GeV of 1% and 0.2%, respectively, and are negligible above 800 GeV.

Table V summarizes the overall impact of systematic uncertainties in each bin of p_T^{recoil} in the SR, as estimated from the CR-only fit.

B. Signal uncertainties

Sources of systematic uncertainty in the predicted signal yields are considered separately for each model of new physics, using a common set of procedures. Experimental uncertainties include those related to the jet and E_T^{miss} reconstruction, energy scales and resolutions, which introduce uncertainties in the signal yields for the different models that vary in the range between 1% and 3% at low p_T^{recoil}, and between 4% and 7% at large p_T^{recoil}, depending on the parameters of the model. The 1.7% uncertainty in the integrated luminosity is also included. Other uncertainties related to the jet quality requirements are negligible.

Uncertainties affecting the signal acceptance in the generation of signal samples include: uncertainties in the modeling of the initial- and final-state radiation and the underlying event, determined using simulated samples with modified parton-shower parameters (by factors of two or one half); uncertainties due to PDFs and variations of the $\alpha_s(m_Z)$ value employed, as computed from the envelope of CT10 or CT14, MMHT2014 [118] and NNPDF30 error sets; and uncertainties due to the choice of renormalization and factorization scales, which are varied by factors of two or one half. In addition, theoretical uncertainties in the predicted cross sections, including PDF and renormalization- and factorization-scale uncertainties, are assessed and their effect is shown in terms of variations of the observed results.

In the case of WIMP production models, the uncertainty related to the modeling of the initial- and final-state radiation translates into a 3% to 6% uncertainty in the signal acceptance. The choice of different PDF sets results in up to a 10% and a 20% uncertainty in the case of axial-vector and pseudoscalar models, respectively. Varying the renormalization and factorization scales introduces 0.1% to 21% variations in the signal acceptance, depending on the model and the mediator and WIMP masses considered. Renormalization and factorization scale uncertainties introduce an uncertainty in the cross-section predictions of about 10% in the case of the axial-vector mediator model and up to 50% for the pseudoscalar mediator model. Finally, PDF uncertainties translate into cross-section uncertainties of about 5% and 20% for the axial-vector and pseudoscalar mediator models, respectively. The larger uncertainties computed in the case of the pseudoscalar mediator model are attributed to the presence of top-quark

TABLE V. Summary of the impact at low and high $p_{\mathrm{T}}^{\mathrm{recoil}}$ of systematic uncertainties on the total background in the SR, as obtained from the CR-only fit. The impact of each source of systematic uncertainty is shown as the sum in quadrature of the individual contributions represented by the corresponding nuisance parameters. The two reported values refer to the first and last bin of $p_{\mathrm{T}}^{\mathrm{recoil}}$ (EM0 and EM12). Only non-negligible contributions are shown.

Source of uncertainty and effect on the total SR background estimate [%]			
Flavor tagging	0.1–0.9	τ-lepton identification efficiency	0.1–0.07
Jet energy scale	0.17–1.0	Luminosity	0.01–0.05
Jet energy resolution	0.15–1.3	Noncollision background	0.2–0.0
Jet JVT efficiency	0.01–0.03	Multijet background	1.0–0.0
Pileup reweighting	0.4–0.24	Diboson theory	0.01–0.22
$E_{\mathrm{T}}^{\mathrm{miss}}$ resolution	0.34–0.04	Single-top theory	0.13–0.28
$E_{\mathrm{T}}^{\mathrm{miss}}$ scale	0.5–0.25	$t\bar{t}$ theory	0.06–0.7
Electron and photon energy resolution	0.01–0.08	$V+$jets τ-lepton definition	0.04–0.16
Electron and photon energy scale	0.3–0.7	$V+$jets pure QCD corrections	0.24–1.1
Electron identification efficiency	0.5–1.0	$V+$jets pure EW corrections	0.17–2.2
Electron reconstruction efficiency	0.15–0.2	$V+$jets mixed QCD–EW corrections	0.02–0.7
Electron isolation efficiency	0.04–0.19	$V+$jets PDF	0.01–0.7
Muon identification efficiency	0.03–0.9	VBF EW $V+$jets backgrounds	0.02–1.1
Muon reconstruction efficiency	0.4–1.5	Limited MC statistics	0.05–1.9
Muon momentum scale	0.1–0.7		
Total background uncertainty in the signal region: 1.5%–4.2%			

induced loops in the relevant Feynman diagrams, that are absent in the axial-vector mediator model.

Similarly, for SUSY models, the uncertainties related to the modeling of initial- and final-state gluon radiation and the matching between matrix elements and parton showers in the simulation translate into a 7% to 8% uncertainty in the signal acceptance for $E_{\mathrm{T}}^{\mathrm{miss}} > 200$ GeV. Variations of the renormalization and factorization scales introduce an uncertainty of about 3% in the signal acceptance. Uncertainties in the predicted cross sections, including both renormalization/factorization scale and PDF uncertainties, increase with the squark masses and range between 7% for a mass of 100 GeV and about 11% for a mass of about 1 TeV.

In the case of dark-energy-inspired models, uncertainties related to renormalization/factorization scales, PDFs, and parton-shower modeling vary the signal acceptance by 0.1% to 3.5%, 1% to 16%, and 0.1% to 5%, respectively, with increasing $E_{\mathrm{T}}^{\mathrm{miss}}$. Renormalization/factorization scale and PDF uncertainties introduce variations in the cross-section predictions of about 30% each.

For the ADD model, the uncertainties related to the modeling of the initial- and final-state gluon radiation translate into uncertainties in the ADD signal acceptance which vary between 11% and 13% with increasing $E_{\mathrm{T}}^{\mathrm{miss}}$ and are approximately independent of n. The uncertainties due to the PDFs, affecting both signal normalization and acceptance, increase from 11% at $n = 2$ to 43% at $n = 6$. Similarly, the variations of the renormalization and factorization scales introduce a signal yield uncertainty of 23% to 36%, growing with increasing n.

For the ALPs production model, theoretical uncertainties related to PDFs, affecting signal normalization and acceptance, translate into uncertainties in the signal yields that vary in the range between 2% and 14%. Variations of the renormalization and factorization scales and matrix-elements to parton-shower matching scales, introduce uncertainties in the signal yields that vary between 5% and 50%. Variations in the parton-shower modeling translate into uncertainties in the signal acceptance in the range between 1% and 20%, depending on the $E_{\mathrm{T}}^{\mathrm{miss}}$ bin considered.

Finally, for the interpretation of an invisibly decaying Higgs boson, uncertainties related to PDFs, affecting both signal normalization and signal acceptance, translate into 0.4% to 0.8% variations in the Higgs signal yields as $E_{\mathrm{T}}^{\mathrm{miss}}$ increases. Variations in the renormalization and factorization scales introduce a 10% uncertainty in the signal yields. Uncertainties in the parton-shower modeling translate into uncertainties in the signal acceptance that vary between 3% and 9% with increasing $E_{\mathrm{T}}^{\mathrm{miss}}$. Uncertainties in the higher-order electroweak corrections, especially relevant for VBF and VH processes, translate into uncertainties in the signal yield that vary between 1.4% and 10% with increasing $E_{\mathrm{T}}^{\mathrm{miss}}$.

VIII. RESULTS AND INTERPRETATIONS

Figure 4 shows several measured distributions in the signal region compared with the SM predictions obtained from the fit to CRs. As discussed in Sec. VI, the SM predictions are normalized with normalization factors determined from the global fit carried out in exclusive $p_{\mathrm{T}}^{\mathrm{recoil}}$ bins. The fitting procedure also constrains the background uncertainties, resulting in a precise SM

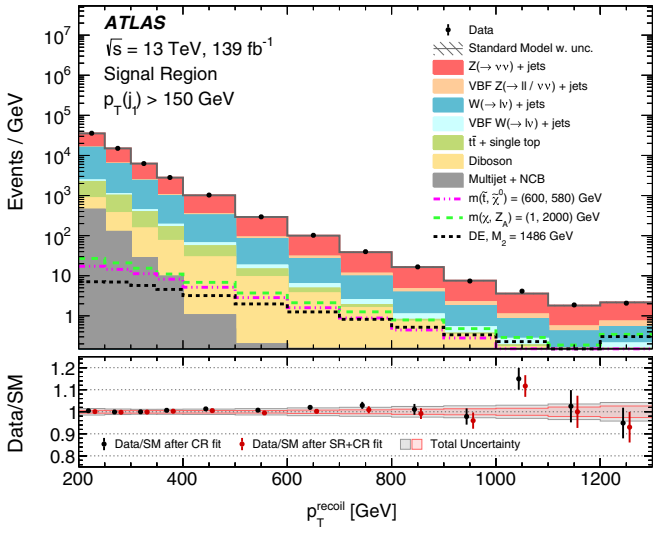

FIG. 4. Measured distributions of $p_{\mathrm{T}}^{\mathrm{recoil}}$ for the $p_{\mathrm{T}}^{\mathrm{recoil}} > 200$ GeV selection compared with the SM predictions in the signal region. The latter are normalized with normalization factors as determined by the global fit that considers exclusive $p_{\mathrm{T}}^{\mathrm{recoil}}$ control regions ("CR fit"). For illustration purposes, the distributions of examples of dark energy (DE), SUSY, and WIMP scenarios are included. The ratios of data to SM predictions after the CR fit are shown in the lower panel (black dots), and compared with the same quantities when SM predictions are normalized to the results of the global background-only fit when the signal region is also included ("SR + CR fit", red dots). The error bands in the ratio shown in the lower panel include both the statistical and systematic uncertainties in the background predictions. Events with values beyond the range of the histogram are included in the last bin.

prediction in almost the whole $p_{\mathrm{T}}^{\mathrm{recoil}}$ spectrum. As an example, the SM predictions are determined with a total uncertainty of 1.5%, 1.2%, and 4.1% for the EM0, EM4, and EM12 signal regions, respectively, which include correlations between uncertainties in the individual background contributions. For illustration purposes, the ratios of data to SM predictions are shown in the lower panel, both after the CR fit and after a global background-only fit when the signal region is also included ("SR+CR fit").

The number of events in the data and the individual background predictions are presented in Tables VI and VII for inclusive and exclusive $p_{\mathrm{T}}^{\mathrm{recoil}}$ bins, respectively. The results for all the signal regions are summarized in Table VIII. Overall, good agreement between data and SM predictions is observed. The compatibility of the data with a SM background hypothesis is tested using the binned profile likelihood fit described above. The resulting statistical tests for a background-only hypothesis, in the presence of different potential signal contributions, give p-values in the range between 0.02 and 1.0, where the minimum corresponds to a signal for stop-pair production in the $\tilde{t}_1 \to c + \tilde{\chi}_1^0$ decay channel with $m_{\tilde{t}_1} = 500$ GeV and $m_{\tilde{\chi}_1^0} = 420$ GeV and a deviation of about 2σ from the background-only hypothesis.

The results are translated into upper limits on the presence of new phenomena, using a simultaneous likelihood fit in both the control and signal regions, and the $\mathrm{CL_s}$ modified frequentist approach [119]. As already mentioned, inclusive regions with minimum $p_{\mathrm{T}}^{\mathrm{recoil}}$ thresholds are used to set model-independent exclusion limits, and the exclusive regions are used for the interpretation of the results within different models of new physics. For the latter, the presence of a slight excess of events at high $p_{\mathrm{T}}^{\mathrm{recoil}}$ limits the reach of the observed limits, mostly for those models in which the expected signal would accumulate in the tail of the $p_{\mathrm{T}}^{\mathrm{recoil}}$ distribution.

A. Model-independent exclusion limits

Results obtained in inclusive $p_{\mathrm{T}}^{\mathrm{recoil}}$ regions are translated into model-independent observed and expected 95% CL upper limits on the visible cross section, defined as the product of the production cross section, acceptance and efficiency $\sigma \times A \times \epsilon$. The limits are extracted by dividing the 95% CL upper limit on the number of signal events by the integrated luminosity, taking into consideration the systematic uncertainties in the SM backgrounds and the uncertainty in the integrated luminosity. A likelihood fit is performed separately for each of the inclusive regions IM0–IM12. The results are collected in Table IX. Values of $\sigma \times A \times \epsilon$ above 736 fb (for IM0) and above 0.3 fb (for IM12) are excluded at 95% CL.

B. Model-dependent exclusion limits

A simultaneous fit to the signal and control regions in the exclusive $p_{\mathrm{T}}^{\mathrm{recoil}}$ bins is performed, and used to set observed and expected 95% CL exclusion limits on the parameters of the different models under consideration. Uncertainties in the signal and background predictions, and in the luminosity are considered, and correlations between experimental systematic uncertainties in signal and background predictions are taken into account. The contamination of the control regions by signal events is negligible.

1. Weakly interacting massive particles

As discussed in Sec. I, simplified models are considered with the exchange of an axial-vector or a pseudoscalar mediator in the s-channel. In the case of the exchange of an axial-vector mediator, and for WIMP-pair production with $m_{Z_A} > 2m_\chi$, typical $A \times \epsilon$ values for the signal models with a 2 TeV mediator range from 13% to less than 1% for the EM0 and EM12 selections, respectively, where the values refer to an initial simulated sample generated with a minimum transverse momentum of 150 GeV. Similarly, values for $A \times \epsilon$ in the range between 13% and less than 1% are computed for the pseudoscalar mediator model with $m_{Z_P} = 350$ GeV and $m_\chi = 1$ GeV, where 1% is

TABLE VI. Data and SM background predictions in the signal region for several inclusive $p_{\mathrm{T}}^{\mathrm{recoil}}$ selections, as determined using separate one-bin likelihood fits in the control regions. For the SM prediction, both the statistical and systematic uncertainties are included. In each signal region, the individual uncertainties for the different background processes can be correlated, and do not necessarily add in quadrature to equal the total background uncertainty. The … denotes negligible background contributions. For illustration, the expected event yields for particular signals for new phenomena are provided; in this case, the quoted errors include experimental uncertainties and theory uncertainties on the signal acceptance, as described in Sec. VII B.

Inclusive Signal Region	IM1	IM3	IM5	IM7	IM10	IM12
Data events (139 fb^{-1})	1 357 019	290 779	46 855	7194	807	207
SM prediction	1 346 000 ± 16 000	286 000 ± 4000	45 550 ± 1000	7070 ± 240	720 ± 60	223 ± 19
$W \to e\nu$	72 000 ± 5000	11 900 ± 800	1400 ± 100	166 ± 12	12.4 ± 1.5	2.8 ± 0.4
$W \to \mu\nu$	105 800 ± 2200	17 600 ± 400	2220 ± 70	305 ± 14	38 ± 4	14.6 ± 1.7
$W \to \tau\nu$	243 900 ± 3500	44 900 ± 800	5890 ± 160	790 ± 40	66 ± 7	17.6 ± 2.1
VBF W + jets	7900 ± 1700	2200 ± 600	450 ± 160	80 ± 40	10 ± 8	3.9 ± 3.5
$Z \to ee$	…	…	…	…	…	…
$Z \to \mu\mu$	2970 ± 130	…	…	…	…	…
$Z \to \tau\tau$	2550 ± 110	…	…	…	…	…
$Z \to \nu\nu$	816 000 ± 10 000	189 000 ± 4000	32 000 ± 1000	5120 ± 250	520 ± 50	157 ± 18
VBF Z + jets	13 600 ± 2800	4800 ± 1200	1210 ± 350	260 ± 90	35 ± 14	13 ± 6
$t\bar{t}$ and single-t	46 700 ± 2100	6900 ± 400	610 ± 70	45 ± 14	…	…
Diboson	26 000 ± 5000	7700 ± 1500	1600 ± 400	310 ± 80	38 ± 12	13 ± 4
Multijet	7000 ± 7000	500 ± 500	5.3 ± 5.3	0.2 ± 0.2	…	…
Noncollision background	1200 ± 1200	160 ± 160	29 ± 29	6 ± 6	…	…
SUSY, $m(\tilde{t},\tilde{\chi}^0) = (600, 580)$ GeV	2840 ± 340	1560 ± 190	640 ± 80	195 ± 24	34 ± 4	10.8 ± 1.3
DMA, $m(\chi, Z_A) = (1, 2000)$ GeV	3960 ± 160	2150 ± 80	918 ± 34	330 ± 13	82 ± 4	34.5 ± 1.7
Dark energy, $M_2 = 1486$ GeV	1740 ± 50	1106 ± 33	558 ± 27	235 ± 16	68 ± 6	30.4 ± 3.3

TABLE VII. Data and SM background predictions in the signal region for several exclusive $p_{\mathrm{T}}^{\mathrm{recoil}}$ selections, as determined using a binned likelihood fit in the control regions. For the SM prediction, both the statistical and systematic uncertainties are included. In each signal region, the individual uncertainties for the different background processes can be correlated, and do not necessarily add in quadrature to equal the total background uncertainty. The … denotes negligible background contributions. For illustration, the expected event yields for particular signals for new phenomena are provided; in this case, the quoted errors include experimental uncertainties and theory uncertainties on the signal acceptance, as described in Sec. VII B.

Exclusive Signal Region	EM2	EM4	EM6	EM8	EM9	EM11
Data events (139 fb^{-1})	313 912	102 888	10 203	1663	738	187
SM prediction	314 000 ± 3500	101 600 ± 1200	10 000 ± 180	1640 ± 40	754 ± 20	182 ± 6
$W \to e\nu$	16 000 ± 1000	3980 ± 250	280 ± 19	35.8 ± 2.6	13.4 ± 1.0	3.01 ± 0.24
$W \to \mu\nu$	23 600 ± 500	5940 ± 120	481 ± 12	66.8 ± 2.3	31.2 ± 1.2	7.8 ± 0.4
$W \to \tau\nu$	54 900 ± 800	15 430 ± 260	1243 ± 29	167 ± 6	77.4 ± 2.9	15.5 ± 0.8
VBF W + jets	2340 ± 300	1010 ± 150	140 ± 27	29 ± 7	16 ± 5	5.0 ± 1.9
$Z \to ee$	…	…	…	…	…	…
$Z \to \mu\mu$	597 ± 15	97.4 ± 2.7	4.51 ± 0.15	1.49 ± 0.05	0.60 ± 0.02	…
$Z \to \tau\tau$	530 ± 14	115.0 ± 3.3	8.31 ± 0.28	0.90 ± 0.04	0.40 ± 0.02	2.10 ± 0.08
$Z \to \nu\nu$	192 800 ± 2100	67 400 ± 1000	7000 ± 170	1180 ± 40	534 ± 20	126 ± 6
VBF Z + jets	3900 ± 500	2170 ± 310	370 ± 60	86 ± 17	45 ± 10	13.7 ± 3.3
single-t	2800 ± 700	550 ± 180	15 ± 8	…	…	…
$t\bar{t}$	8900 ± 700	2000 ± 150	100 ± 8	8.2 ± 1.0	2.4 ± 0.4	0.30 ± 0.05
Diboson	6200 ± 1000	2700 ± 500	350 ± 70	71 ± 15	33 ± 8	…
Multijet	1100 ± 1100	57 ± 57	0.6 ± 0.6	0.1 ± 0.1	…	…
Noncollision background	240 ± 240	46 ± 46	8 ± 8	6 ± 6	…	…
SUSY, $m(\tilde{t},\tilde{\chi}^0) = (600, 580)$ GeV	562 ± 70	516 ± 60	159 ± 19	44 ± 6	28 ± 4	8.2 ± 1.1
DMA, $m(\chi, Z_A) = (1, 2000)$ GeV	770 ± 30	684 ± 27	212 ± 9	79 ± 4	47.9 ± 2.3	18.7 ± 1.1
Dark energy, $M_2 = 1486$ GeV	286 ± 7	320 ± 11	125 ± 7	52 ± 5	33.6 ± 3.2	14.6 ± 1.8

TABLE VIII. Data and SM background predictions in the signal region for the different selections, as determined using a binned likelihood fit in the control regions. For the SM predictions both the statistical and systematic uncertainties are included.

Inclusive Signal Region			Exclusive Signal Region		
Region	Predicted	Observed	Region	Predicted	Observed
IM0	$3\,120\,000 \pm 40\,000$	3 148 643	EM0	$1\,783\,000 \pm 26\,000$	1 791 624
IM1	$1\,346\,000 \pm 16\,000$	1 357 019	EM1	$753\,000 \pm 9000$	752 328
IM2	$597\,000 \pm 8000$	604 691	EM2	$314\,000 \pm 3500$	313 912
IM3	$286\,000 \pm 4000$	290 779	EM3	$140\,100 \pm 1600$	141 036
IM4	$146\,400 \pm 2300$	149 743	EM4	$101\,600 \pm 1200$	102 888
IM5	$45\,550 \pm 1000$	46 855	EM5	$29\,200 \pm 400$	29 458
IM6	$16\,800 \pm 500$	17 397	EM6	$10\,000 \pm 180$	10 203
IM7	7070 ± 240	7194	EM7	3870 ± 80	3986
IM8	3180 ± 130	3208	EM8	1640 ± 40	1663
IM9	1560 ± 80	1545	EM9	754 ± 20	738
IM10	720 ± 60	807	EM10	359 ± 10	413
IM11	407 ± 34	394	EM11	182 ± 6	187
IM12	223 ± 19	207	EM12	218 ± 9	207

already reached for the EM5 selection due to the softer $p_{\mathrm{T}}^{\mathrm{recoil}}$ spectrum.

Figure 5(a) shows the observed and expected 95% CL exclusion contours in the $m_{Z_A} - m_\chi$ parameter plane for a simplified model with an axial-vector mediator, Dirac WIMPs, and couplings $g_q = 1/4$ and $g_\chi = 1$. In the region $m_{Z_A} > 2 \times m_\chi$, mediator masses up to about 2.1 TeV are excluded for $m_\chi = 1$ GeV, extending significantly beyond previous bounds. The masses corresponding to the relic density [120] as determined by the Planck and WMAP satellites [15,16], within the WIMP dark-matter model and in the absence of any interaction other than the one considered, are indicated in this figure as a line that crosses the excluded region at $m_{Z_A} \sim 1500$ GeV and $m_\chi \sim 585$ GeV.

Similarly, Figure 5(b) presents observed and expected 95% CL exclusion contours in the $m_{Z_P} - m_\chi$ parameter plane for a simplified model with a pseudoscalar mediator, Dirac WIMPs, and couplings $g_q = 1$ and $g_\chi = 1$. For the first time, the monojet final state in the ATLAS experiment has enough sensitivity to exclude a part of the parameter space in such a model. Mediator masses below 376 GeV are excluded for very light WIMP candidates.

In the case of the axial-vector mediator model, the results are translated into 90% CL exclusion limits on the spin-dependent WIMP-nucleon scattering cross section σ_{SD} as a function of the WIMP mass, following the prescriptions from Refs. [19,120]. Figure 6 shows exclusion limits for WIMP-proton and WIMP-neutron scattering cross sections as a function of the WIMP mass, compared with the results from the PICO [122] experiment, and from the LUX [123] and XENON1T [124] experiments, respectively. Stringent limits on the scattering cross section of the order of 1.4×10^{-43} cm^2 for WIMP masses of about 100 GeV, and 3×10^{-44} cm^2 for WIMP masses below 10 GeV are inferred from this analysis, which complement the results from direct-detection experiments.

TABLE IX. Observed and expected 95% CL upper limits on the number of signal events, S_{obs}^{95} and S_{exp}^{95}, and on the visible cross section, defined as the product of cross section, acceptance and efficiency, $\langle\sigma\rangle_{\mathrm{obs}}^{95}$, for the IM0–IM12 selections.

Selection	$\langle\sigma\rangle_{\mathrm{obs}}^{95}$ [fb]	S_{obs}^{95}	S_{exp}^{95}
$p_{\mathrm{T}}^{\mathrm{recoil}} > 200$ GeV	736	102 274	83000^{+22000}_{-23000}
$p_{\mathrm{T}}^{\mathrm{recoil}} > 250$ GeV	296	41 158	33800^{+11300}_{-9400}
$p_{\mathrm{T}}^{\mathrm{recoil}} > 300$ GeV	150	20 893	15400^{+5900}_{-4300}
$p_{\mathrm{T}}^{\mathrm{recoil}} > 350$ GeV	86	11 937	8300^{+3100}_{-2300}
$p_{\mathrm{T}}^{\mathrm{recoil}} > 400$ GeV	52	7214	4700^{+1800}_{-1300}
$p_{\mathrm{T}}^{\mathrm{recoil}} > 500$ GeV	21	2918	1930^{+730}_{-540}
$p_{\mathrm{T}}^{\mathrm{recoil}} > 600$ GeV	10	1391	940^{+360}_{-260}
$p_{\mathrm{T}}^{\mathrm{recoil}} > 700$ GeV	4.1	574	490^{+190}_{-140}
$p_{\mathrm{T}}^{\mathrm{recoil}} > 800$ GeV	2.1	298	277^{+106}_{-77}
$p_{\mathrm{T}}^{\mathrm{recoil}} > 900$ GeV	1.2	164	168^{+65}_{-47}
$p_{\mathrm{T}}^{\mathrm{recoil}} > 1000$ GeV	1.3	186	119^{+45}_{-33}
$p_{\mathrm{T}}^{\mathrm{recoil}} > 1100$ GeV	0.5	73	75^{+28}_{-21}
$p_{\mathrm{T}}^{\mathrm{recoil}} > 1200$ GeV	0.3	40	49^{+19}_{-14}

2. Squark-pair production

As in previous publications, different models of squark-pair production are considered: stop-pair production with $\tilde{t}_1 \to c + \tilde{\chi}_1^0$, stop-pair production with $\tilde{t}_1 \to b + ff' + \tilde{\chi}_1^0$, sbottom-pair production with $\tilde{b}_1 \to b + \tilde{\chi}_1^0$, and squark-pair production with $\tilde{q} \to q + \tilde{\chi}_1^0$ ($q = u, d, c, s$). In each case separately, the results are translated into exclusion limits as a function of the squark mass for different neutralino masses. The region with stop-neutralino or sbottom-neutralino mass differences below 5 GeV is not considered

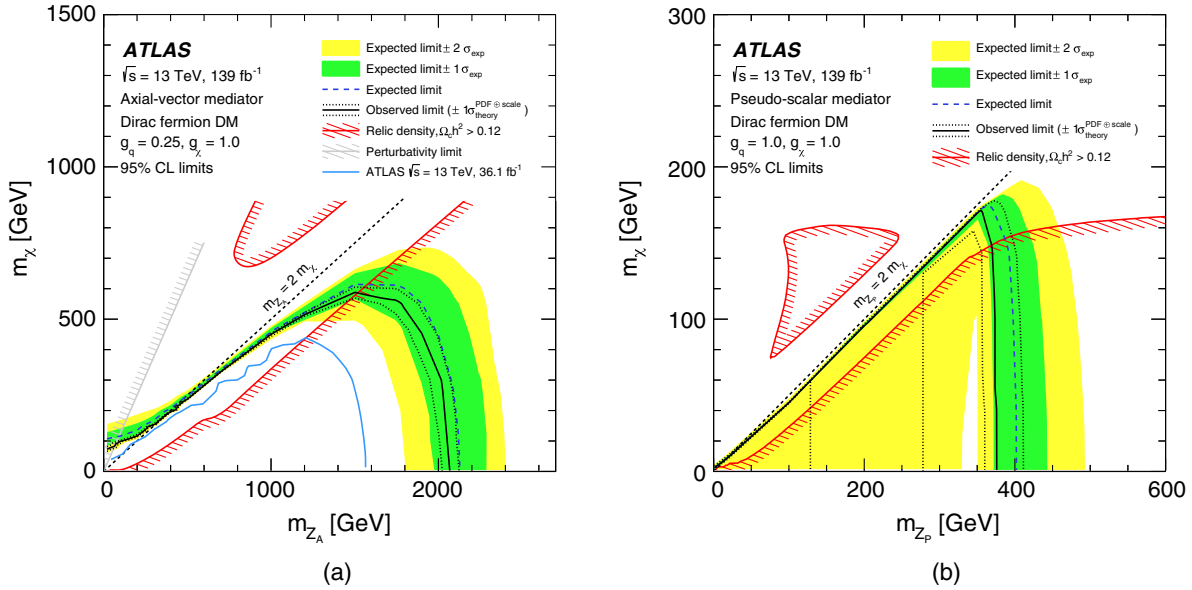

FIG. 5. (a) 95% CL exclusion contours in the $m_{Z_A} - m_\chi$ parameter plane for the axial-vector mediator model. (b) 95% CL exclusion contours in the $m_{Z_P} - m_\chi$ parameter plane for the pseudoscalar mediator model. The solid (dashed) curves show the observed (expected) limits, while the bands indicate the $\pm 1\sigma$ theory uncertainties in the observed limit and the $\pm 1\sigma$ and $\pm 2\sigma$ ranges of the expected limit in the absence of a signal. The red curves correspond to the set of points for which the expected relic density is consistent with the WMAP measurements (i.e., $\Omega h^2 = 0.12$), as computed with MADDM [121]. The area on the hashed side of the red contour (e.g., to the right of the red contour in the region $m_{Z_A} > 2m_\chi$) corresponds to predicted values of the relic density abundance inconsistent with the WMAP measurements. The region excluded due to perturbativity, defined by $m_\chi > \sqrt{\pi/2} m_{Z_A}$, is indicated by the gray hatched area. The dotted lines indicate the kinematic limit for on-shell production $m_{Z_{A,P}} = 2 \times m_\chi$. In the case of the pseudoscalar mediator model, the shape of the 2σ band at $m_{Z_P} \sim 350$ GeV is related to the rapid increase of the signal cross section at the threshold at which the mediator mass equals twice the mass of the top quark. The same applies to the 1σ band on the observed limit. In the case of the axial-vector mediator model, the results are compared with previous results from the ATLAS Collaboration at $\sqrt{s} = 13$ TeV using 36.1 fb^{-1} [4].

in the exclusion since in this regime the squarks could become long-lived. In such a compressed scenario, and for stop sbottom masses of about 600 GeV, the typical value of $A \times \epsilon$ for the selection criteria varies between 11% for EM0 and less than 1% for EM12, as computed using a sample with a minimum missing transverse momentum of 150 GeV. Comparable values for $A \times \epsilon$ are obtained in the rest of the squark-neutralino mass plane.

Figure 7(a) presents the results in the case of the $\tilde{t}_1 \to c + \tilde{\chi}_1^0$ decays. In the compressed scenario with stop and neutralino nearly degenerate in mass, masses up to 550 GeV are excluded. Similarly, Fig. 7(b) shows the observed and expected 95% CL exclusion limits as a function of the stop and neutralino masses for the $\tilde{t}_1 \to b + ff' + \tilde{\chi}_1^0$ decay channel, assuming a branching ratio $\mathcal{B} = 100\%$. For $m_{\tilde{t}_1} - m_{\tilde{\chi}_1^0} \sim m_b$, stop masses up to 550 GeV are also excluded. Figure 8(a) presents the observed and expected 95% CL exclusion limits as a function of the sbottom and neutralino masses for the $\tilde{b}_1 \to b + \tilde{\chi}_1^0$ ($\mathcal{B} = 100\%$) decay channel. In the scenario with $m_{\tilde{b}_1} - m_{\tilde{\chi}_1^0} \sim m_b$, this analysis extends the 95% CL exclusion limits up to a sbottom mass of 545 GeV. Finally, Figure 8(b) presents the observed and expected 95% CL exclusion limits as a function of the squark mass and the squark-neutralino mass difference for $\tilde{q} \to q + \tilde{\chi}_1^0$ ($q = u$, d, c, s). In the compressed scenario, squark masses below 925 GeV are excluded at 95% CL. Altogether, these results significantly improve upon the previous exclusion limits based on 36.1 fb^{-1} of total integrated luminosity [4]. In the very compressed scenario, the observed limits on the squark masses are extended by more than 100 GeV.

3. Dark-energy-inspired model

Exclusion limits are computed for the Horndeski dark-energy model (see Sec. I) with $m_\varphi = 0.1$ GeV, and considering only the terms relevant for the monojet final state, following the work described in Ref. [6]. The sensitivity remains independent of the m_φ value considered for light particles up to masses of the order of 1 GeV. The typical value of $A \times \epsilon$ for the selection criteria varies between 8.2% for EM0 and less than 1% for EM12, as computed using a sample with a minimum missing transverse momentum of 150 GeV. Figure 9 shows the observed and expected contours at 95% CL on the σ-M_2 plane. Values for M_2 below 1486 GeV are excluded, which represents a significant improvement over the limits previously obtained.

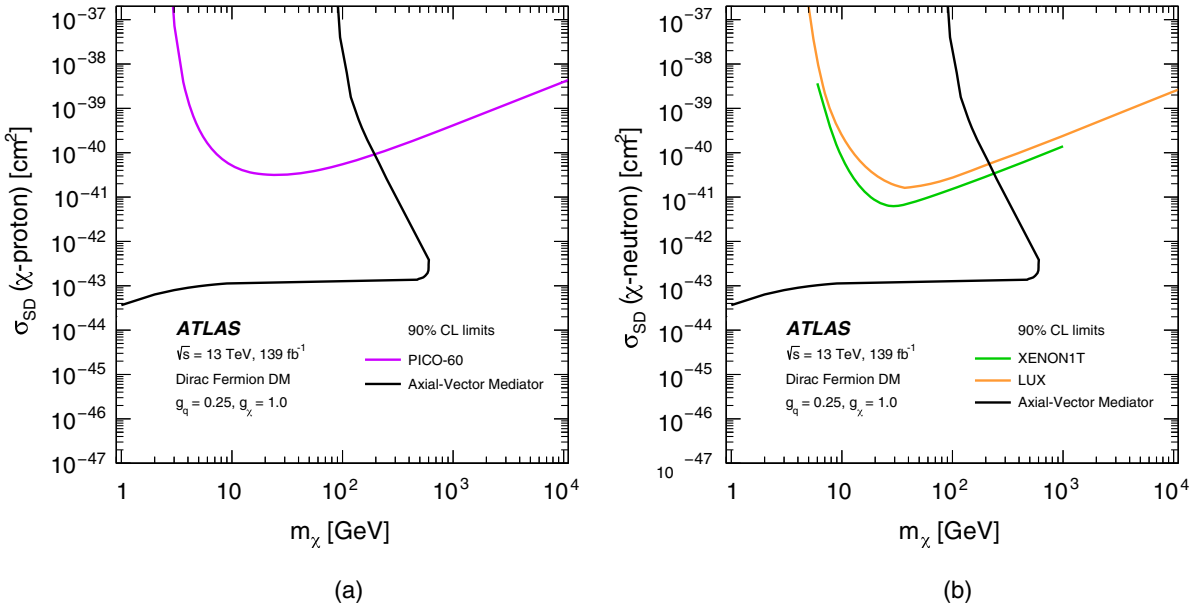

FIG. 6. A comparison of the inferred limits (black line) with the constraints from direct-detection experiments on the spin-dependent (a) WIMP-proton scattering cross section and (b) WIMP-neutron scattering cross section as a function of the WIMP mass, in the context of the simplified model with axial-vector couplings. Unlike in the $m_{Z_A} - m_\chi$ parameter plane, the limits are shown at 90% CL. The results from this analysis, excluding the region to the left of the contour, are compared with limits from the PICO [122] (purple line), LUX [123] (orange line), and XENON1T [124] (green line) experiments. The comparison is model-dependent and solely valid in the context of this model, assuming minimal mediator width and the coupling values $g_q = 1/4$ and $g_\chi = 1$.

The validity of the effective implementation of the model at the LHC energies was studied previously [6] by truncating the signal contributions with $\sqrt{\hat{s}} < g_* M_2$, where $\sqrt{\hat{s}}$ is the center-of-mass energy of the hard interaction and g_* is a number that depends on the UV completion of the model which must satisfy $g_* < 4\pi$ in order for the couplings to be in the perturbative regime, leading to a negligible effect on the obtained exclusion limits for $g_* > 3.5$.

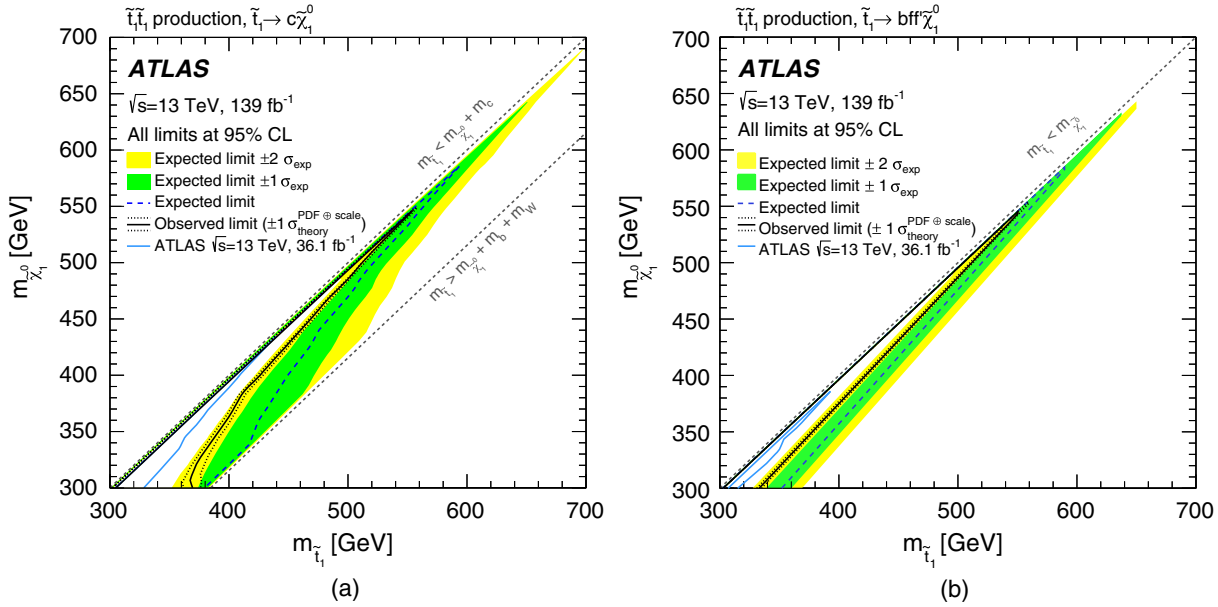

FIG. 7. Excluded regions at the 95% CL in the $(\tilde{t}_1, \tilde{\chi}_1^0)$ mass plane for (a) the decay channel $\tilde{t}_1 \to c + \tilde{\chi}_1^0$ ($\mathcal{B} = 100\%$) and (b) the decay channel $\tilde{t}_1 \to b + ff' + \tilde{\chi}_1^0$ ($\mathcal{B} = 100\%$). The dotted lines around the observed limits indicate the range of observed limits corresponding to $\pm 1\sigma$ variations of the NNLO + NNLL SUSY cross-section predictions. The bands around the expected limits indicate the expected $\pm 1\sigma$ and $\pm 2\sigma$ ranges of limits in the absence of a signal. The results from this analysis are compared with previous results from the ATLAS Collaboration at $\sqrt{s} = 13$ TeV using 36.1 fb^{-1} [4].

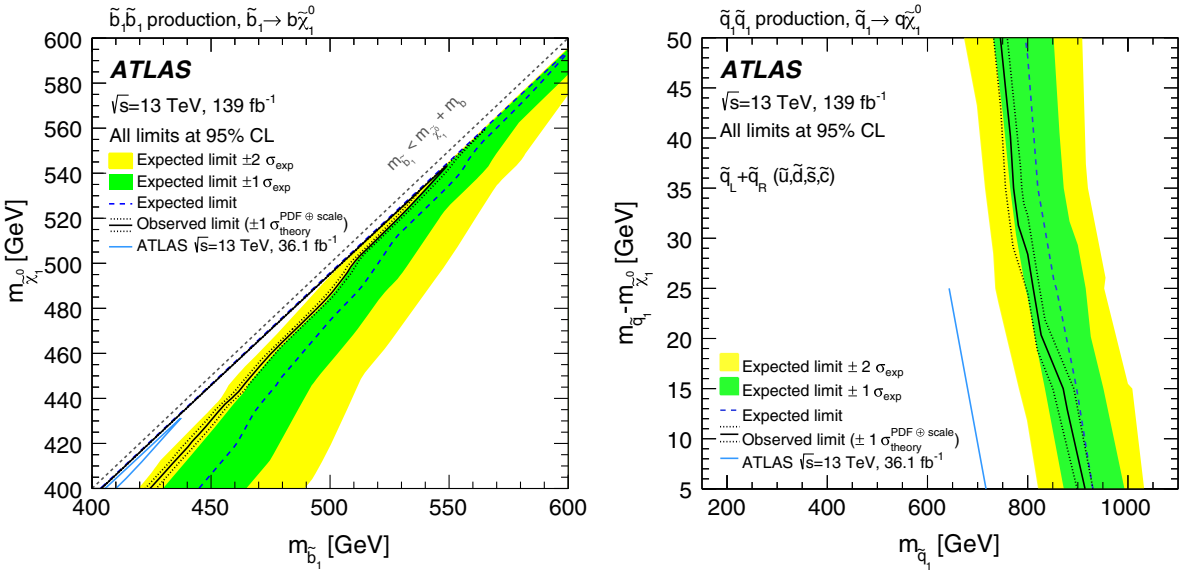

FIG. 8. (a) Exclusion plane at 95% CL as a function of sbottom and neutralino masses for the decay channel $\tilde{b}_1 \to b + \tilde{\chi}_1^0$ ($\mathcal{B} = 100\%$). (b) Exclusion region at 95% CL as a function of squark mass and the squark–neutralino mass difference for $\tilde{q} \to q + \tilde{\chi}_1^0$ and $\tilde{q}_L + \tilde{q}_R$ with $(\tilde{u}, \tilde{d}, \tilde{c}, \tilde{s})$. The dotted lines around the observed limit indicate the range of observed limits corresponding to $\pm 1\sigma$ variations of the NNLO + NNLL SUSY cross-section predictions. The bands around the expected limit indicates the expected $\pm 1\sigma$ and $\pm 2\sigma$ ranges of limits in the absence of a signal. The results from this analysis are compared with previous results from the ATLAS Collaboration at $\sqrt{s} = 13$ TeV using 36.1 fb^{-1} [4].

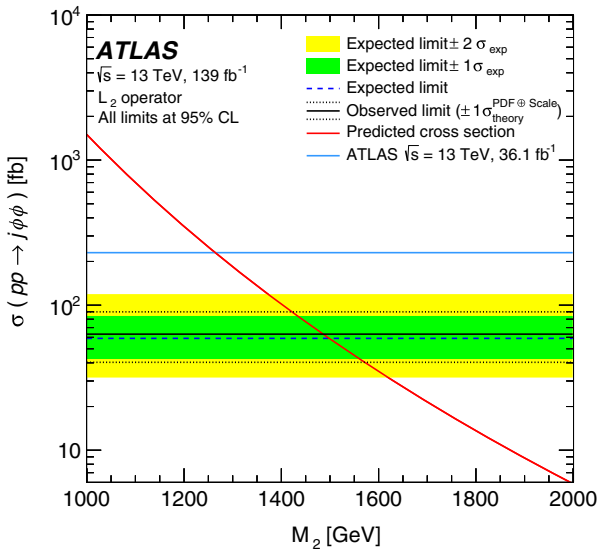

FIG. 9. Observed (solid line) and expected (dashed line) exclusions at 95% CL on the Horndeski dark-energy model for $m_\phi = 0.1$ GeV and $c_{i\neq 2} = 0$, $c_2 = 1$ [6], expressed in terms of the visible cross section as a function of the suppression scale M_2. The results are compared with the theoretical predictions. The dotted lines around the observed limits indicate the range of observed limits corresponding to $\pm 1\sigma$ variations of the cross-section predictions. The results from this analysis are compared with previous results from the ATLAS Collaboration at $\sqrt{s} = 13$ TeV using 36.1 fb^{-1} [6].

4. Large extra spatial dimensions

The results are translated into limits on the parameters of the ADD model. As in previous analyses, only the signal regions with $p_{\mathrm{T}}^{\mathrm{recoil}} > 400$ GeV are employed, with sufficient sensitivity to ADD signal. The typical value of $A \times \epsilon$ for the selection criteria, as computed from a simulated sample with missing transverse momentum above 350 GeV, is of the order of 6% for EM4 and is less than 1% for EM12. Figure 10 and Table X present the results. Values of M_D below 11.2 TeV at $n = 2$ and below 5.9 TeV at $n = 6$ are excluded at 95% CL, which improve on the exclusion limits from previous results using 36.1 fb^{-1} of 13 TeV data [4]. As already noted in Ref. [4], the analysis partially probes the phase-space region with $\hat{s} > M_D^2$. The suppression of this kinematic region in computing the 95% CL lower limits on M_D translates into a negligible effect on the results.

5. Axionlike particles

Results are expressed in terms of 95% CL limits on the parameters of the ALP model. As in the case of the ADD model, the kinematic region with $p_{\mathrm{T}}^{\mathrm{recoil}} > 400$ GeV provides the best sensitivity. Figure 11 shows 95% exclusion contours in the $c_{\tilde{G}}$-f_a plane, for an axion mass of 1 MeV. The exclusion does not depend significantly on the axion mass for masses up to at least 1 GeV. The limits on $c_{\tilde{G}}$

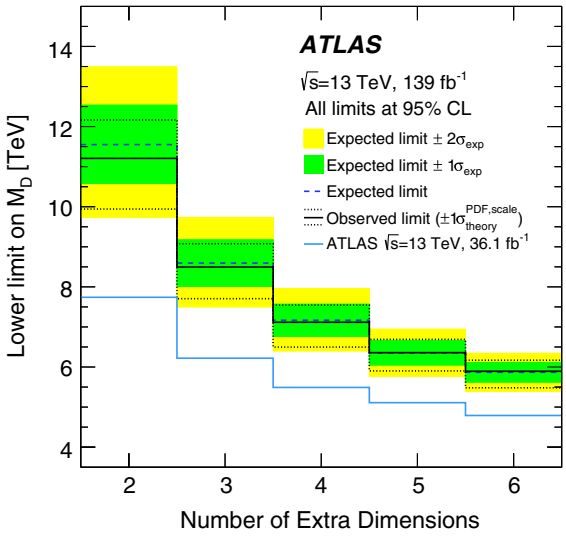

FIG. 10. Observed and expected 95% CL lower limits on the fundamental Planck scale in $4+n$ dimensions, M_D, as a function of the number of extra dimensions. The bands indicate the $\pm 1\sigma$ theory uncertainties in the observed limit and the $\pm 1\sigma$ and $\pm 2\sigma$ ranges of the expected limit in the absence of a signal. The results from this analysis are compared with previous results from the ATLAS Collaboration using 36.1 fb^{-1} of $\sqrt{s} = 13$ TeV data [4].

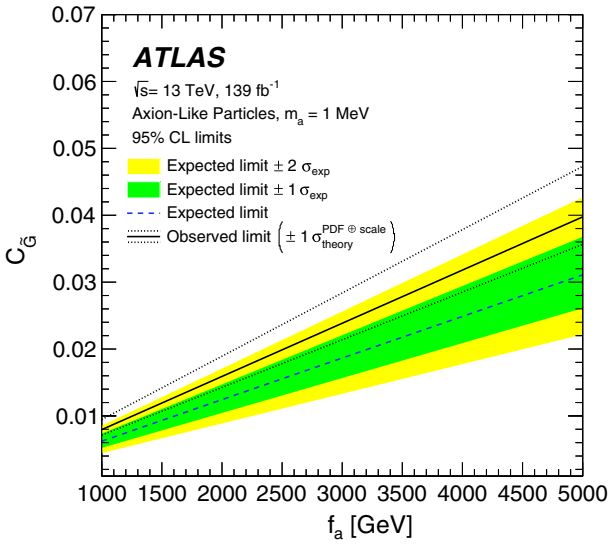

FIG. 11. Observed and expected 95% CL upper limits on the coupling $c_{\tilde{G}}$ as a function of the effective scale f_a for ALP mass of 1 MeV. The bands indicate the $\pm 1\sigma$ theory uncertainties in the observed limit and the $\pm 1\sigma$ and $\pm 2\sigma$ ranges of the expected limit in the absence of a signal. The 95% CL limits are computed with no suppression of the events with $\hat{s} > f_a^2$.

increase linearly with f_a. For $f_a = 1$ TeV, couplings $c_{\tilde{G}}$ above 0.008 are excluded. Expressed in terms of the $c_{\tilde{G}}/f_a$ ratio, values above $8 \times 10^{-6}\text{GeV}^{-1}$ are excluded at 95% CL. As in the case of the dark energy and ADD models, the validity of the effective field implementation of the model is challenged for $\hat{s} > f_a^2$. For values of f_a below 2 TeV, the signal yields are reduced significantly when applying a suppressing weighting factor $f_a^4/\hat{s}^2$ for events with $\hat{s} > f_a^2$. The effect is reduced to about 5% for $f_a = 2$ TeV and it is negligible for f_a above 3 TeV.

6. Invisibly decaying Higgs boson

The results are interpreted in terms of 95% CL upper limits on the branching ratio for an invisibly decaying Higgs boson. The signal yields are dominated by gluon-gluon fusion production processes (about 73%), followed by the contributions from VBF (18%), VH (8%), and $t\bar{t}+H$ (1%) processes. The low $E_{\mathrm{T}}^{\mathrm{miss}}$ region plays an important role in enhancing the sensitivity of the data to the Higgs signal and the full $E_{\mathrm{T}}^{\mathrm{miss}}$ spectrum is employed in computing the limits. The observed agreement between data and the SM background predictions in the measured $E_{\mathrm{T}}^{\mathrm{miss}}$ distribution leads to a 95% CL observed (expected) exclusion limit on the invisible branching ratio of the Higgs boson of 0.34 ($0.39^{+0.16}_{-0.11}$).

TABLE X. The 95% CL observed and expected lower limits on the fundamental Planck scale in $4+n$ dimensions, M_D, as a function of the number of extra dimensions n, considering nominal LO signal cross sections. The impact of the $\pm 1\sigma$ theoretical uncertainty on the observed limits and the expected $\pm 1\sigma$ range of limits in the absence of a signal are also given.

	ADD Model Limits on M_D (95% CL)	
	Expected [TeV]	Observed [TeV]
$n=2$	$11.6^{+1.0}_{-1.0}$	$11.2^{+1.0}_{-1.3}$
$n=3$	$8.6^{+0.6}_{-0.6}$	$8.5^{+0.6}_{-0.8}$
$n=4$	$7.2^{+0.4}_{-0.4}$	$7.1^{+0.4}_{-0.6}$
$n=5$	$6.4^{+0.3}_{-0.3}$	$6.4^{+0.3}_{-0.5}$
$n=6$	$5.9^{+0.2}_{-0.2}$	$5.9^{+0.3}_{-0.4}$

IX. CONCLUSIONS

Results are reported from a search for new phenomena in events with an energetic jet and large missing transverse momentum in proton-proton collisions at $\sqrt{s} = 13$ TeV at the LHC, based on data corresponding to an integrated luminosity of 139 fb^{-1} collected by the ATLAS detector during 2015–2018. Compared to previous publications, in addition to an increase of almost a factor of four in the data size, the analysis implements a number of improvements in the signal selection and the background determination leading to enhanced sensitivity. The measurements are in agreement with the SM predictions. The results are translated into model-independent 95% CL upper limits on the visible cross section for new phenomena, and these range from 736 fb to 0.3 fb with increasing missing transverse momentum. Improved bounds on the parameters for a variety of models for new phenomena have been derived. In the case of simplified models for WIMP-pair

production in the s-channel, with Dirac fermions as dark-matter candidates, an axial-vector mediator with masses below 2.1 TeV is excluded at 95% CL for very light WIMPs and coupling values $g_q = 1/4$ and $g_\chi = 1$. For the first time, the ATLAS monojet analysis reaches sensitivity for excluding pseudoscalar mediators with masses below 376 GeV, for very light WIMPs and coupling values $g_q = 1$ and $g_\chi = 1$.

Similarly, the results are interpreted in terms of a search for squark-pair production in a compressed-mass supersymmetric scenario. In the case of stop- and sbottom-pair production with $\tilde{t}_1 \to c + \tilde{\chi}_1^0$ or $\tilde{t}_1 \to b + ff' + \tilde{\chi}_1^0$ and $\tilde{b}_1 \to b + \tilde{\chi}_1^0$, respectively, squark masses below about 550 GeV and 550 GeV are excluded at 95% CL, thus surpassing previous exclusions by almost 100 GeV. In the case of squark-pair production with $\tilde{q} \to q + \tilde{\chi}_1^0 (q = u, d, c, s)$, squark masses below 925 GeV are excluded.

The results are expressed in terms of 95% CL limits on the suppression scale M_2 for the Horndeski dark-energy model with $m_\phi = 0.1$ GeV and $c_{i\neq 2} = 0$, $c_2 = 1$. Suppression scales M_2 below about 1.5 TeV are excluded. In the case of the ADD model with large extra spatial dimensions, 95% CL lower limits on the fundamental Planck scale M_D in $4 + n$ dimensions vary in the range between 11.2 TeV and 5.9 TeV for $n = 2$ and $n = 6$, respectively. In models with axionlike particles with coupling to gluons, couplings-to-effective-scale ratios $c_{\tilde{G}}/f_a$ above 8×10^{-6} GeV^{-1} are excluded at 95% CL for axion masses up to 1 GeV. Finally, limits are obtained for the branching ratio of an invisibly decaying Higgs boson. Branching fractions above 0.34 are excluded at 95% CL.

ACKNOWLEDGMENTS

We thank CERN for the very successful operation of the LHC, as well as the support staff from our institutions without whom ATLAS could not be operated efficiently. We acknowledge the support of ANPCyT, Argentina; YerPhI, Armenia; ARC, Australia; BMWFW and FWF, Austria; ANAS, Azerbaijan; SSTC, Belarus; CNPq and FAPESP, Brazil; NSERC, NRC and CFI, Canada; CERN; ANID, Chile; CAS, MOST and NSFC, China; COLCIENCIAS, Colombia; MSMT CR, MPO CR and VSC CR, Czech Republic; DNRF and DNSRC, Denmark; IN2P3-CNRS and CEA-DRF/IRFU, France; SRNSFG, Georgia; BMBF, HGF and MPG, Germany; GSRT, Greece; RGC and Hong Kong SAR, China; ISF and Benoziyo Center, Israel; INFN, Italy; MEXT and JSPS, Japan; CNRST, Morocco; NWO, Netherlands; RCN, Norway; MNiSW and NCN, Poland; FCT, Portugal; MNE/IFA, Romania; JINR; MES of Russia and NRC KI, Russian Federation; MESTD, Serbia; MSSR, Slovakia; ARRS and MIZŠ, Slovenia; DST/NRF, South Africa; MICINN, Spain; SRC and Wallenberg Foundation, Sweden; SERI, SNSF and Cantons of Bern and Geneva, Switzerland; MOST, Taiwan; TAEK, Turkey; STFC, United Kingdom; DOE and NSF, United States of America. In addition, individual groups and members have received support from BCKDF, CANARIE, Compute Canada, CRC and IVADO, Canada; Beijing Municipal Science & Technology Commission, China; COST, ERC, ERDF, Horizon 2020 and Marie Skłodowska-Curie Actions, European Union; Investissements d'Avenir Labex, Investissements d'Avenir Idex and ANR, France; DFG and AvH Foundation, Germany; Herakleitos, Thales and Aristeia programmes co-financed by EU-ESF and the Greek NSRF, Greece; BSF-NSF and GIF, Israel; La Caixa Banking Foundation, CERCA Programme Generalitat de Catalunya and PROMETEO and GenT Programmes Generalitat Valenciana, Spain; Göran Gustafssons Stiftelse, Sweden; The Royal Society and Leverhulme Trust, United Kingdom. The crucial computing support from all WLCG partners is acknowledged gratefully, in particular from CERN, the ATLAS Tier-1 facilities at TRIUMF (Canada), NDGF (Denmark, Norway, Sweden), CC-IN2P3 (France), KIT/GridKA (Germany), INFN-CNAF (Italy), NL-T1 (Netherlands), PIC (Spain), ASGC (Taiwan), RAL (UK) and BNL (USA), the Tier-2 facilities worldwide and large non-WLCG resource providers. Major contributors of computing resources are listed in Ref. [125].

[1] ATLAS Collaboration, Search for new phenomena in final states with an energetic jet and large missing transverse momentum in pp collisions at $\sqrt{s} = 13$ TeV using the ATLAS detector, Phys. Rev. D **94**, 032005 (2016).

[2] CMS Collaboration, Search for dark matter produced with an energetic jet or a hadronically decaying W or Z boson at $\sqrt{s} = 13$ TeV, J. High Energy Phys. 07 (2017) 014.

[3] ATLAS Collaboration, Measurement of detector-corrected observables sensitive to the anomalous production of events with jets and large missing transverse momentum in pp collisions at $\sqrt{s} = 13$ TeV using the ATLAS detector, Eur. Phys. J. C **77**, 765 (2017).

[4] ATLAS Collaboration, Search for dark matter and other new phenomena in events with an energetic jet and large missing transverse momentum using the ATLAS detector, J. High Energy Phys. 01 (2018) 126.

[5] CMS Collaboration, Search for dark matter, extra dimensions, and unparticles in monojet events in proton-proton collisions at $\sqrt{s} = 8$ TeV, Eur. Phys. J. C **75**, 1 (2015).

[6] ATLAS Collaboration, Constraints on mediator-based dark matter and scalar dark energy models using $\sqrt{s} = 13$ TeV pp collision data collected by the ATLAS detector, J. High Energy Phys. 05 (2019) 142.

[7] K. Mimasu and V. Sanz, ALPs at colliders, J. High Energy Phys. 06 (2015) 173.

[8] ATLAS Collaboration, Search for new phenomena in final states with an energetic jet and large missing transverse momentum in pp collisions at $\sqrt{s} = 8$ TeV with the ATLAS detector, Eur. Phys. J. C **75**, 299 (2015); , Erratum, Eur. Phys. J. C **75**, 408 (2015).

[9] CMS Collaboration, Searches for invisible decays of the Higgs boson in pp collisions at $\sqrt{s} = 7$, 8, and 13 TeV, J. High Energy Phys. 02 (2017) 135.

[10] V. Trimble, Existence and nature of dark matter in the universe, Annu. Rev. Astron. Astrophys. **25**, 425 (1987).

[11] G. Bertone, D. Hooper, and J. Silk, Particle dark matter: Evidence, candidates and constraints, Phys. Rep. **405**, 279 (2005).

[12] J. L. Feng, Dark matter candidates from particle physics and methods of detection, Annu. Rev. Astron. Astrophys. **48**, 495 (2010).

[13] G. Steigman and M. S. Turner, Cosmological constraints on the properties of weakly interacting massive particles, Nucl. Phys. **B253**, 375 (1985).

[14] E. W. Kolb and M. S. Turner, The early universe, Front. Phys. **69**, 1 (1990).

[15] N. Aghanim *et al.* (Planck Collaboration), Planck 2018 results. VI. Cosmological parameters, Astron. Astrophys. **641**, A6 (2020).

[16] G. Hinshaw *et al.*, Nine-year Wilkinson microwave anisotropy probe (WMAP) observations: Cosmological parameter results, Astrophys. J. Suppl. Ser. **208**, 19 (2013).

[17] J. Abdallah *et al.*, Simplified models for dark matter searches at the LHC, Phys. Dark Universe **9–10**, 8 (2015).

[18] D. Abercrombie *et al.*, Dark matter benchmark models for early LHC Run-2 searches: Report of the ATLAS/CMS dark matter forum, Phys. Dark Universe **27**, 100371 (2020).

[19] O. Buchmueller, M. J. Dolan, S. A. Malik, and C. McCabe, Characterising dark matter searches at colliders and direct detection experiments: Vector mediators, J. High Energy Phys. 01 (2015) 037.

[20] Y. A. Golfand and E. P. Likhtman, Extension of the algebra of Poincare group generators and violation of p invariance, JETP Lett. **13**, 323 (1971).

[21] D. V. Volkov and V. P. Akulov, Is the neutrino a Goldstone particle?, Phys. Lett. **46B**, 109 (1973).

[22] J. Wess and B. Zumino, Supergauge transformations in four-dimensions, Nucl. Phys. **B70**, 39 (1974).

[23] J. Wess and B. Zumino, Supergauge invariant extension of quantum electrodynamics, Nucl. Phys. **B78**, 1 (1974).

[24] S. Ferrara and B. Zumino, Supergauge invariant Yang-Mills theories, Nucl. Phys. **B79**, 413 (1974).

[25] A. Salam and J. Strathdee, Super-symmetry and non-Abelian gauges, Phys. Lett. **51B**, 353 (1974).

[26] G. R. Farrar and P. Fayet, Phenomenology of the production, decay, and detection of new hadronic states associated with supersymmetry, Phys. Lett. **76B**, 575 (1978).

[27] H. Goldberg, Constraint on the Photino Mass from Cosmology, Phys. Rev. Lett. **50**, 1419 (1983); , Erratum, Phys. Rev. Lett. **103**, 099905 (2009).

[28] J. Ellis, J. Hagelin, D. V. Nanopoulos, K. A. Olive, and M. Srednicki, Supersymmetric relics from the big bang, Nucl. Phys. **B238**, 453 (1984).

[29] A. G. Riess *et al.*, Observational evidence from supernovae for an accelerating universe and a cosmological constant, Astron. J. **116**, 1009 (1998).

[30] S. Perlmutter *et al.*, Measurements of Ω and Λ from 42 high-redshift supernovae, Astrophys. J. **517**, 565 (1999).

[31] P. Brax, C. Burrage, C. Englert, and M. Spannowsky, LHC signatures of scalar dark energy, Phys. Rev. D **94**, 084054 (2016).

[32] G. W. Horndeski, Second-order scalar-tensor field equations in a four-dimensional space, Int. J. Theor. Phys. **10**, 363 (1974).

[33] H. Georgi, Effective field theory, Annu. Rev. Nucl. Part. Sci. **43**, 209 (1993).

[34] N. Arkani-Hamed, S. Dimopoulos, and G. Dvali, The hierarchy problem and new dimensions at a millimeter, Phys. Lett. B **429**, 263 (1998).

[35] R. D. Peccei and H. R. Quinn, *CP* Conservation in the Presence of Pseudoparticles, Phys. Rev. Lett. **38**, 1440 (1977).

[36] I. Brivio, M. B. Gavela, L. Merlo, K. Mimasu, J. M. No, R. del Rey, and V. Sanz, ALPs effective field theory and collider signatures, Eur. Phys. J. C **77**, 572 (2017).

[37] ATLAS Collaboration, Combination of Searches for Invisible Higgs Boson Decays with the ATLAS Experiment, Phys. Rev. Lett. **122**, 231801 (2019).

[38] CMS Collaboration, Search for invisible decays of a Higgs boson produced through vector boson fusion in proton-proton collisions at $\sqrt{s} = 13$ TeV, Phys. Lett. B **793**, 520 (2019).

[39] ATLAS Collaboration, The ATLAS experiment at the CERN large hadron collider, J. Instrum. **3**, S08003 (2008).

[40] ATLAS Collaboration, ATLAS insertable B-Layer technical design report, Reports No. ATLAS-TDR-19, No. CERN-LHCC-2010-013, 2010, https://cds.cern.ch/record/1291633.

[41] ATLAS Collaboration, Production and integration of the ATLAS insertable B-Layer, J. Instrum. **13**, T05008 (2018).

[42] ATLAS Collaboration, Performance of the ATLAS trigger system in 2015, Eur. Phys. J. C **77**, 317 (2017).

[43] ATLAS Collaboration, The ATLAS simulation infrastructure, Eur. Phys. J. C **70**, 823 (2010).

[44] S. Agostinelli *et al.*, GEANT4—a simulation toolkit, Nucl. Instrum. Methods Phys. Res., Sect. A **506**, 250 (2003).

[45] T. Sjöstrand, S. Mrenna, and P. Z. Skands, PYTHIA 6.4 physics and manual, J. High Energy Phys. 05 (2006) 026.

[46] ATLAS Collaboration, The PYTHIA 8 A3 tune description of ATLAS minimum bias and inelastic measurements incorporating the Donnachie–Landshoff diffractive model, Report No. ATL-PHYS-PUB-2016-017, 2016, https://cds.cern.ch/record/2206965.

[47] R. D. Ball *et al.*, Parton distributions for the LHC run II, J. High Energy Phys. 04 (2015) 040.
[48] S. Alioli, P. Nason, C. Oleari, and E. Re, A general framework for implementing NLO calculations in shower Monte Carlo programs: The POWHEG BOX, J. High Energy Phys. 06 (2010) 043.
[49] S. Frixione, P. Nason, and C. Oleari, Matching NLO QCD computations with parton shower simulations: The POWHEG method, J. High Energy Phys. 11 (2007) 070.
[50] P. Nason, A new method for combining NLO QCD with shower Monte Carlo algorithms, J. High Energy Phys. 11 (2004) 040.
[51] U. Haisch, F. Kahlhöfer, and E. Re, QCD effects in mono-jet searches for dark matter, J. High Energy Phys. 12 (2013) 007.
[52] U. Haisch and E. Re, Simplified dark matter top-quark interactions at the LHC, J. High Energy Phys. 06 (2015) 078.
[53] ATLAS Collaboration, ATLAS PYTHIA 8 tunes to 7 TeV data, Report No. ATL-PHYS-PUB-2014-021, 2014, https://cds.cern.ch/record/1966419.
[54] J. Alwall, R. Frederix, S. Frixione, V. Hirschi, F. Maltoni, O. Mattelaer, H.-S. Shao, T. Stelzer, P. Torrielli, and M. Zaro, The automated computation of tree-level and next-to-leading order differential cross sections, and their matching to parton shower simulations, J. High Energy Phys. 07 (2014) 079.
[55] L. Lönnblad and S. Prestel, Matching tree-level matrix elements with interleaved showers, J. High Energy Phys. 03 (2012) 019.
[56] W. Beenakker, M. Kramer, T. Plehn, M. Spira, and P. M. Zerwas, Stop production at hadron colliders, Nucl. Phys. **B515**, 3 (1998).
[57] W. Beenakker, S. Brensing, M. Krämer, A. Kulesza, E. Laenen, and I. Niessen, Supersymmetric top and bottom squark production at hadron colliders, J. High Energy Phys. 08 (2010) 098.
[58] W. Beenakker, C. Borschensky, M. Krämer, A. Kulesza, and E. Laenen, NNLL-fast: Predictions for coloured supersymmetric particle production at the LHC with threshold and Coulomb resummation, J. High Energy Phys. 12 (2016) 133.
[59] W. Beenakker, C. Borschensky, R. Heger, M. Krämer, A. Kulesza, and E. Laenen, NNLL resummation for stop pair-production at the LHC, J. High Energy Phys. 05 (2016) 153.
[60] C. Borschensky, M. Krämer, A. Kulesza, M. Mangano, S. Padhi, T. Plehn, and X. Portell, Squark and gluino production cross sections in pp collisions at $\sqrt{s} = 13$, 14, 33 and 100 TeV, Eur. Phys. J. C **74**, 3174 (2014).
[61] S. Frixione, P. Nason, and G. Ridolfi, A positive-weight next-to-leading-order Monte Carlo for heavy flavour hadroproduction, J. High Energy Phys. 09 (2007) 126.
[62] ATLAS Collaboration, Measurement of the Z/γ^* boson transverse momentum distribution in pp collisions at $\sqrt{s} = 7$ TeV with the ATLAS detector, J. High Energy Phys. 09 (2014) 145.
[63] D. de Florian *et al.* (LHC Higgs Cross Section Working Group), Handbook of LHC Higgs cross sections: 4. Deciphering the nature of the Higgs sector, arXiv:1610.07922.
[64] T. Gleisberg, S. Höche, F. Krauss, M. Schönherr, S. Schumann, F. Siegert, and J. Winter, Event generation with SHERPA 1.1, J. High Energy Phys. 02 (2009) 007.
[65] F. Cascioli, P. Maierhöfer, and S. Pozzorini, Scattering Amplitudes with Open Loops, Phys. Rev. Lett. **108**, 111601 (2012).
[66] T. Gleisberg and S. Höche, Comix, a new matrix element generator, J. High Energy Phys. 12 (2008) 039.
[67] S. Schumann and F. Krauss, A parton shower algorithm based on Catani–Seymour dipole factorisation, J. High Energy Phys. 03 (2008) 038.
[68] S. Höche, F. Krauss, M. Schönherr, and F. Siegert, QCD matrix elements + parton showers. The NLO case, J. High Energy Phys. 04 (2013) 027.
[69] S. Catani, L. Cieri, G. Ferrera, D. de Florian, and M. Grazzini, Vector Boson Production at Hadron Colliders: A Fully Exclusive QCD Calculation at Next-to-Next-to-Leading Order, Phys. Rev. Lett. **103**, 082001 (2009).
[70] S. Catani and M. Grazzini, Next-to-Next-to-Leading-Order Subtraction Formalism in Hadron Collisions and its Application to Higgs-Boson Production at the Large Hadron Collider, Phys. Rev. Lett. **98**, 222002 (2007).
[71] A. D. Martin, W. J. Stirling, R. S. Thorne, and G. Watt, Parton distributions for the LHC, Eur. Phys. J. C **63**, 189 (2009).
[72] J. Lindert *et al.*, Precise predictions for V + jets dark matter backgrounds, Eur. Phys. J. C **77**, 829 (2017).
[73] A. Gehrmann-De Ridder, T. Gehrmann, E. Glover, A. Huss, and T. Morgan, Precise QCD Predictions for the Production of a Z Boson in Association with a Hadronic Jet, Phys. Rev. Lett. **117**, 022001 (2016).
[74] A. Gehrmann-De Ridder, T. Gehrmann, E. Glover, A. Huss, and T. Morgan, The NNLO QCD corrections to Z boson production at large transverse momentum, J. High Energy Phys. 07 (2016) 133.
[75] R. Boughezal, X. Liu, and F. Petriello, Phenomenology of the Z-boson plus jet process at NNLO, Phys. Rev. D **94**, 074015 (2016).
[76] R. Boughezal, X. Liu, and F. Petriello, W-boson plus jet differential distributions at NNLO in QCD, Phys. Rev. D **94**, 113009 (2016).
[77] A. Denner, S. Dittmaier, T. Kasprzik, and A. Muck, Electroweak corrections to dilepton + jet production at hadron colliders, J. High Energy Phys. 06 (2011) 069.
[78] A. Denner, S. Dittmaier, T. Kasprzik, and A. Mück, Electroweak corrections to monojet production at the LHC, Eur. Phys. J. C **73**, 2297 (2013).
[79] S. Kallweit, J. M. Lindert, P. Maierhofer, S. Pozzorini, and M. Schönherr, NLO QCD + EW predictions for V + jets including off-shell vector-boson decays and multijet merging, J. High Energy Phys. 04 (2016) 021.
[80] A. Denner, S. Dittmaier, T. Kasprzik, and A. Muck, Electroweak corrections to W + jet hadroproduction including leptonic W-boson decays, J. High Energy Phys. 08 (2009) 075.
[81] J. H. Kuhn, A. Kulesza, S. Pozzorini, and M. Schulze, Logarithmic electroweak corrections to hadronic $Z + 1$ jet production at large transverse momentum, Phys. Lett. B **609**, 277 (2005).
[82] J. H. Kuhn, A. Kulesza, S. Pozzorini, and M. Schulze, Electroweak corrections to large transverse momentum

production of W bosons at the LHC, Phys. Lett. B **651**, 160 (2007).
[83] J. H. Kuhn, A. Kulesza, S. Pozzorini, and M. Schulze, One-loop weak corrections to hadronic production of Z bosons at large transverse momenta, Nucl. Phys. **B727**, 368 (2005).
[84] J. H. Kuhn, A. Kulesza, S. Pozzorini, and M. Schulze, Electroweak corrections to hadronic production of W bosons at large transverse momenta, Nucl. Phys. **B797**, 27 (2008).
[85] ATLAS Collaboration, Measurements of the production cross section of a Z boson in association with jets in pp collisions at $\sqrt{s} = 13$ TeV with the ATLAS detector, Eur. Phys. J. C **77**, 361 (2017).
[86] M. Bahr *et al.*, Herwig++ physics and manual, Eur. Phys. J. C **58**, 639 (2008).
[87] J. Baglio *et al.*, Release Note—VBFNLO 2.7.0, arXiv:1404.3940.
[88] D. J. Lange, The EvtGen particle decay simulation package, Nucl. Instrum. Methods Phys. Res., Sect. A **462**, 152 (2001).
[89] H.-L. Lai, M. Guzzi, J. Huston, Z. Li, P. M. Nadolsky, J. Pumplin, and C.-P. Yuan, New parton distributions for collider physics, Phys. Rev. D **82**, 074024 (2010).
[90] C. D. White, S. Frixione, E. Laenen, and F. Maltoni, Isolating Wt production at the LHC, J. High Energy Phys. 11 (2009) 074.
[91] J. M. Campbell, R. K. Ellis, and C. Williams, Vector boson pair production at the LHC, J. High Energy Phys. 07 (2011) 018.
[92] ATLAS Collaboration, Topological cell clustering in the ATLAS calorimeters and its performance in LHC Run 1, Eur. Phys. J. C **77**, 490 (2017).
[93] M. Cacciari, G. P. Salam, and G. Soyez, The anti-k_t jet clustering algorithm, J. High Energy Phys. 04 (2008) 063.
[94] M. Cacciari, G. P. Salam, and G. Soyez, FastJet user manual, Eur. Phys. J. C **72**, 1896 (2012).
[95] ATLAS Collaboration, Jet energy scale and resolution measured in proton-proton collisions at $\sqrt{s} = 13$ TeV with the ATLAS detector, arXiv:2007.02645.
[96] ATLAS Collaboration, Tagging and suppression of pileup jets with the ATLAS detector, Report No. ATLAS-CONF-2014-018, 2014, https://cds.cern.ch/record/1700870.
[97] ATLAS Collaboration, Performance of b-jet identification in the ATLAS experiment, J. Instrum. **11**, P04008 (2016).
[98] ATLAS Collaboration, Optimisation of the ATLAS b-tagging performance for the 2016 LHC Run, Report No. ATL-PHYS-PUB-2016-012, 2016, https://cds.cern.ch/record/2160731.
[99] ATLAS Collaboration, Electron and photon performance measurements with the ATLAS detector using the 2015–2017 LHC proton-proton collision data, J. Instrum. **14**, P12006 (2019).
[100] ATLAS Collaboration, Muon reconstruction performance of the ATLAS detector in proton-proton collision data at $\sqrt{s} = 13$ TeV, Eur. Phys. J. C **76**, 292 (2016).
[101] ATLAS Collaboration, Identification and energy calibration of hadronically decaying tau leptons with the ATLAS experiment in pp collisions at $\sqrt{s} = 8$ TeV, Eur. Phys. J. C **75**, 303 (2015).
[102] ATLAS Collaboration, Measurement of the tau lepton reconstruction and identification performance in the ATLAS experiment using pp collisions at $\sqrt{s} = 13$ TeV, Report No. ATLAS-CONF-2017-029, 2017, https://cds.cern.ch/record/2261772.
[103] ATLAS Collaboration, Reconstruction, energy calibration, and identification of hadronically decaying tau leptons in the ATLAS experiment for Run-2 of the LHC, Report No. ATL-PHYS-PUB-2015-045, 2015, https://cds.cern.ch/record/2064383.
[104] ATLAS Collaboration, Performance of missing transverse momentum reconstruction with the ATLAS detector using proton-proton collisions at $\sqrt{s} = 13$ TeV, Eur. Phys. J. C **78**, 903 (2018).
[105] ATLAS Collaboration, Performance of the missing transverse momentum triggers for the ATLAS detector during Run-2 data taking, J. High Energy Phys. 08 (2020) 080.
[106] ATLAS Collaboration, Selection of jets produced in 13 TeV proton-proton collisions with the ATLAS detector, Report No. ATLAS-CONF-2015-029, 2015, https://cds.cern.ch/record/2037702.
[107] ATLAS Collaboration, Characterisation and mitigation of beam-induced backgrounds observed in the ATLAS detector during the 2011 proton-proton run, J. Instrum. **8**, P07004 (2013).
[108] ATLAS Collaboration, Search for squarks and gluinos with the ATLAS detector in final states with jets and missing transverse momentum using 4.7 fb^{-1} of $\sqrt{s} = 7$ TeV proton-proton collision data, Phys. Rev. D **87**, 012008 (2013).
[109] G. Cowan, K. Cranmer, E. Gross, and O. Vitells, Asymptotic formulae for likelihood-based tests of new physics, Eur. Phys. J. C **71**, 1554 (2011).
[110] ATLAS Collaboration, Luminosity determination in pp collisions at $\sqrt{s} = 8$ TeV using the ATLAS detector at the LHC, Eur. Phys. J. C **76**, 653 (2016).
[111] ATLAS Collaboration, The new LUCID-2 detector for luminosity measurement and monitoring in ATLAS, J. Instrum. **13**, P07017 (2018).
[112] ATLAS Collaboration, Performance of pile-up mitigation techniques for jets in pp collisions at $\sqrt{s} = 8$ TeV using the ATLAS detector, Eur. Phys. J. C **76**, 581 (2016).
[113] ATLAS Collaboration, Measurements of b-jet tagging efficiency with the ATLAS detector using $t\bar{t}$ events at $\sqrt{s} = 13$ TeV, J. High Energy Phys. 08 (2018) 089.
[114] ATLAS Collaboration, Electron and photon energy calibration with the ATLAS detector using 2015–2016 LHC proton-proton collision data, J. Instrum. **14**, P03017 (2019).
[115] J. Butterworth *et al.*, PDF4LHC recommendations for LHC Run II, J. Phys. G **43**, 023001 (2016).
[116] ATLAS Collaboration, Studies on top-quark Monte Carlo modelling with Sherpa and MG5_aMC@NLO, Report No. ATL-PHYS-PUB-2017-007, 2017, https://cds.cern.ch/record/2261938.
[117] ATLAS Collaboration, Studies on top-quark Monte Carlo modelling for Top2016, Report No. ATL-PHYS-PUB-2016-020, 2016, https://cds.cern.ch/record/2216168.

[118] L. Harland-Lang, A. Martin, P. Motylinski, and R. Thorne, Parton distributions in the LHC era: MMHT 2014 PDFs, Eur. Phys. J. C **75**, 204 (2015).
[119] A. L. Read, Presentation of search results: the CLS technique, J. Phys. G **28**, 2693 (2002).
[120] G. Busoni *et al.*, Recommendations on presenting LHC searches for missing transverse energy signals using simplified *s*-channel models of dark matter, Phys. Dark Universe **27**, 100365 (2020).
[121] M. Backovic, A. Martini, O. Mattelaer, K. Kong, and G. Mohlabeng, Direct detection of dark matter with MadDM v.2.0, Phys. Dark Universe **9–10**, 37 (2015).
[122] C. Amole *et al.*, Dark matter search results from the complete exposure of the PICO-60 C3F8 bubble chamber, Phys. Rev. D **100**, 022001 (2019).
[123] D. Akerib *et al.*, Limits on Spin-Dependent WIMP-Nucleon Cross Section Obtained from the Complete LUX Exposure, Phys. Rev. Lett. **118**, 251302 (2017).
[124] E. Aprile *et al.*, Constraining the Spin-Dependent WIMP-Nucleon Cross Sections with XENON1T, Phys. Rev. Lett. **122**, 141301 (2019).
[125] ATLAS Collaboration, ATLAS Computing Acknowledgements, Technical Report No. ATL-SOFT-PUB-2020-001, CERN, 2020, http://cds.cern.ch/record/2717821.

G. Aad,[102] B. Abbott,[128] D. C. Abbott,[103] A. Abed Abud,[36] K. Abeling,[53] D. K. Abhayasinghe,[94] S. H. Abidi,[167] O. S. AbouZeid,[40] N. L. Abraham,[156] H. Abramowicz,[161] H. Abreu,[160] Y. Abulaiti,[6] B. S. Acharya,[67a,67b,b] B. Achkar,[53] L. Adam,[100] C. Adam Bourdarios,[5] L. Adamczyk,[84a] L. Adamek,[167] J. Adelman,[121] A. Adiguzel,[12c,c] S. Adorni,[54] T. Adye,[143] A. A. Affolder,[145] Y. Afik,[160] C. Agapopoulou,[65] M. N. Agaras,[38] A. Aggarwal,[119] C. Agheorghiesei,[27c] J. A. Aguilar-Saavedra,[139f,139a,d] A. Ahmad,[36] F. Ahmadov,[80] W. S. Ahmed,[104] X. Ai,[18] G. Aielli,[74a,74b] S. Akatsuka,[86] M. Akbiyik,[100] T. P. A. Åkesson,[97] E. Akilli,[54] A. V. Akimov,[111] K. Al Khoury,[65] G. L. Alberghi,[23b,23a] J. Albert,[176] M. J. Alconada Verzini,[161] S. Alderweireldt,[36] M. Aleksa,[36] I. N. Aleksandrov,[80] C. Alexa,[27b] T. Alexopoulos,[10] A. Alfonsi,[120] F. Alfonsi,[23b,23a] M. Alhroob,[128] B. Ali,[141] S. Ali,[158] M. Aliev,[166] G. Alimonti,[69a] C. Allaire,[36] B. M. M. Allbrooke,[156] B. W. Allen,[131] P. P. Allport,[21] A. Aloisio,[70a,70b] F. Alonso,[89] C. Alpigiani,[148] E. Alunno Camelia,[74a,74b] M. Alvarez Estevez,[99] M. G. Alviggi,[70a,70b] Y. Amaral Coutinho,[81b] A. Ambler,[104] L. Ambroz,[134] C. Amelung,[36] D. Amidei,[106] S. P. Amor Dos Santos,[139a] S. Amoroso,[46] C. S. Amrouche,[54] F. An,[79] C. Anastopoulos,[149] N. Andari,[144] T. Andeen,[11] J. K. Anders,[20] S. Y. Andrean,[45a,45b] A. Andreazza,[69a,69b] V. Andrei,[61a] C. R. Anelli,[176] S. Angelidakis,[9] A. Angerami,[39] A. V. Anisenkov,[122b,122a] A. Annovi,[72a] C. Antel,[54] M. T. Anthony,[149] E. Antipov,[129] M. Antonelli,[51] D. J. A. Antrim,[18] F. Anulli,[73a] M. Aoki,[82] J. A. Aparisi Pozo,[174] M. A. Aparo,[156] L. Aperio Bella,[46] N. Aranzabal,[36] V. Araujo Ferraz,[81a] R. Araujo Pereira,[81b] C. Arcangeletti,[51] A. T. H. Arce,[49] J-F. Arguin,[110] S. Argyropoulos,[52] J.-H. Arling,[46] A. J. Armbruster,[36] O. Arnaez,[167] H. Arnold,[120] Z. P. Arrubarrena Tame,[114] G. Artoni,[134] H. Asada,[117] K. Asai,[126] S. Asai,[163] T. Asawatavonvanich,[165] N. A. Asbah,[59] E. M. Asimakopoulou,[172] L. Asquith,[156] J. Assahsah,[35e] K. Assamagan,[29] R. Astalos,[28a] R. J. Atkin,[33a] M. Atkinson,[173] N. B. Atlay,[19] H. Atmani,[65] P. A. Atmasiddha,[106] K. Augsten,[141] V. A. Austrup,[182] G. Avolio,[36] M. K. Ayoub,[15a] G. Azuelos,[110,e] D. Babal,[28a] H. Bachacou,[144] K. Bachas,[162] F. Backman,[45a,45b] P. Bagnaia,[73a,73b] H. Bahrasemani,[152] A. J. Bailey,[174] V. R. Bailey,[173] J. T. Baines,[143] C. Bakalis,[10] O. K. Baker,[183] P. J. Bakker,[120] E. Bakos,[16] D. Bakshi Gupta,[8] S. Balaji,[157] R. Balasubramanian,[120] E. M. Baldin,[122b,122a] P. Balek,[180] F. Balli,[144] W. K. Balunas,[134] J. Balz,[100] E. Banas,[85] M. Bandieramonte,[138] A. Bandyopadhyay,[19] Sw. Banerjee,[181,f] L. Barak,[161] W. M. Barbe,[38] E. L. Barberio,[105] D. Barberis,[55b,55a] M. Barbero,[102] G. Barbour,[95] T. Barillari,[115] M-S. Barisits,[36] J. Barkeloo,[131] T. Barklow,[153] R. Barnea,[160] B. M. Barnett,[143] R. M. Barnett,[18] Z. Barnovska-Blenessy,[60a] A. Baroncelli,[60a] G. Barone,[29] A. J. Barr,[134] L. Barranco Navarro,[45a,45b] F. Barreiro,[99] J. Barreiro Guimarães da Costa,[15a] U. Barron,[161] S. Barsov,[137] F. Bartels,[61a] R. Bartoldus,[153] G. Bartolini,[102] A. E. Barton,[90] P. Bartos,[28a] A. Basalaev,[46] A. Basan,[100] A. Bassalat,[65,g] M. J. Basso,[167] R. L. Bates,[57] S. Batlamous,[35f] J. R. Batley,[32] B. Batool,[151] M. Battaglia,[145] M. Bauce,[73a,73b] F. Bauer,[144,a] P. Bauer,[24] H. S. Bawa,[31] A. Bayirli,[12c] J. B. Beacham,[49] T. Beau,[135] P. H. Beauchemin,[170] F. Becherer,[52] P. Bechtle,[24] H. C. Beck,[53] H. P. Beck,[20,h] K. Becker,[178] C. Becot,[46] A. Beddall,[12d] A. J. Beddall,[12a] V. A. Bednyakov,[80] M. Bedognetti,[120] C. P. Bee,[155] T. A. Beermann,[182] M. Begalli,[81b] M. Begel,[29] A. Behera,[155] J. K. Behr,[46] F. Beisiegel,[24] M. Belfkir,[5] A. S. Bell,[95] G. Bella,[161] L. Bellagamba,[23b] A. Bellerive,[34] P. Bellos,[9] K. Beloborodov,[122b,122a] K. Belotskiy,[112] N. L. Belyaev,[112] D. Benchekroun,[35a] N. Benekos,[10] Y. Benhammou,[161] D. P. Benjamin,[6] M. Benoit,[29] J. R. Bensinger,[26] S. Bentvelsen,[120] L. Beresford,[134] M. Beretta,[51] D. Berge,[19] E. Bergeaas Kuutmann,[172] N. Berger,[5] B. Bergmann,[141] L. J. Bergsten,[26] J. Beringer,[18] S. Berlendis,[7] G. Bernardi,[135] C. Bernius,[153] F. U. Bernlochner,[24] T. Berry,[94] P. Berta,[100] A. Berthold,[48] I. A. Bertram,[90] N. Besson,[144] S. Bethke,[115] A. Betti,[42] A. J. Bevan,[93] J. Beyer,[115] S. Bhatta,[155] D. S. Bhattacharya,[177]

P. Bhattarai,[26] V. S. Bhopatkar,[6] R. Bi,[138] R. M. Bianchi,[138] O. Biebel,[114] D. Biedermann,[19] R. Bielski,[36] K. Bierwagen,[100] M. Biglietti,[75a] T. R. V. Billoud,[141] M. Bindi,[53] A. Bingul,[12d] C. Bini,[73a,73b] S. Biondi,[23b,23a] C. J. Birch-sykes,[101] M. Birman,[180] T. Bisanz,[36] J. P. Biswal,[3] D. Biswas,[181,f] A. Bitadze,[101] C. Bittrich,[48] K. Bjørke,[133] T. Blazek,[28a] I. Bloch,[46] C. Blocker,[26] A. Blue,[57] U. Blumenschein,[93] G. J. Bobbink,[120] V. S. Bobrovnikov,[122b,122a] S. S. Bocchetta,[97] D. Bogavac,[14] A. G. Bogdanchikov,[122b,122a] C. Bohm,[45a] V. Boisvert,[94] P. Bokan,[172,53] T. Bold,[84a] A. E. Bolz,[61b] M. Bomben,[135] M. Bona,[93] J. S. Bonilla,[131] M. Boonekamp,[144] C. D. Booth,[94] A. G. Borbély,[57] H. M. Borecka-Bielska,[91] L. S. Borgna,[95] A. Borisov,[123] G. Borissov,[90] D. Bortoletto,[134] D. Boscherini,[23b] M. Bosman,[14] J. D. Bossio Sola,[104] K. Bouaouda,[35a] J. Boudreau,[138] E. V. Bouhova-Thacker,[90] D. Boumediene,[38] A. Boveia,[127] J. Boyd,[36] D. Boye,[33c] I. R. Boyko,[80] A. J. Bozson,[94] J. Bracinik,[21] N. Brahimi,[60d,60c] G. Brandt,[182] O. Brandt,[32] F. Braren,[46] B. Brau,[103] J. E. Brau,[131] W. D. Breaden Madden,[57] K. Brendlinger,[46] R. Brener,[160] L. Brenner,[36] R. Brenner,[172] S. Bressler,[180] B. Brickwedde,[100] D. L. Briglin,[21] D. Britton,[57] D. Britzger,[115] I. Brock,[24] R. Brock,[107] G. Brooijmans,[39] W. K. Brooks,[146d] E. Brost,[29] P. A. Bruckman de Renstrom,[85] B. Brüers,[46] D. Bruncko,[28b] A. Bruni,[23b] G. Bruni,[23b] M. Bruschi,[23b] N. Bruscino,[73a,73b] L. Bryngemark,[153] T. Buanes,[17] Q. Buat,[155] P. Buchholz,[151] A. G. Buckley,[57] I. A. Budagov,[80] M. K. Bugge,[133] O. Bulekov,[112] B. A. Bullard,[59] T. J. Burch,[121] S. Burdin,[91] C. D. Burgard,[120] A. M. Burger,[129] B. Burghgrave,[8] J. T. P. Burr,[46] C. D. Burton,[11] J. C. Burzynski,[103] V. Büscher,[100] E. Buschmann,[53] P. J. Bussey,[57] J. M. Butler,[25] C. M. Buttar,[57] J. M. Butterworth,[95] P. Butti,[36] W. Buttinger,[143] C. J. Buxo Vazquez,[107] A. Buzatu,[158] A. R. Buzykaev,[122b,122a] G. Cabras,[23b,23a] S. Cabrera Urbán,[174] D. Caforio,[56] H. Cai,[138] V. M. M. Cairo,[153] O. Cakir,[4a] N. Calace,[36] P. Calafiura,[18] G. Calderini,[135] P. Calfayan,[66] G. Callea,[57] L. P. Caloba,[81b] A. Caltabiano,[74a,74b] S. Calvente Lopez,[99] D. Calvet,[38] S. Calvet,[38] T. P. Calvet,[102] M. Calvetti,[72a,72b] R. Camacho Toro,[135] S. Camarda,[36] D. Camarero Munoz,[99] P. Camarri,[74a,74b] M. T. Camerlingo,[75a,75b] D. Cameron,[133] C. Camincher,[36] S. Campana,[36] M. Campanelli,[95] A. Camplani,[40] V. Canale,[70a,70b] A. Canesse,[104] M. Cano Bret,[78] J. Cantero,[129] T. Cao,[161] Y. Cao,[173] M. Capua,[41b,41a] R. Cardarelli,[74a] F. Cardillo,[174] G. Carducci,[41b,41a] I. Carli,[142] T. Carli,[36] G. Carlino,[70a] B. T. Carlson,[138] E. M. Carlson,[176,168a] L. Carminati,[69a,69b] R. M. D. Carney,[153] S. Caron,[119] E. Carquin,[146d] S. Carrá,[46] G. Carratta,[23b,23a] J. W. S. Carter,[167] T. M. Carter,[50] M. P. Casado,[14,i] A. F. Casha,[167] E. G. Castiglia,[183] F. L. Castillo,[174] L. Castillo Garcia,[14] V. Castillo Gimenez,[174] N. F. Castro,[139a,139e] A. Catinaccio,[36] J. R. Catmore,[133] A. Cattai,[36] V. Cavaliere,[29] V. Cavasinni,[72a,72b] E. Celebi,[12b] F. Celli,[134] K. Cerny,[130] A. S. Cerqueira,[81a] A. Cerri,[156] L. Cerrito,[74a,74b] F. Cerutti,[18] A. Cervelli,[23b,23a] S. A. Cetin,[12b] Z. Chadi,[35a] D. Chakraborty,[121] J. Chan,[181] W. S. Chan,[120] W. Y. Chan,[91] J. D. Chapman,[32] B. Chargeishvili,[159b] D. G. Charlton,[21] T. P. Charman,[93] M. Chatterjee,[20] C. C. Chau,[34] S. Che,[127] S. Chekanov,[6] S. V. Chekulaev,[168a] G. A. Chelkov,[80,j] B. Chen,[79] C. Chen,[60a] C. H. Chen,[79] H. Chen,[15c] H. Chen,[29] J. Chen,[60a] J. Chen,[39] J. Chen,[26] S. Chen,[136] S. J. Chen,[15c] X. Chen,[15b] Y. Chen,[60a] Y-H. Chen,[46] H. C. Cheng,[63a] H. J. Cheng,[15a] A. Cheplakov,[80] E. Cheremushkina,[123] R. Cherkaoui El Moursli,[35f] E. Cheu,[7] K. Cheung,[64] T. J. A. Chevalérias,[144] L. Chevalier,[144] V. Chiarella,[51] G. Chiarelli,[72a] G. Chiodini,[68a] A. S. Chisholm,[21] A. Chitan,[27b] I. Chiu,[163] Y. H. Chiu,[176] M. V. Chizhov,[80] K. Choi,[11] A. R. Chomont,[73a,73b] Y. Chou,[103] Y. S. Chow,[120] L. D. Christopher,[33f] M. C. Chu,[63a] X. Chu,[15a,15d] J. Chudoba,[140] J. J. Chwastowski,[85] L. Chytka,[130] D. Cieri,[115] K. M. Ciesla,[85] V. Cindro,[92] I. A. Cioară,[27b] A. Ciocio,[18] F. Cirotto,[70a,70b] Z. H. Citron,[180,k] M. Citterio,[69a] D. A. Ciubotaru,[27b] B. M. Ciungu,[167] A. Clark,[54] P. J. Clark,[50] S. E. Clawson,[101] C. Clement,[45a,45b] L. Clissa,[23b,23a] Y. Coadou,[102] M. Cobal,[67a,67c] A. Coccaro,[55b] J. Cochran,[79] R. Coelho Lopes De Sa,[103] H. Cohen,[161] A. E. C. Coimbra,[36] B. Cole,[39] A. P. Colijn,[120] J. Collot,[58] P. Conde Muiño,[139a,139h] S. H. Connell,[33c] I. A. Connelly,[57] S. Constantinescu,[27b] F. Conventi,[70a,l] A. M. Cooper-Sarkar,[134] F. Cormier,[175] K. J. R. Cormier,[167] L. D. Corpe,[95] M. Corradi,[73a,73b] E. E. Corrigan,[97] F. Corriveau,[104,m] M. J. Costa,[174] F. Costanza,[5] D. Costanzo,[149] G. Cowan,[94] J. W. Cowley,[32] J. Crane,[101] K. Cranmer,[125] R. A. Creager,[136] S. Crépé-Renaudin,[58] F. Crescioli,[135] M. Cristinziani,[24] V. Croft,[170] G. Crosetti,[41b,41a] A. Cueto,[5] T. Cuhadar Donszelmann,[171] H. Cui,[15a,15d] A. R. Cukierman,[153] W. R. Cunningham,[57] S. Czekierda,[85] P. Czodrowski,[36] M. M. Czurylo,[61b] M. J. Da Cunha Sargedas De Sousa,[60b] J. V. Da Fonseca Pinto,[81b] C. Da Via,[101] W. Dabrowski,[84a] F. Dachs,[36] T. Dado,[47] S. Dahbi,[33f] T. Dai,[106] C. Dallapiccola,[103] M. Dam,[40] G. D'amen,[29] V. D'Amico,[75a,75b] J. Damp,[100] J. R. Dandoy,[136] M. F. Daneri,[30] M. Danninger,[152] V. Dao,[36] G. Darbo,[55b] O. Dartsi,[5] A. Dattagupta,[131] T. Daubney,[46] S. D'Auria,[69a,69b] C. David,[168b] T. Davidek,[142] D. R. Davis,[49] I. Dawson,[149] K. De,[8] R. De Asmundis,[70a] M. De Beurs,[120] S. De Castro,[23b,23a] N. De Groot,[119] P. de Jong,[120] H. De la Torre,[107] A. De Maria,[15c] D. De Pedis,[73a] A. De Salvo,[73a] U. De Sanctis,[74a,74b] A. De Santo,[156] J. B. De Vivie De Regie,[65] D. V. Dedovich,[80] A. M. Deiana,[42] J. Del Peso,[99] Y. Delabat Diaz,[46] D. Delgove,[65] F. Deliot,[144] C. M. Delitzsch,[7] M. Della Pietra,[70a,70b] D. Della Volpe,[54] A. Dell'Acqua,[36] L. Dell'Asta,[74a,74b] M. Delmastro,[5] C. Delporte,[65] P. A. Delsart,[58] S. Demers,[183] M. Demichev,[80] G. Demontigny,[110]

S. P. Denisov,[123] L. D'Eramo,[121] D. Derendarz,[85] J. E. Derkaoui,[35e] F. Derue,[135] P. Dervan,[91] K. Desch,[24] K. Dette,[167] C. Deutsch,[24] M. R. Devesa,[30] P. O. Deviveiros,[36] F. A. Di Bello,[73a,73b] A. Di Ciaccio,[74a,74b] L. Di Ciaccio,[5] C. Di Donato,[70a,70b] A. Di Girolamo,[36] G. Di Gregorio,[72a,72b] A. Di Luca,[76a,76b] B. Di Micco,[75a,75b] R. Di Nardo,[75a,75b] K. F. Di Petrillo,[59] R. Di Sipio,[167] C. Diaconu,[102] F. A. Dias,[120] T. Dias Do Vale,[139a] M. A. Diaz,[146a] F. G. Diaz Capriles,[24] J. Dickinson,[18] M. Didenko,[166] E. B. Diehl,[106] J. Dietrich,[19] S. Díez Cornell,[46] C. Diez Pardos,[151] A. Dimitrievska,[18] W. Ding,[15b] J. Dingfelder,[24] S. J. Dittmeier,[61b] F. Dittus,[36] F. Djama,[102] T. Djobava,[159b] J. I. Djuvsland,[17] M. A. B. Do Vale,[147] M. Dobre,[27b] D. Dodsworth,[26] C. Doglioni,[97] J. Dolejsi,[142] Z. Dolezal,[142] M. Donadelli,[81c] B. Dong,[60c] J. Donini,[38] A. D'onofrio,[15c] M. D'Onofrio,[91] J. Dopke,[143] A. Doria,[70a] M. T. Dova,[89] A. T. Doyle,[57] E. Drechsler,[152] E. Dreyer,[152] T. Dreyer,[53] A. S. Drobac,[170] D. Du,[60b] T. A. du Pree,[120] Y. Duan,[60d] F. Dubinin,[111] M. Dubovsky,[28a] A. Dubreuil,[54] E. Duchovni,[180] G. Duckeck,[114] O. A. Ducu,[36,27b] D. Duda,[115] A. Dudarev,[36] A. C. Dudder,[100] E. M. Duffield,[18] M. D'uffizi,[101] L. Duflot,[65] M. Dührssen,[36] C. Dülsen,[182] M. Dumancic,[180] A. E. Dumitriu,[27b] M. Dunford,[61a] S. Dungs,[47] A. Duperrin,[102] H. Duran Yildiz,[4a] M. Düren,[56] A. Durglishvili,[159b] D. Duschinger,[48] B. Dutta,[46] D. Duvnjak,[1] G. I. Dyckes,[136] M. Dyndal,[36] S. Dysch,[101] B. S. Dziedzic,[85] M. G. Eggleston,[49] T. Eifert,[8] G. Eigen,[17] K. Einsweiler,[18] T. Ekelof,[172] H. El Jarrari,[35f] V. Ellajosyula,[172] M. Ellert,[172] F. Ellinghaus,[182] A. A. Elliot,[93] N. Ellis,[36] J. Elmsheuser,[29] M. Elsing,[36] D. Emeliyanov,[143] A. Emerman,[39] Y. Enari,[163] M. B. Epland,[49] J. Erdmann,[47] A. Ereditato,[20] P. A. Erland,[85] M. Errenst,[182] M. Escalier,[65] C. Escobar,[174] O. Estrada Pastor,[174] E. Etzion,[161] G. Evans,[139a] H. Evans,[66] M. O. Evans,[156] A. Ezhilov,[137] F. Fabbri,[57] L. Fabbri,[23b,23a] V. Fabiani,[119] G. Facini,[178] R. M. Fakhrutdinov,[123] S. Falciano,[73a] P. J. Falke,[24] S. Falke,[36] J. Faltova,[142] Y. Fang,[15a] Y. Fang,[15a] G. Fanourakis,[44] M. Fanti,[69a,69b] M. Faraj,[67a,67c] A. Farbin,[8] A. Farilla,[75a] E. M. Farina,[71a,71b] T. Farooque,[107] S. M. Farrington,[50] P. Farthouat,[36] F. Fassi,[35f] P. Fassnacht,[36] D. Fassouliotis,[9] M. Faucci Giannelli,[50] W. J. Fawcett,[32] L. Fayard,[65] O. L. Fedin,[137,n] W. Fedorko,[175] A. Fehr,[20] M. Feickert,[173] L. Feligioni,[102] A. Fell,[149] C. Feng,[60b] M. Feng,[49] M. J. Fenton,[171] A. B. Fenyuk,[123] S. W. Ferguson,[43] J. Ferrando,[46] A. Ferrari,[172] P. Ferrari,[120] R. Ferrari,[71a] D. E. Ferreira de Lima,[61b] A. Ferrer,[174] D. Ferrere,[54] C. Ferretti,[106] F. Fiedler,[100] A. Filipčič,[92] F. Filthaut,[119] K. D. Finelli,[25] M. C. N. Fiolhais,[139a,139c,o] L. Fiorini,[174] F. Fischer,[114] J. Fischer,[100] W. C. Fisher,[107] T. Fitschen,[21] I. Fleck,[151] P. Fleischmann,[106] T. Flick,[182] B. M. Flierl,[114] L. Flores,[136] L. R. Flores Castillo,[63a] F. M. Follega,[76a,76b] N. Fomin,[17] J. H. Foo,[167] G. T. Forcolin,[76a,76b] B. C. Forland,[66] A. Formica,[144] F. A. Förster,[14] A. C. Forti,[101] E. Fortin,[102] M. G. Foti,[134] D. Fournier,[65] H. Fox,[90] P. Francavilla,[72a,72b] S. Francescato,[73a,73b] M. Franchini,[23b,23a] S. Franchino,[61a] D. Francis,[36] L. Franco,[5] L. Franconi,[20] M. Franklin,[59] G. Frattari,[73a,73b] A. N. Fray,[93] P. M. Freeman,[21] B. Freund,[110] W. S. Freund,[81b] E. M. Freundlich,[47] D. C. Frizzell,[128] D. Froidevaux,[36] J. A. Frost,[134] M. Fujimoto,[126] C. Fukunaga,[164] E. Fullana Torregrosa,[174] T. Fusayasu,[116] J. Fuster,[174] A. Gabrielli,[23b,23a] A. Gabrielli,[36] S. Gadatsch,[54] P. Gadow,[115] G. Gagliardi,[55b,55a] L. G. Gagnon,[110] G. E. Gallardo,[134] E. J. Gallas,[134] B. J. Gallop,[143] R. Gamboa Goni,[93] K. K. Gan,[127] S. Ganguly,[180] J. Gao,[60a] Y. Gao,[50] Y. S. Gao,[31,p] F. M. Garay Walls,[146a] C. García,[174] J. E. García Navarro,[174] J. A. García Pascual,[15a] C. Garcia-Argos,[52] M. Garcia-Sciveres,[18] R. W. Gardner,[37] N. Garelli,[153] S. Gargiulo,[52] C. A. Garner,[167] V. Garonne,[133] S. J. Gasiorowski,[148] P. Gaspar,[81b] A. Gaudiello,[55b,55a] G. Gaudio,[71a] P. Gauzzi,[73a,73b] I. L. Gavrilenko,[111] A. Gavrilyuk,[124] C. Gay,[175] G. Gaycken,[46] E. N. Gazis,[10] A. A. Geanta,[27b] C. M. Gee,[145] C. N. P. Gee,[143] J. Geisen,[97] M. Geisen,[100] C. Gemme,[55b] M. H. Genest,[58] C. Geng,[106] S. Gentile,[73a,73b] S. George,[94] T. Geralis,[44] L. O. Gerlach,[53] P. Gessinger-Befurt,[100] G. Gessner,[47] M. Ghasemi Bostanabad,[176] M. Ghneimat,[151] A. Ghosh,[65] A. Ghosh,[78] B. Giacobbe,[23b] S. Giagu,[73a,73b] N. Giangiacomi,[167] P. Giannetti,[72a] A. Giannini,[70a,70b] G. Giannini,[14] S. M. Gibson,[94] M. Gignac,[145] D. T. Gil,[84b] B. J. Gilbert,[39] D. Gillberg,[34] G. Gilles,[182] N. E. K. Gillwald,[46] D. M. Gingrich,[3,e] M. P. Giordani,[67a,67c] P. F. Giraud,[144] G. Giugliarelli,[67a,67c] D. Giugni,[69a] F. Giuli,[74a,74b] S. Gkaitatzis,[162] I. Gkialas,[9,q] E. L. Gkougkousis,[14] P. Gkountoumis,[10] L. K. Gladilin,[113] C. Glasman,[99] J. Glatzer,[14] P. C. F. Glaysher,[46] A. Glazov,[46] G. R. Gledhill,[131] I. Gnesi,[41b,r] M. Goblirsch-Kolb,[26] D. Godin,[110] S. Goldfarb,[105] T. Golling,[54] D. Golubkov,[123] A. Gomes,[139a,139b] R. Goncalves Gama,[53] R. Gonçalo,[139a,139c] G. Gonella,[131] L. Gonella,[21] A. Gongadze,[80] F. Gonnella,[21] J. L. Gonski,[39] S. González de la Hoz,[174] S. Gonzalez Fernandez,[14] R. Gonzalez Lopez,[91] C. Gonzalez Renteria,[18] R. Gonzalez Suarez,[172] S. Gonzalez-Sevilla,[54] G. R. Gonzalvo Rodriguez,[174] L. Goossens,[36] N. A. Gorasia,[21] P. A. Gorbounov,[124] H. A. Gordon,[29] B. Gorini,[36] E. Gorini,[68a,68b] A. Gorišek,[92] A. T. Goshaw,[49] M. I. Gostkin,[80] C. A. Gottardo,[119] M. Gouighri,[35b] A. G. Goussiou,[148] N. Govender,[33c] C. Goy,[5] I. Grabowska-Bold,[84a] E. C. Graham,[91] J. Gramling,[171] E. Gramstad,[133] S. Grancagnolo,[19] M. Grandi,[156] V. Gratchev,[137] P. M. Gravila,[27f] F. G. Gravili,[68a,68b] C. Gray,[57] H. M. Gray,[18] C. Grefe,[24] K. Gregersen,[97] I. M. Gregor,[46] P. Grenier,[153] K. Grevtsov,[46] C. Grieco,[14] N. A. Grieser,[128] A. A. Grillo,[145] K. Grimm,[31,s] S. Grinstein,[14,t] J.-F. Grivaz,[65] S. Groh,[100] E. Gross,[180] J. Grosse-Knetter,[53]

Z. J. Grout,[95] C. Grud,[106] A. Grummer,[118] J. C. Grundy,[134] L. Guan,[106] W. Guan,[181] C. Gubbels,[175] J. Guenther,[77] A. Guerguichon,[65] J. G. R. Guerrero Rojas,[174] F. Guescini,[115] D. Guest,[77] R. Gugel,[100] A. Guida,[46] T. Guillemin,[5] S. Guindon,[36] J. Guo,[60c] W. Guo,[106] Y. Guo,[60a] Z. Guo,[102] R. Gupta,[46] S. Gurbuz,[12c] G. Gustavino,[128] M. Guth,[52] P. Gutierrez,[128] C. Gutschow,[95] C. Guyot,[144] C. Gwenlan,[134] C. B. Gwilliam,[91] E. S. Haaland,[133] A. Haas,[125] C. Haber,[18] H. K. Hadavand,[8] A. Hadef,[100] M. Haleem,[177] J. Haley,[129] J. J. Hall,[149] G. Halladjian,[107] G. D. Hallewell,[102] K. Hamano,[176] H. Hamdaoui,[35f] M. Hamer,[24] G. N. Hamity,[50] K. Han,[60a] L. Han,[15c] L. Han,[60a] S. Han,[18] Y. F. Han,[167] K. Hanagaki,[82,u] M. Hance,[145] D. M. Handl,[114] M. D. Hank,[37] R. Hankache,[135] E. Hansen,[97] J. B. Hansen,[40] J. D. Hansen,[40] M. C. Hansen,[24] P. H. Hansen,[40] E. C. Hanson,[101] K. Hara,[169] T. Harenberg,[182] S. Harkusha,[108] P. F. Harrison,[178] N. M. Hartman,[153] N. M. Hartmann,[114] Y. Hasegawa,[150] A. Hasib,[50] S. Hassani,[144] S. Haug,[20] R. Hauser,[107] M. Havranek,[141] C. M. Hawkes,[21] R. J. Hawkings,[36] S. Hayashida,[117] D. Hayden,[107] C. Hayes,[106] R. L. Hayes,[175] C. P. Hays,[134] J. M. Hays,[93] H. S. Hayward,[91] S. J. Haywood,[143] F. He,[60a] Y. He,[165] M. P. Heath,[50] V. Hedberg,[97] A. L. Heggelund,[133] N. D. Hehir,[93] C. Heidegger,[52] K. K. Heidegger,[52] W. D. Heidorn,[79] J. Heilman,[34] S. Heim,[46] T. Heim,[18] B. Heinemann,[46,v] J. G. Heinlein,[136] J. J. Heinrich,[131] L. Heinrich,[36] J. Hejbal,[140] L. Helary,[46] A. Held,[125] S. Hellesund,[133] C. M. Helling,[145] S. Hellman,[45a,45b] C. Helsens,[36] R. C. W. Henderson,[90] L. Henkelmann,[32] A. M. Henriques Correia,[36] H. Herde,[26] Y. Hernández Jiménez,[33f] H. Herr,[100] M. G. Herrmann,[114] T. Herrmann,[48] G. Herten,[52] R. Hertenberger,[114] L. Hervas,[36] G. G. Hesketh,[95] N. P. Hessey,[168a] H. Hibi,[83] S. Higashino,[82] E. Higón-Rodriguez,[174] K. Hildebrand,[37] J. C. Hill,[32] K. K. Hill,[29] K. H. Hiller,[46] S. J. Hillier,[21] M. Hils,[48] I. Hinchliffe,[18] F. Hinterkeuser,[24] M. Hirose,[132] S. Hirose,[169] D. Hirschbuehl,[182] B. Hiti,[92] O. Hladik,[140] J. Hobbs,[155] R. Hobincu,[27e] N. Hod,[180] M. C. Hodgkinson,[149] A. Hoecker,[36] D. Hohn,[52] D. Hohov,[65] T. Holm,[24] T. R. Holmes,[37] M. Holzbock,[115] L. B. A. H. Hommels,[32] T. M. Hong,[138] J. C. Honig,[52] A. Hönle,[115] B. H. Hooberman,[173] W. H. Hopkins,[6] Y. Horii,[117] P. Horn,[48] L. A. Horyn,[37] S. Hou,[158] A. Hoummada,[35a] J. Howarth,[57] J. Hoya,[89] M. Hrabovsky,[130] J. Hrivnac,[65] A. Hrynevich,[109] T. Hryn'ova,[5] P. J. Hsu,[64] S.-C. Hsu,[148] Q. Hu,[39] S. Hu,[60c] Y. F. Hu,[15a,15d,w] D. P. Huang,[95] X. Huang,[15c] Y. Huang,[60a] Y. Huang,[15a] Z. Hubacek,[141] F. Hubaut,[102] M. Huebner,[24] F. Huegging,[24] T. B. Huffman,[134] M. Huhtinen,[36] R. Hulsken,[58] R. F. H. Hunter,[34] N. Huseynov,[80,x] J. Huston,[107] J. Huth,[59] R. Hyneman,[153] S. Hyrych,[28a] G. Iacobucci,[54] G. Iakovidis,[29] I. Ibragimov,[151] L. Iconomidou-Fayard,[65] P. Iengo,[36] R. Ignazzi,[40] R. Iguchi,[163] T. Iizawa,[54] Y. Ikegami,[82] M. Ikeno,[82] N. Ilic,[119,167,m] F. Iltzsche,[48] H. Imam,[35a] G. Introzzi,[71a,71b] M. Iodice,[75a] K. Iordanidou,[168a] V. Ippolito,[73a,73b] M. F. Isacson,[172] M. Ishino,[163] W. Islam,[129] C. Issever,[19,46] S. Istin,[160] J. M. Iturbe Ponce,[63a] R. Iuppa,[76a,76b] A. Ivina,[180] J. M. Izen,[43] V. Izzo,[70a] P. Jacka,[140] P. Jackson,[1] R. M. Jacobs,[46] B. P. Jaeger,[152] V. Jain,[2] G. Jäkel,[182] K. B. Jakobi,[100] K. Jakobs,[52] T. Jakoubek,[180] J. Jamieson,[57] K. W. Janas,[84a] R. Jansky,[54] M. Janus,[53] P. A. Janus,[84a] G. Jarlskog,[97] A. E. Jaspan,[91] N. Javadov,[80,x] T. Javůrek,[36] M. Javurkova,[103] F. Jeanneau,[144] L. Jeanty,[131] J. Jejelava,[159a] P. Jenni,[52,y] N. Jeong,[46] S. Jézéquel,[5] J. Jia,[155] Z. Jia,[15c] H. Jiang,[79] Y. Jiang,[60a] Z. Jiang,[153] S. Jiggins,[52] F. A. Jimenez Morales,[38] J. Jimenez Pena,[115] S. Jin,[15c] A. Jinaru,[27b] O. Jinnouchi,[165] P. Johansson,[149] K. A. Johns,[7] C. A. Johnson,[66] E. Jones,[178] R. W. L. Jones,[90] S. D. Jones,[156] T. J. Jones,[91] J. Jovicevic,[36] X. Ju,[18] J. J. Junggeburth,[115] A. Juste Rozas,[14,t] A. Kaczmarska,[85] M. Kado,[73a,73b] H. Kagan,[127] M. Kagan,[153] A. Kahn,[39] C. Kahra,[100] T. Kaji,[179] E. Kajomovitz,[160] C. W. Kalderon,[29] A. Kaluza,[100] M. Kaneda,[163] N. J. Kang,[145] S. Kang,[79] Y. Kano,[117] J. Kanzaki,[82] L. S. Kaplan,[181] D. Kar,[33f] K. Karava,[134] M. J. Kareem,[168b] I. Karkanias,[162] S. N. Karpov,[80] Z. M. Karpova,[80] V. Kartvelishvili,[90] A. N. Karyukhin,[123] E. Kasimi,[162] A. Kastanas,[45a,45b] C. Kato,[60d] J. Katzy,[46] K. Kawade,[150] K. Kawagoe,[88] T. Kawaguchi,[117] T. Kawamoto,[144] G. Kawamura,[53] E. F. Kay,[176] F. I. Kaya,[170] S. Kazakos,[14] V. F. Kazanin,[122b,122a] J. M. Keaveney,[33a] R. Keeler,[176] J. S. Keller,[34] E. Kellermann,[97] D. Kelsey,[156] J. J. Kempster,[21] J. Kendrick,[21] K. E. Kennedy,[39] O. Kepka,[140] S. Kersten,[182] B. P. Kerševan,[92] S. Ketabchi Haghighat,[167] F. Khalil-Zada,[13] M. Khandoga,[144] A. Khanov,[129] A. G. Kharlamov,[122b,122a] T. Kharlamova,[122b,122a] E. E. Khoda,[175] T. J. Khoo,[77] G. Khoriauli,[177] E. Khramov,[80] J. Khubua,[159b] S. Kido,[83] M. Kiehn,[36] E. Kim,[165] Y. K. Kim,[37] N. Kimura,[95] A. Kirchhoff,[53] D. Kirchmeier,[48] J. Kirk,[143] A. E. Kiryunin,[115] T. Kishimoto,[163] D. P. Kisliuk,[167] V. Kitali,[46] C. Kitsaki,[10] O. Kivernyk,[24] T. Klapdor-Kleingrothaus,[52] M. Klassen,[61a] C. Klein,[34] M. H. Klein,[106] M. Klein,[91] U. Klein,[91] K. Kleinknecht,[100] P. Klimek,[36] A. Klimentov,[29] F. Klimpel,[36] T. Klingl,[24] T. Klioutchnikova,[36] F. F. Klitzner,[114] P. Kluit,[120] S. Kluth,[115] E. Kneringer,[77] E. B. F. G. Knoops,[102] A. Knue,[52] D. Kobayashi,[88] M. Kobel,[48] M. Kocian,[153] T. Kodama,[163] P. Kodys,[142] D. M. Koeck,[156] P. T. Koenig,[24] T. Koffas,[34] N. M. Köhler,[36] M. Kolb,[144] I. Koletsou,[5] T. Komarek,[130] T. Kondo,[82] K. Köneke,[52] A. X. Y. Kong,[1] A. C. König,[119] T. Kono,[126] V. Konstantinides,[95] N. Konstantinidis,[95] B. Konya,[97] R. Kopeliansky,[66] S. Koperny,[84a] K. Korcyl,[85] K. Kordas,[162] G. Koren,[161] A. Korn,[95] I. Korolkov,[14] E. V. Korolkova,[149] N. Korotkova,[113] O. Kortner,[115] S. Kortner,[115] V. V. Kostyukhin,[149,166] A. Kotsokechagia,[65] A. Kotwal,[49] A. Koulouris,[10]

A. Kourkoumeli-Charalampidi,[71a,71b] C. Kourkoumelis,[9] E. Kourlitis,[6] V. Kouskoura,[29] R. Kowalewski,[176] W. Kozanecki,[101] A. S. Kozhin,[123] V. A. Kramarenko,[113] G. Kramberger,[92] D. Krasnopevtsev,[60a] M. W. Krasny,[135] A. Krasznahorkay,[36] D. Krauss,[115] J. A. Kremer,[100] J. Kretzschmar,[91] K. Kreul,[19] P. Krieger,[167] F. Krieter,[114] S. Krishnamurthy,[103] A. Krishnan,[61b] M. Krivos,[142] K. Krizka,[18] K. Kroeninger,[47] H. Kroha,[115] J. Kroll,[140] J. Kroll,[136] K. S. Krowpman,[107] U. Kruchonak,[80] H. Krüger,[24] N. Krumnack,[79] M. C. Kruse,[49] J. A. Krzysiak,[85] A. Kubota,[165] O. Kuchinskaia,[166] S. Kuday,[4b] D. Kuechler,[46] J. T. Kuechler,[46] S. Kuehn,[36] T. Kuhl,[46] V. Kukhtin,[80] Y. Kulchitsky,[108,z] S. Kuleshov,[146b] Y. P. Kulinich,[173] M. Kuna,[58] A. Kupco,[140] T. Kupfer,[47] O. Kuprash,[52] H. Kurashige,[83] L. L. Kurchaninov,[168a] Y. A. Kurochkin,[108] A. Kurova,[112] M. G. Kurth,[15a,15d] E. S. Kuwertz,[36] M. Kuze,[165] A. K. Kvam,[148] J. Kvita,[130] T. Kwan,[104] C. Lacasta,[174] F. Lacava,[73a,73b] D. P. J. Lack,[101] H. Lacker,[19] D. Lacour,[135] E. Ladygin,[80] R. Lafaye,[5] B. Laforge,[135] T. Lagouri,[146c] S. Lai,[53] I. K. Lakomiec,[84a] J. E. Lambert,[128] S. Lammers,[66] W. Lampl,[7] C. Lampoudis,[162] E. Lançon,[29] U. Landgraf,[52] M. P. J. Landon,[93] V. S. Lang,[52] J. C. Lange,[53] R. J. Langenberg,[103] A. J. Lankford,[171] F. Lanni,[29] K. Lantzsch,[24] A. Lanza,[71a] A. Lapertosa,[55b,55a] J. F. Laporte,[144] T. Lari,[69a] F. Lasagni Manghi,[23b,23a] M. Lassnig,[36] V. Latonova,[140] T. S. Lau,[63a] A. Laudrain,[100] A. Laurier,[34] M. Lavorgna,[70a,70b] S. D. Lawlor,[94] M. Lazzaroni,[69a,69b] B. Le,[101] E. Le Guirriec,[102] A. Lebedev,[79] M. LeBlanc,[7] T. LeCompte,[6] F. Ledroit-Guillon,[58] A. C. A. Lee,[95] C. A. Lee,[29] G. R. Lee,[17] L. Lee,[59] S. C. Lee,[158] S. Lee,[79] B. Lefebvre,[168a] H. P. Lefebvre,[94] M. Lefebvre,[176] C. Leggett,[18] K. Lehmann,[152] N. Lehmann,[20] G. Lehmann Miotto,[36] W. A. Leight,[46] A. Leisos,[162,aa] M. A. L. Leite,[81c] C. E. Leitgeb,[114] R. Leitner,[142] K. J. C. Leney,[42] T. Lenz,[24] S. Leone,[72a] C. Leonidopoulos,[50] A. Leopold,[135] C. Leroy,[110] R. Les,[107] C. G. Lester,[32] M. Levchenko,[137] J. Levêque,[5] D. Levin,[106] L. J. Levinson,[180] D. J. Lewis,[21] B. Li,[15b] B. Li,[106] C-Q. Li,[60c,60d] F. Li,[60c] H. Li,[60a] H. Li,[60b] J. Li,[60c] K. Li,[148] L. Li,[60c] M. Li,[15a,15d] Q. Y. Li,[60a] S. Li,[60d,60c,bb] X. Li,[46] Y. Li,[46] Z. Li,[60b] Z. Li,[134] Z. Li,[104] Z. Li,[91] Z. Liang,[15a] M. Liberatore,[46] B. Liberti,[74a] K. Lie,[63c] S. Lim,[29] C. Y. Lin,[32] K. Lin,[107] R. A. Linck,[66] R. E. Lindley,[7] J. H. Lindon,[21] A. Linss,[46] A. L. Lionti,[54] E. Lipeles,[136] A. Lipniacka,[17] T. M. Liss,[173,cc] A. Lister,[175] J. D. Little,[8] B. Liu,[79] B. X. Liu,[152] H. B. Liu,[29] J. B. Liu,[60a] J. K. K. Liu,[37] K. Liu,[60d,60c] M. Liu,[60a] M. Y. Liu,[60a] P. Liu,[15a] X. Liu,[60a] Y. Liu,[46] Y. Liu,[15a,15d] Y. L. Liu,[106] Y. W. Liu,[60a] M. Livan,[71a,71b] A. Lleres,[58] J. Llorente Merino,[152] S. L. Lloyd,[93] C. Y. Lo,[63b] E. M. Lobodzinska,[46] P. Loch,[7] S. Loffredo,[74a,74b] T. Lohse,[19] K. Lohwasser,[149] M. Lokajicek,[140] J. D. Long,[173] R. E. Long,[90] I. Longarini,[73a,73b] L. Longo,[36] I. Lopez Paz,[101] A. Lopez Solis,[149] J. Lorenz,[114] N. Lorenzo Martinez,[5] A. M. Lory,[114] A. Lösle,[52] X. Lou,[45a,45b] X. Lou,[15a] A. Lounis,[65] J. Love,[6] P. A. Love,[90] J. J. Lozano Bahilo,[174] M. Lu,[60a] Y. J. Lu,[64] H. J. Lubatti,[148] C. Luci,[73a,73b] F. L. Lucio Alves,[15c] A. Lucotte,[58] F. Luehring,[66] I. Luise,[155] L. Luminari,[73a] B. Lund-Jensen,[154] N. A. Luongo,[131] M. S. Lutz,[161] D. Lynn,[29] H. Lyons,[91] R. Lysak,[140] E. Lytken,[97] F. Lyu,[15a] V. Lyubushkin,[80] T. Lyubushkina,[80] H. Ma,[29] L. L. Ma,[60b] Y. Ma,[95] D. M. Mac Donell,[176] G. Maccarrone,[51] C. M. Macdonald,[149] J. C. MacDonald,[149] J. Machado Miguens,[136] R. Madar,[38] W. F. Mader,[48] M. Madugoda Ralalage Don,[129] N. Madysa,[48] J. Maeda,[83] T. Maeno,[29] M. Maerker,[48] V. Magerl,[52] N. Magini,[79] J. Magro,[67a,67c,dd] D. J. Mahon,[39] C. Maidantchik,[81b] A. Maio,[139a,139b,139d] K. Maj,[84a] O. Majersky,[28a] S. Majewski,[131] Y. Makida,[82] N. Makovec,[65] B. Malaescu,[135] Pa. Malecki,[85] V. P. Maleev,[137] F. Malek,[58] D. Malito,[41b,41a] U. Mallik,[78] C. Malone,[32] S. Maltezos,[10] S. Malyukov,[80] J. Mamuzic,[174] G. Mancini,[51] J. P. Mandalia,[93] I. Mandić,[92] L. Manhaes de Andrade Filho,[81a] I. M. Maniatis,[162] J. Manjarres Ramos,[48] K. H. Mankinen,[97] A. Mann,[114] A. Manousos,[77] B. Mansoulie,[144] I. Manthos,[162] S. Manzoni,[120] A. Marantis,[162,aa] G. Marceca,[30] L. Marchese,[134] G. Marchiori,[135] M. Marcisovsky,[140] L. Marcoccia,[74a,74b] C. Marcon,[97] M. Marjanovic,[128] Z. Marshall,[18] M. U. F. Martensson,[172] S. Marti-Garcia,[174] C. B. Martin,[127] T. A. Martin,[178] V. J. Martin,[50] B. Martin dit Latour,[17] L. Martinelli,[75a,75b] M. Martinez,[14,t] P. Martinez Agullo,[174] V. I. Martinez Outschoorn,[103] S. Martin-Haugh,[143] V. S. Martoiu,[27b] A. C. Martyniuk,[95] A. Marzin,[36] S. R. Maschek,[115] L. Masetti,[100] T. Mashimo,[163] R. Mashinistov,[111] J. Masik,[101] A. L. Maslennikov,[122b,122a] L. Massa,[23b,23a] P. Massarotti,[70a,70b] P. Mastrandrea,[72a,72b] A. Mastroberardino,[41b,41a] T. Masubuchi,[163] D. Matakias,[29] A. Matic,[114] N. Matsuzawa,[163] P. Mättig,[24] J. Maurer,[27b] B. Maček,[92] D. A. Maximov,[122b,122a] R. Mazini,[158] I. Maznas,[162] S. M. Mazza,[145] J. P. Mc Gowan,[104] S. P. Mc Kee,[106] T. G. McCarthy,[115] W. P. McCormack,[18] E. F. McDonald,[105] A. E. McDougall,[120] J. A. Mcfayden,[18] G. Mchedlidze,[159b] M. A. McKay,[42] K. D. McLean,[176] S. J. McMahon,[143] P. C. McNamara,[105] C. J. McNicol,[178] R. A. McPherson,[176,m] Z. A. Meadows,[103] S. Meehan,[36] T. Megy,[38] S. Mehlhase,[114] A. Mehta,[91] B. Meirose,[43] D. Melini,[160] B. R. Mellado Garcia,[33f] J. D. Mellenthin,[53] M. Melo,[28a] F. Meloni,[46] A. Melzer,[24] E. D. Mendes Gouveia,[139a,139e] A. M. Mendes Jacques Da Costa,[21] H. Y. Meng,[167] L. Meng,[36] X. T. Meng,[106] S. Menke,[115] E. Meoni,[41b,41a] S. Mergelmeyer,[19] S. A. M. Merkt,[138] C. Merlassino,[134] P. Mermod,[54,a] L. Merola,[70a,70b] C. Meroni,[69a] G. Merz,[106] O. Meshkov,[113,111] J. K. R. Meshreki,[151]

J. Metcalfe,[6] A. S. Mete,[6] C. Meyer,[66] J-P. Meyer,[144] M. Michetti,[19] R. P. Middleton,[143] L. Mijović,[50] G. Mikenberg,[180] M. Mikestikova,[140] M. Mikuž,[92] H. Mildner,[149] A. Milic,[167] C. D. Milke,[42] D. W. Miller,[37] L. S. Miller,[34] A. Milov,[180] D. A. Milstead,[45a,45b] A. A. Minaenko,[123] I. A. Minashvili,[159b] L. Mince,[57] A. I. Mincer,[125] B. Mindur,[84a] M. Mineev,[80] Y. Minegishi,[163] Y. Mino,[86] L. M. Mir,[14] M. Mironova,[134] T. Mitani,[179] J. Mitrevski,[114] V. A. Mitsou,[174] M. Mittal,[60c] O. Miu,[167] A. Miucci,[20] P. S. Miyagawa,[93] A. Mizukami,[82] J. U. Mjörnmark,[97] T. Mkrtchyan,[61a] M. Mlynarikova,[121] T. Moa,[45a,45b] S. Mobius,[53] K. Mochizuki,[110] P. Moder,[46] P. Mogg,[114] S. Mohapatra,[39] R. Moles-Valls,[24] K. Mönig,[46] E. Monnier,[102] A. Montalbano,[152] J. Montejo Berlingen,[36] M. Montella,[95] F. Monticelli,[89] S. Monzani,[69a] N. Morange,[65] A. L. Moreira De Carvalho,[139a] D. Moreno,[22a] M. Moreno Llácer,[174] C. Moreno Martinez,[14] P. Morettini,[55b] M. Morgenstern,[160] S. Morgenstern,[48] D. Mori,[152] M. Morii,[59] M. Morinaga,[179] V. Morisbak,[133] A. K. Morley,[36] G. Mornacchi,[36] A. P. Morris,[95] L. Morvaj,[36] P. Moschovakos,[36] B. Moser,[120] M. Mosidze,[159b] T. Moskalets,[144] P. Moskvitina,[119] J. Moss,[31,ee] E. J. W. Moyse,[103] S. Muanza,[102] J. Mueller,[138] R. S. P. Mueller,[114] D. Muenstermann,[90] G. A. Mullier,[97] D. P. Mungo,[69a,69b] J. L. Munoz Martinez,[14] F. J. Munoz Sanchez,[101] P. Murin,[28b] W. J. Murray,[178,143] A. Murrone,[69a,69b] J. M. Muse,[128] M. Muškinja,[18] C. Mwewa,[33a] A. G. Myagkov,[123,j] A. A. Myers,[138] G. Myers,[66] J. Myers,[131] M. Myska,[141] B. P. Nachman,[18] O. Nackenhorst,[47] A. Nag Nag,[48] K. Nagai,[134] K. Nagano,[82] Y. Nagasaka,[62] J. L. Nagle,[29] E. Nagy,[102] A. M. Nairz,[36] Y. Nakahama,[117] K. Nakamura,[82] T. Nakamura,[163] H. Nanjo,[132] F. Napolitano,[61a] R. F. Naranjo Garcia,[46] R. Narayan,[42] I. Naryshkin,[137] M. Naseri,[34] T. Naumann,[46] G. Navarro,[22a] P. Y. Nechaeva,[111] F. Nechansky,[46] T. J. Neep,[21] A. Negri,[71a,71b] M. Negrini,[23b] C. Nellist,[119] C. Nelson,[104] M. E. Nelson,[45a,45b] S. Nemecek,[140] M. Nessi,[36,ff] M. S. Neubauer,[173] F. Neuhaus,[100] M. Neumann,[182] R. Newhouse,[175] P. R. Newman,[21] C. W. Ng,[138] Y. S. Ng,[19] Y. W. Y. Ng,[171] B. Ngair,[35f] H. D. N. Nguyen,[102] T. Nguyen Manh,[110] E. Nibigira,[38] R. B. Nickerson,[134] R. Nicolaidou,[144] D. S. Nielsen,[40] J. Nielsen,[145] M. Niemeyer,[53] N. Nikiforou,[11] V. Nikolaenko,[123,j] I. Nikolic-Audit,[135] K. Nikolopoulos,[21] P. Nilsson,[29] H. R. Nindhito,[54] A. Nisati,[73a] N. Nishu,[60c] R. Nisius,[115] I. Nitsche,[47] T. Nitta,[179] T. Nobe,[163] D. L. Noel,[32] Y. Noguchi,[86] I. Nomidis,[135] M. A. Nomura,[29] M. Nordberg,[36] J. Novak,[92] T. Novak,[92] O. Novgorodova,[48] R. Novotny,[118] L. Nozka,[130] K. Ntekas,[171] E. Nurse,[95] F. G. Oakham,[34,e] J. Ocariz,[135] A. Ochi,[83] I. Ochoa,[139a] J. P. Ochoa-Ricoux,[146a] K. O'Connor,[26] S. Odaka,[82] S. Oerdek,[53] A. Ogrodnik,[84a] A. Oh,[101] C. C. Ohm,[154] H. Oide,[165] R. Oishi,[163] M. L. Ojeda,[167] H. Okawa,[169] Y. Okazaki,[86] M. W. O'Keefe,[91] Y. Okumura,[163] A. Olariu,[27b] L. F. Oleiro Seabra,[139a] S. A. Olivares Pino,[146a] D. Oliveira Damazio,[29] J. L. Oliver,[1] M. J. R. Olsson,[171] A. Olszewski,[85] J. Olszowska,[85] Ö. O. Öncel,[24] D. C. O'Neil,[152] A. P. O'neill,[134] A. Onofre,[139a,139e] P. U. E. Onyisi,[11] H. Oppen,[133] R. G. Oreamuno Madriz,[121] M. J. Oreglia,[37] G. E. Orellana,[89] D. Orestano,[75a,75b] N. Orlando,[14] R. S. Orr,[167] V. O'Shea,[57] R. Ospanov,[60a] G. Otero y Garzon,[30] H. Otono,[88] P. S. Ott,[61a] G. J. Ottino,[18] M. Ouchrif,[35e] J. Ouellette,[29] F. Ould-Saada,[133] A. Ouraou,[144,a] Q. Ouyang,[15a] M. Owen,[57] R. E. Owen,[143] V. E. Ozcan,[12c] N. Ozturk,[8] J. Pacalt,[130] H. A. Pacey,[32] K. Pachal,[49] A. Pacheco Pages,[14] C. Padilla Aranda,[14] S. Pagan Griso,[18] G. Palacino,[66] S. Palazzo,[50] S. Palestini,[36] M. Palka,[84b] P. Palni,[84a] C. E. Pandini,[54] J. G. Panduro Vazquez,[94] P. Pani,[46] G. Panizzo,[67a,67c] L. Paolozzi,[54] C. Papadatos,[110] K. Papageorgiou,[9,q] S. Parajuli,[42] A. Paramonov,[6] C. Paraskevopoulos,[10] D. Paredes Hernandez,[63b] S. R. Paredes Saenz,[134] B. Parida,[180] T. H. Park,[167] A. J. Parker,[31] M. A. Parker,[32] F. Parodi,[55b,55a] E. W. Parrish,[121] J. A. Parsons,[39] U. Parzefall,[52] L. Pascual Dominguez,[135] V. R. Pascuzzi,[18] J. M. P. Pasner,[145] F. Pasquali,[120] E. Pasqualucci,[73a] S. Passaggio,[55b] F. Pastore,[94] P. Pasuwan,[45a,45b] S. Pataraia,[100] J. R. Pater,[101] A. Pathak,[181,f] J. Patton,[91] T. Pauly,[36] J. Pearkes,[153] M. Pedersen,[133] L. Pedraza Diaz,[119] R. Pedro,[139a] T. Peiffer,[53] S. V. Peleganchuk,[122b,122a] O. Penc,[140] C. Peng,[63b] H. Peng,[60a] B. S. Peralva,[81a] M. M. Perego,[65] A. P. Pereira Peixoto,[139a] L. Pereira Sanchez,[45a,45b] D. V. Perepelitsa,[29] E. Perez Codina,[168a] L. Perini,[69a,69b] H. Pernegger,[36] S. Perrella,[36] A. Perrevoort,[120] K. Peters,[46] R. F. Y. Peters,[101] B. A. Petersen,[36] T. C. Petersen,[40] E. Petit,[102] V. Petousis,[141] C. Petridou,[162] F. Petrucci,[75a,75b] M. Pettee,[183] N. E. Pettersson,[103] K. Petukhova,[142] A. Peyaud,[144] R. Pezoa,[146d] L. Pezzotti,[71a,71b] T. Pham,[105] P. W. Phillips,[143] M. W. Phipps,[173] G. Piacquadio,[155] E. Pianori,[18] A. Picazio,[103] R. H. Pickles,[101] R. Piegaia,[30] D. Pietreanu,[27b] J. E. Pilcher,[37] A. D. Pilkington,[101] M. Pinamonti,[67a,67c] J. L. Pinfold,[3] C. Pitman Donaldson,[95] M. Pitt,[161] L. Pizzimento,[74a,74b] A. Pizzini,[120] M.-A. Pleier,[29] V. Plesanovs,[52] V. Pleskot,[142] E. Plotnikova,[80] P. Podberezko,[122b,122a] R. Poettgen,[97] R. Poggi,[54] L. Poggioli,[135] I. Pogrebnyak,[107] D. Pohl,[24] I. Pokharel,[53] G. Polesello,[71a] A. Poley,[152,168a] A. Policicchio,[73a,73b] R. Polifka,[142] A. Polini,[23b] C. S. Pollard,[46] V. Polychronakos,[29] D. Ponomarenko,[112] L. Pontecorvo,[36] S. Popa,[27a] G. A. Popeneciu,[27d] L. Portales,[5] D. M. Portillo Quintero,[58] S. Pospisil,[141] K. Potamianos,[46] I. N. Potrap,[80] C. J. Potter,[32] H. Potti,[11] T. Poulsen,[97] J. Poveda,[174] T. D. Powell,[149] G. Pownall,[46] M. E. Pozo Astigarraga,[36] A. Prades Ibanez,[174] P. Pralavorio,[102] M. M. Prapa,[44] S. Prell,[79] D. Price,[101] M. Primavera,[68a] M. L. Proffitt,[148] N. Proklova,[112] K. Prokofiev,[63c] F. Prokoshin,[80] S. Protopopescu,[29] J. Proudfoot,[6] M. Przybycien,[84a]

D. Pudzha,[137] A. Puri,[173] P. Puzo,[65] D. Pyatiizbyantseva,[112] J. Qian,[106] Y. Qin,[101] A. Quadt,[53] M. Queitsch-Maitland,[36] G. Rabanal Bolanos,[59] M. Racko,[28a] F. Ragusa,[69a,69b] G. Rahal,[98] J. A. Raine,[54] S. Rajagopalan,[29] A. Ramirez Morales,[93] K. Ran,[15a,15d] D. F. Rassloff,[61a] D. M. Rauch,[46] F. Rauscher,[114] S. Rave,[100] B. Ravina,[57] I. Ravinovich,[180] J. H. Rawling,[101] M. Raymond,[36] A. L. Read,[133] N. P. Readioff,[149] M. Reale,[68a,68b] D. M. Rebuzzi,[71a,71b] G. Redlinger,[29] K. Reeves,[43] D. Reikher,[161] A. Reiss,[100] A. Rej,[151] C. Rembser,[36] A. Renardi,[46] M. Renda,[27b] M. B. Rendel,[115] A. G. Rennie,[57] S. Resconi,[69a] E. D. Resseguie,[18] S. Rettie,[95] B. Reynolds,[127] E. Reynolds,[21] O. L. Rezanova,[122b,122a] P. Reznicek,[142] E. Ricci,[76a,76b] R. Richter,[115] S. Richter,[46] E. Richter-Was,[84b] M. Ridel,[135] P. Rieck,[115] O. Rifki,[46] M. Rijssenbeek,[155] A. Rimoldi,[71a,71b] M. Rimoldi,[46] L. Rinaldi,[23b] T. T. Rinn,[173] G. Ripellino,[154] I. Riu,[14] P. Rivadeneira,[46] J. C. Rivera Vergara,[176] F. Rizatdinova,[129] E. Rizvi,[93] C. Rizzi,[36] S. H. Robertson,[104,m] M. Robin,[46] D. Robinson,[32] C. M. Robles Gajardo,[146d] M. Robles Manzano,[100] A. Robson,[57] A. Rocchi,[74a,74b] C. Roda,[72a,72b] S. Rodriguez Bosca,[174] A. Rodriguez Rodriguez,[52] A. M. Rodríguez Vera,[168b] S. Roe,[36] J. Roggel,[182] O. Røhne,[133] R. Röhrig,[115] R. A. Rojas,[146d] B. Roland,[52] C. P. A. Roland,[66] J. Roloff,[29] A. Romaniouk,[112] M. Romano,[23b,23a] N. Rompotis,[91] M. Ronzani,[125] L. Roos,[135] S. Rosati,[73a] G. Rosin,[103] B. J. Rosser,[136] E. Rossi,[46] E. Rossi,[75a,75b] E. Rossi,[70a,70b] L. P. Rossi,[55b] L. Rossini,[46] R. Rosten,[14] M. Rotaru,[27b] B. Rottler,[52] D. Rousseau,[65] G. Rovelli,[71a,71b] A. Roy,[11] D. Roy,[33f] A. Rozanov,[102] Y. Rozen,[160] X. Ruan,[33f] T. A. Ruggeri,[1] F. Rühr,[52] A. Ruiz-Martinez,[174] A. Rummler,[36] Z. Rurikova,[52] N. A. Rusakovich,[80] H. L. Russell,[104] L. Rustige,[38,47] J. P. Rutherfoord,[7] E. M. Rüttinger,[149] M. Rybar,[142] G. Rybkin,[65] E. B. Rye,[133] A. Ryzhov,[123] J. A. Sabater Iglesias,[46] P. Sabatini,[174] L. Sabetta,[73a,73b] S. Sacerdoti,[65] H. F-W. Sadrozinski,[145] R. Sadykov,[80] F. Safai Tehrani,[73a] B. Safarzadeh Samani,[156] M. Safdari,[153] P. Saha,[121] S. Saha,[104] M. Sahinsoy,[115] A. Sahu,[182] M. Saimpert,[36] M. Saito,[163] T. Saito,[163] H. Sakamoto,[163] D. Salamani,[54] G. Salamanna,[75a,75b] A. Salnikov,[153] J. Salt,[174] A. Salvador Salas,[14] D. Salvatore,[41b,41a] F. Salvatore,[156] A. Salvucci,[63a] A. Salzburger,[36] J. Samarati,[36] D. Sammel,[52] D. Sampsonidis,[162] D. Sampsonidou,[60d,60c] J. Sánchez,[174] A. Sanchez Pineda,[67a,36,67c] H. Sandaker,[133] C. O. Sander,[46] I. G. Sanderswood,[90] M. Sandhoff,[182] C. Sandoval,[22b] D. P. C. Sankey,[143] M. Sannino,[55b,55a] Y. Sano,[117] A. Sansoni,[51] C. Santoni,[38] H. Santos,[139a,139b] S. N. Santpur,[18] A. Santra,[174] K. A. Saoucha,[149] A. Sapronov,[80] J. G. Saraiva,[139a,139d] O. Sasaki,[82] K. Sato,[169] F. Sauerburger,[52] E. Sauvan,[5] P. Savard,[167,e] R. Sawada,[163] C. Sawyer,[143] L. Sawyer,[96] I. Sayago Galvan,[174] C. Sbarra,[23b] A. Sbrizzi,[67a,67c] T. Scanlon,[95] J. Schaarschmidt,[148] P. Schacht,[115] D. Schaefer,[37] L. Schaefer,[136] U. Schäfer,[100] A. C. Schaffer,[65] D. Schaile,[114] R. D. Schamberger,[155] E. Schanet,[114] C. Scharf,[19] N. Scharmberg,[101] V. A. Schegelsky,[137] D. Scheirich,[142] F. Schenck,[19] M. Schernau,[171] C. Schiavi,[55b,55a] L. K. Schildgen,[24] Z. M. Schillaci,[26] E. J. Schioppa,[68a,68b] M. Schioppa,[41b,41a] K. E. Schleicher,[52] S. Schlenker,[36] K. R. Schmidt-Sommerfeld,[115] K. Schmieden,[100] C. Schmitt,[100] S. Schmitt,[46] L. Schoeffel,[144] A. Schoening,[61b] P. G. Scholer,[52] E. Schopf,[134] M. Schott,[100] J. F. P. Schouwenberg,[119] J. Schovancova,[36] S. Schramm,[54] F. Schroeder,[182] A. Schulte,[100] H-C. Schultz-Coulon,[61a] M. Schumacher,[52] B. A. Schumm,[145] Ph. Schune,[144] A. Schwartzman,[153] T. A. Schwarz,[106] Ph. Schwemling,[144] R. Schwienhorst,[107] A. Sciandra,[145] G. Sciolla,[26] F. Scuri,[72a] F. Scutti,[105] L. M. Scyboz,[115] C. D. Sebastiani,[91] K. Sedlaczek,[47] P. Seema,[19] S. C. Seidel,[118] A. Seiden,[145] B. D. Seidlitz,[29] T. Seiss,[37] C. Seitz,[46] J. M. Seixas,[81b] G. Sekhniaidze,[70a] S. J. Sekula,[42] N. Semprini-Cesari,[23b,23a] S. Sen,[49] C. Serfon,[29] L. Serin,[65] L. Serkin,[67a,67b] M. Sessa,[60a] H. Severini,[128] S. Sevova,[153] F. Sforza,[55b,55a] A. Sfyrla,[54] E. Shabalina,[53] J. D. Shahinian,[136] N. W. Shaikh,[45a,45b] D. Shaked Renous,[180] L. Y. Shan,[15a] M. Shapiro,[18] A. Sharma,[36] A. S. Sharma,[1] P. B. Shatalov,[124] K. Shaw,[156] S. M. Shaw,[101] M. Shehade,[180] Y. Shen,[128] A. D. Sherman,[25] P. Sherwood,[95] L. Shi,[95] C. O. Shimmin,[183] Y. Shimogama,[179] M. Shimojima,[116] J. D. Shinner,[94] I. P. J. Shipsey,[134] S. Shirabe,[165] M. Shiyakova,[80,gg] J. Shlomi,[180] A. Shmeleva,[111] M. J. Shochet,[37] J. Shojaii,[105] D. R. Shope,[154] S. Shrestha,[127] E. M. Shrif,[33f] M. J. Shroff,[176] E. Shulga,[180] P. Sicho,[140] A. M. Sickles,[173] E. Sideras Haddad,[33f] O. Sidiropoulou,[36] A. Sidoti,[23b,23a] F. Siegert,[48] Dj. Sijacki,[16] M. Silva Jr.,[181] M. V. Silva Oliveira,[36] S. B. Silverstein,[45a] S. Simion,[65] R. Simoniello,[100] C. J. Simpson-allsop,[21] S. Simsek,[12b] P. Sinervo,[167] V. Sinetckii,[113] S. Singh,[152] S. Sinha,[33f] M. Sioli,[23b,23a] I. Siral,[131] S. Yu. Sivoklokov,[113] J. Sjölin,[45a,45b] A. Skaf,[53] E. Skorda,[97] P. Skubic,[128] M. Slawinska,[85] K. Sliwa,[170] V. Smakhtin,[180] B. H. Smart,[143] J. Smiesko,[28b] N. Smirnov,[112] S. Yu. Smirnov,[112] Y. Smirnov,[112] L. N. Smirnova,[113,hh] O. Smirnova,[97] E. A. Smith,[37] H. A. Smith,[134] M. Smizanska,[90] K. Smolek,[141] A. Smykiewicz,[85] A. A. Snesarev,[111] H. L. Snoek,[120] I. M. Snyder,[131] S. Snyder,[29] R. Sobie,[176,m] A. Soffer,[161] A. Søgaard,[50] F. Sohns,[53] C. A. Solans Sanchez,[36] E. Yu. Soldatov,[112] U. Soldevila,[174] A. A. Solodkov,[123] A. Soloshenko,[80] O. V. Solovyanov,[123] V. Solovyev,[137] P. Sommer,[149] H. Son,[170] A. Sonay,[14] W. Song,[143] W. Y. Song,[168b] A. Sopczak,[141] A. L. Sopio,[95] F. Sopkova,[28b] S. Sottocornola,[71a,71b] R. Soualah,[67a,67c] A. M. Soukharev,[122b,122a] D. South,[46] S. Spagnolo,[68a,68b] M. Spalla,[115] M. Spangenberg,[178] F. Spanò,[94] D. Sperlich,[52] T. M. Spieker,[61a] G. Spigo,[36] M. Spina,[156]

D. P. Spiteri,[57] M. Spousta,[142] A. Stabile,[69a,69b] B. L. Stamas,[121] R. Stamen,[61a] M. Stamenkovic,[120] A. Stampekis,[21] E. Stanecka,[85] B. Stanislaus,[134] M. M. Stanitzki,[46] M. Stankaityte,[134] B. Stapf,[120] E. A. Starchenko,[123] G. H. Stark,[145] J. Stark,[58] P. Staroba,[140] P. Starovoitov,[61a] S. Stärz,[104] R. Staszewski,[85] G. Stavropoulos,[44] M. Stegler,[46] P. Steinberg,[29] A. L. Steinhebel,[131] B. Stelzer,[152,168a] H. J. Stelzer,[138] O. Stelzer-Chilton,[168a] H. Stenzel,[56] T. J. Stevenson,[156] G. A. Stewart,[36] M. C. Stockton,[36] G. Stoicea,[27b] M. Stolarski,[139a] S. Stonjek,[115] A. Straessner,[48] J. Strandberg,[154] S. Strandberg,[45a,45b] M. Strauss,[128] T. Strebler,[102] P. Strizenec,[28b] R. Ströhmer,[177] D. M. Strom,[131] R. Stroynowski,[42] A. Strubig,[45a,45b] S. A. Stucci,[29] B. Stugu,[17] J. Stupak,[128] N. A. Styles,[46] D. Su,[153] W. Su,[60d,148,60c] X. Su,[60a] N. B. Suarez,[138] V. V. Sulin,[111] M. J. Sullivan,[91] D. M. S. Sultan,[54] S. Sultansoy,[4c] T. Sumida,[86] S. Sun,[106] X. Sun,[101] C. J. E. Suster,[157] M. R. Sutton,[156] S. Suzuki,[82] M. Svatos,[140] M. Swiatlowski,[168a] S. P. Swift,[2] T. Swirski,[177] A. Sydorenko,[100] I. Sykora,[28a] M. Sykora,[142] T. Sykora,[142] D. Ta,[100] K. Tackmann,[46,ii] J. Taenzer,[161] A. Taffard,[171] R. Tafirout,[168a] E. Tagiev,[123] R. H. M. Taibah,[135] R. Takashima,[87] K. Takeda,[83] T. Takeshita,[150] E. P. Takeva,[50] Y. Takubo,[82] M. Talby,[102] A. A. Talyshev,[122b,122a] K. C. Tam,[63b] N. M. Tamir,[161] J. Tanaka,[163] R. Tanaka,[65] S. Tapia Araya,[173] S. Tapprogge,[100] A. Tarek Abouelfadl Mohamed,[107] S. Tarem,[160] K. Tariq,[60b] G. Tarna,[27b,jj] G. F. Tartarelli,[69a] P. Tas,[142] M. Tasevsky,[140] E. Tassi,[41b,41a] G. Tateno,[163] A. Tavares Delgado,[139a] Y. Tayalati,[35f] A. J. Taylor,[50] G. N. Taylor,[105] W. Taylor,[168b] H. Teagle,[91] A. S. Tee,[90] R. Teixeira De Lima,[153] P. Teixeira-Dias,[94] H. Ten Kate,[36] J. J. Teoh,[120] K. Terashi,[163] J. Terron,[99] S. Terzo,[14] M. Testa,[51] R. J. Teuscher,[167,m] N. Themistokleous,[50] T. Theveneaux-Pelzer,[19] D. W. Thomas,[94] J. P. Thomas,[21] E. A. Thompson,[46] P. D. Thompson,[21] E. Thomson,[136] E. J. Thorpe,[93] V. O. Tikhomirov,[111,kk] Yu. A. Tikhonov,[122b,122a] S. Timoshenko,[112] P. Tipton,[183] S. Tisserant,[102] K. Todome,[23b,23a] S. Todorova-Nova,[142] S. Todt,[48] J. Tojo,[88] S. Tokár,[28a] K. Tokushuku,[82] E. Tolley,[127] R. Tombs,[32] K. G. Tomiwa,[33f] M. Tomoto,[82,117] L. Tompkins,[153] P. Tornambe,[103] E. Torrence,[131] H. Torres,[48] E. Torró Pastor,[174] M. Toscani,[30] C. Tosciri,[134] J. Toth,[102,ll] D. R. Tovey,[149] A. Traeet,[17] C. J. Treado,[125] T. Trefzger,[177] F. Tresoldi,[156] A. Tricoli,[29] I. M. Trigger,[168a] S. Trincaz-Duvoid,[135] D. A. Trischuk,[175] W. Trischuk,[167] B. Trocmé,[58] A. Trofymov,[65] C. Troncon,[69a] F. Trovato,[156] L. Truong,[33c] M. Trzebinski,[85] A. Trzupek,[85] F. Tsai,[46] P. V. Tsiareshka,[108,z] A. Tsirigotis,[162,aa] V. Tsiskaridze,[155] E. G. Tskhadadze,[159a] M. Tsopoulou,[162] I. I. Tsukerman,[124] V. Tsulaia,[18] S. Tsuno,[82] D. Tsybychev,[155] Y. Tu,[63b] A. Tudorache,[27b] V. Tudorache,[27b] A. N. Tuna,[36] S. Turchikhin,[80] D. Turgeman,[180] I. Turk Cakir,[4b,mm] R. J. Turner,[21] R. Turra,[69a] P. M. Tuts,[39] S. Tzamarias,[162] E. Tzovara,[100] K. Uchida,[163] F. Ukegawa,[169] G. Unal,[36] M. Unal,[11] A. Undrus,[29] G. Unel,[171] F. C. Ungaro,[105] Y. Unno,[82] K. Uno,[163] J. Urban,[28b] P. Urquijo,[105] G. Usai,[8] Z. Uysal,[12d] V. Vacek,[141] B. Vachon,[104] K. O. H. Vadla,[133] T. Vafeiadis,[36] A. Vaidya,[95] C. Valderanis,[114] E. Valdes Santurio,[45a,45b] M. Valente,[168a] S. Valentinetti,[23b,23a] A. Valero,[174] L. Valéry,[46] R. A. Vallance,[21] A. Vallier,[36] J. A. Valls Ferrer,[174] T. R. Van Daalen,[14] P. Van Gemmeren,[6] S. Van Stroud,[95] I. Van Vulpen,[120] M. Vanadia,[74a,74b] W. Vandelli,[36] M. Vandenbroucke,[144] E. R. Vandewall,[129] D. Vannicola,[73a,73b] R. Vari,[73a] E. W. Varnes,[7] C. Varni,[55b,55a] T. Varol,[158] D. Varouchas,[65] K. E. Varvell,[157] M. E. Vasile,[27b] G. A. Vasquez,[176] F. Vazeille,[38] D. Vazquez Furelos,[14] T. Vazquez Schroeder,[36] J. Veatch,[53] V. Vecchio,[101] M. J. Veen,[120] L. M. Veloce,[167] F. Veloso,[139a,139c] S. Veneziano,[73a] A. Ventura,[68a,68b] A. Verbytskyi,[115] V. Vercesi,[71a] M. Verducci,[72a,72b] C. M. Vergel Infante,[79] C. Vergis,[24] W. Verkerke,[120] A. T. Vermeulen,[120] J. C. Vermeulen,[120] C. Vernieri,[153] P. J. Verschuuren,[94] M. C. Vetterli,[152,e] N. Viaux Maira,[146d] T. Vickey,[149] O. E. Vickey Boeriu,[149] G. H. A. Viehhauser,[134] L. Vigani,[61b] M. Villa,[23b,23a] M. Villaplana Perez,[174] E. M. Villhauer,[50] E. Vilucchi,[51] M. G. Vincter,[34] G. S. Virdee,[21] A. Vishwakarma,[50] C. Vittori,[23b,23a] I. Vivarelli,[156] M. Vogel,[182] P. Vokac,[141] J. Von Ahnen,[46] S. E. von Buddenbrock,[33f] E. Von Toerne,[24] V. Vorobel,[142] K. Vorobev,[112] M. Vos,[174] J. H. Vossebeld,[91] M. Vozak,[101] N. Vranjes,[16] M. Vranjes Milosavljevic,[16] V. Vrba,[141,a] M. Vreeswijk,[120] N. K. Vu,[102] R. Vuillermet,[36] I. Vukotic,[37] S. Wada,[169] P. Wagner,[24] W. Wagner,[182] J. Wagner-Kuhr,[114] S. Wahdan,[182] H. Wahlberg,[89] R. Wakasa,[169] V. M. Walbrecht,[115] J. Walder,[143] R. Walker,[114] S. D. Walker,[94] W. Walkowiak,[151] V. Wallangen,[45a,45b] A. M. Wang,[59] A. Z. Wang,[181] C. Wang,[60a] C. Wang,[60c] H. Wang,[18] H. Wang,[3] J. Wang,[63a] P. Wang,[42] Q. Wang,[128] R.-J. Wang,[100] R. Wang,[60a] R. Wang,[6] S. M. Wang,[158] W. T. Wang,[60a] W. Wang,[15c] W. X. Wang,[60a] Y. Wang,[60a] Z. Wang,[106] C. Wanotayaroj,[46] A. Warburton,[104] C. P. Ward,[32] R. J. Ward,[21] N. Warrack,[57] A. T. Watson,[21] M. F. Watson,[21] G. Watts,[148] B. M. Waugh,[95] A. F. Webb,[11] C. Weber,[29] M. S. Weber,[20] S. A. Weber,[34] S. M. Weber,[61a] Y. Wei,[134] A. R. Weidberg,[134] J. Weingarten,[47] M. Weirich,[100] C. Weiser,[52] P. S. Wells,[36] T. Wenaus,[29] B. Wendland,[47] T. Wengler,[36] S. Wenig,[36] N. Wermes,[24] M. Wessels,[61a] T. D. Weston,[20] K. Whalen,[131] A. M. Wharton,[90] A. S. White,[106] A. White,[8] M. J. White,[1] D. Whiteson,[171] B. W. Whitmore,[90] W. Wiedenmann,[181] C. Wiel,[48] M. Wielers,[143] N. Wieseotte,[100] C. Wiglesworth,[40] L. A. M. Wiik-Fuchs,[52] H. G. Wilkens,[36] L. J. Wilkins,[94] D. M. Williams,[39] H. H. Williams,[136] S. Williams,[32] S. Willocq,[103] P. J. Windischhofer,[134] I. Wingerter-Seez,[5] E. Winkels,[156] F. Winklmeier,[131]

B. T. Winter,[52] M. Wittgen,[153] M. Wobisch,[96] A. Wolf,[100] R. Wölker,[134] J. Wollrath,[52] M. W. Wolter,[85] H. Wolters,[139a,139c] V. W. S. Wong,[175] A. F. Wongel,[46] N. L. Woods,[145] S. D. Worm,[46] B. K. Wosiek,[85] K. W. Woźniak,[85] K. Wraight,[57] S. L. Wu,[181] X. Wu,[54] Y. Wu,[60a] J. Wuerzinger,[134] T. R. Wyatt,[101] B. M. Wynne,[50] S. Xella,[40] J. Xiang,[63c] X. Xiao,[106] X. Xie,[60a] I. Xiotidis,[156] D. Xu,[15a] H. Xu,[60a] H. Xu,[60a] L. Xu,[29] R. Xu,[136] T. Xu,[144] W. Xu,[106] Y. Xu,[15b] Z. Xu,[60b] Z. Xu,[153] B. Yabsley,[157] S. Yacoob,[33a] D. P. Yallup,[95] N. Yamaguchi,[88] Y. Yamaguchi,[165] A. Yamamoto,[82] M. Yamatani,[163] T. Yamazaki,[163] Y. Yamazaki,[83] J. Yan,[60c] Z. Yan,[25] H. J. Yang,[60c,60d] H. T. Yang,[18] S. Yang,[60a] T. Yang,[63c] X. Yang,[60a] X. Yang,[60b,58] Y. Yang,[163] Z. Yang,[106,60a] W-M. Yao,[18] Y. C. Yap,[46] H. Ye,[15c] J. Ye,[42] S. Ye,[29] I. Yeletskikh,[80] M. R. Yexley,[90] E. Yigitbasi,[25] P. Yin,[39] K. Yorita,[179] K. Yoshihara,[79] C. J. S. Young,[36] C. Young,[153] J. Yu,[79] R. Yuan,[60b,nn] X. Yue,[61a] M. Zaazoua,[35f] B. Zabinski,[85] G. Zacharis,[10] E. Zaffaroni,[54] J. Zahreddine,[135] A. M. Zaitsev,[123,j] T. Zakareishvili,[159b] N. Zakharchuk,[34] S. Zambito,[36] D. Zanzi,[36] S. V. Zeißner,[47] C. Zeitnitz,[182] G. Zemaityte,[134] J. C. Zeng,[173] O. Zenin,[123] T. Ženiš,[28a] D. Zerwas,[65] M. Zgubič,[134] B. Zhang,[15c] D. F. Zhang,[15b] G. Zhang,[15b] J. Zhang,[6] K. Zhang,[15a] L. Zhang,[15c] L. Zhang,[60a] M. Zhang,[173] R. Zhang,[181] S. Zhang,[106] X. Zhang,[60c] X. Zhang,[60b] Y. Zhang,[15a,15d] Z. Zhang,[63a] Z. Zhang,[65] P. Zhao,[49] Y. Zhao,[145] Z. Zhao,[60a] A. Zhemchugov,[80] Z. Zheng,[106] D. Zhong,[173] B. Zhou,[106] C. Zhou,[181] H. Zhou,[7] M. Zhou,[155] N. Zhou,[60c] Y. Zhou,[7] C. G. Zhu,[60b] C. Zhu,[15a,15d] H. L. Zhu,[60a] H. Zhu,[15a] J. Zhu,[106] Y. Zhu,[60a] X. Zhuang,[15a] K. Zhukov,[111] V. Zhulanov,[122b,122a] D. Zieminska,[66] N. I. Zimine,[80] S. Zimmermann,[52,a] Z. Zinonos,[115] M. Ziolkowski,[151] L. Živković,[16] G. Zobernig,[181] A. Zoccoli,[23b,23a] K. Zoch,[53] T. G. Zorbas,[149] R. Zou,[37] and L. Zwalinski[36]

(ATLAS Collaboration)

[1]*Department of Physics, University of Adelaide, Adelaide, Australia*
[2]*Physics Department, SUNY Albany, Albany, New York, USA*
[3]*Department of Physics, University of Alberta, Edmonton AB, Canada*
[4a]*Department of Physics, Ankara University, Ankara, Turkey*
[4b]*Istanbul Aydin University, Application and Research Center for Advanced Studies, Istanbul, Turkey*
[4c]*Division of Physics, TOBB University of Economics and Technology, Ankara, Turkey*
[5]*LAPP, Univ. Savoie Mont Blanc, CNRS/IN2P3, Annecy, France*
[6]*High Energy Physics Division, Argonne National Laboratory, Argonne, Illinois, USA*
[7]*Department of Physics, University of Arizona, Tucson, Arizona, USA*
[8]*Department of Physics, University of Texas at Arlington, Arlington, Texas, USA*
[9]*Physics Department, National and Kapodistrian University of Athens, Athens, Greece*
[10]*Physics Department, National Technical University of Athens, Zografou, Greece*
[11]*Department of Physics, University of Texas at Austin, Austin, Texas, USA*
[12a]*Bahcesehir University, Faculty of Engineering and Natural Sciences, Istanbul, Turkey*
[12b]*Istanbul Bilgi University, Faculty of Engineering and Natural Sciences, Istanbul, Turkey*
[12c]*Department of Physics, Bogazici University, Istanbul, Turkey*
[12d]*Department of Physics Engineering, Gaziantep University, Gaziantep, Turkey*
[13]*Institute of Physics, Azerbaijan Academy of Sciences, Baku, Azerbaijan*
[14]*Institut de Física d'Altes Energies (IFAE), Barcelona Institute of Science and Technology, Barcelona, Spain*
[15a]*Institute of High Energy Physics, Chinese Academy of Sciences, Beijing, China*
[15b]*Physics Department, Tsinghua University, Beijing, China*
[15c]*Department of Physics, Nanjing University, Nanjing, China*
[15d]*University of Chinese Academy of Science (UCAS), Beijing, China*
[16]*Institute of Physics, University of Belgrade, Belgrade, Serbia*
[17]*Department for Physics and Technology, University of Bergen, Bergen, Norway*
[18]*Physics Division, Lawrence Berkeley National Laboratory and University of California, Berkeley, California, USA*
[19]*Institut für Physik, Humboldt Universität zu Berlin, Berlin, Germany*
[20]*Albert Einstein Center for Fundamental Physics and Laboratory for High Energy Physics, University of Bern, Bern, Switzerland*
[21]*School of Physics and Astronomy, University of Birmingham, Birmingham, United Kingdom*
[22a]*Facultad de Ciencias y Centro de Investigaciónes, Universidad Antonio Nariño, Bogotá, Colombia*
[22b]*Departamento de Física, Universidad Nacional de Colombia, Bogotá, Colombia, Colombia*
[23a]*INFN Bologna and Universita' di Bologna, Dipartimento di Fisica, Italy*
[23b]*INFN Sezione di Bologna, Italy*
[24]*Physikalisches Institut, Universität Bonn, Bonn, Germany*

[25]*Department of Physics, Boston University, Boston, Massachusetts, USA*
[26]*Department of Physics, Brandeis University, Waltham, Massachusetts, USA*
[27a]*Transilvania University of Brasov, Brasov, Romania*
[27b]*Horia Hulubei National Institute of Physics and Nuclear Engineering, Bucharest, Romania*
[27c]*Department of Physics, Alexandru Ioan Cuza University of Iasi, Iasi, Romania*
[27d]*National Institute for Research and Development of Isotopic and Molecular Technologies, Physics Department, Cluj-Napoca, Romania*
[27e]*University Politehnica Bucharest, Bucharest, Romania*
[27f]*West University in Timisoara, Timisoara, Romania*
[28a]*Faculty of Mathematics, Physics and Informatics, Comenius University, Bratislava, Slovak Republic*
[28b]*Department of Subnuclear Physics, Institute of Experimental Physics of the Slovak Academy of Sciences, Kosice, Slovak Republic*
[29]*Physics Department, Brookhaven National Laboratory, Upton, New York, USA*
[30]*Departamento de Física, Universidad de Buenos Aires, Buenos Aires, Argentina*
[31]*California State University, California, USA*
[32]*Cavendish Laboratory, University of Cambridge, Cambridge, United Kingdom*
[33a]*Department of Physics, University of Cape Town, Cape Town, South Africa*
[33b]*iThemba Labs, Western Cape, South Africa*
[33c]*Department of Mechanical Engineering Science, University of Johannesburg, Johannesburg, South Africa*
[33d]*National Institute of Physics, University of the Philippines Diliman, Philippines*
[33e]*University of South Africa, Department of Physics, Pretoria, South Africa*
[33f]*School of Physics, University of the Witwatersrand, Johannesburg, South Africa*
[34]*Department of Physics, Carleton University, Ottawa ON, Canada*
[35a]*Faculté des Sciences Ain Chock, Réseau Universitaire de Physique des Hautes Energies—Université Hassan II, Casablanca, Morocco*
[35b]*Faculté des Sciences, Université Ibn-Tofail, Kénitra, Morocco*
[35c]*Faculté des Sciences Semlalia, Université Cadi Ayyad, LPHEA-Marrakech, Morocco*
[35d]*Moroccan Foundation for Advanced Science Innovation and Research (MAScIR), Rabat, Morocco*
[35e]*LPMR, Faculté des Sciences, Université Mohamed Premier, Oujda, Morocco*
[35f]*Faculté des sciences, Université Mohammed V, Rabat, Morocco*
[36]*CERN, Geneva, Switzerland*
[37]*Enrico Fermi Institute, University of Chicago, Chicago, Illinois, USA*
[38]*LPC, Université Clermont Auvergne, CNRS/IN2P3, Clermont-Ferrand, France*
[39]*Nevis Laboratory, Columbia University, Irvington, New York, USA*
[40]*Niels Bohr Institute, University of Copenhagen, Copenhagen, Denmark*
[41a]*Dipartimento di Fisica, Università della Calabria, Rende, Italy*
[41b]*INFN Gruppo Collegato di Cosenza, Laboratori Nazionali di Frascati, Italy*
[42]*Physics Department, Southern Methodist University, Dallas, Texas, USA*
[43]*Physics Department, University of Texas at Dallas, Richardson, Texas, USA*
[44]*National Centre for Scientific Research "Demokritos", Agia Paraskevi, Greece*
[45a]*Department of Physics, Stockholm University, Sweden*
[45b]*Oskar Klein Centre, Stockholm, Sweden*
[46]*Deutsches Elektronen-Synchrotron DESY, Hamburg and Zeuthen, Germany*
[47]*Lehrstuhl für Experimentelle Physik IV, Technische Universität Dortmund, Dortmund, Germany*
[48]*Institut für Kern- und Teilchenphysik, Technische Universität Dresden, Dresden, Germany*
[49]*Department of Physics, Duke University, Durham, North Carolina, USA*
[50]*SUPA—School of Physics and Astronomy, University of Edinburgh, Edinburgh, United Kingdom*
[51]*INFN e Laboratori Nazionali di Frascati, Frascati, Italy*
[52]*Physikalisches Institut, Albert-Ludwigs-Universität Freiburg, Freiburg, Germany*
[53]*II. Physikalisches Institut, Georg-August-Universität Göttingen, Göttingen, Germany*
[54]*Département de Physique Nucléaire et Corpusculaire, Université de Genève, Genève, Switzerland*
[55a]*Dipartimento di Fisica, Università di Genova, Genova, Italy*
[55b]*INFN Sezione di Genova, Italy*
[56]*II. Physikalisches Institut, Justus-Liebig-Universität Giessen, Giessen, Germany*
[57]*SUPA—School of Physics and Astronomy, University of Glasgow, Glasgow, United Kingdom*
[58]*LPSC, Université Grenoble Alpes, CNRS/IN2P3, Grenoble INP, Grenoble, France*
[59]*Laboratory for Particle Physics and Cosmology, Harvard University, Cambridge, Massachusetts, USA*
[60a]*Department of Modern Physics and State Key Laboratory of Particle Detection and Electronics, University of Science and Technology of China, Hefei, China*

[60b]Institute of Frontier and Interdisciplinary Science and Key Laboratory of Particle Physics and Particle Irradiation (MOE), Shandong University, Qingdao, China
[60c]School of Physics and Astronomy, Shanghai Jiao Tong University, Key Laboratory for Particle Astrophysics and Cosmology (MOE), SKLPPC, Shanghai, China
[60d]Tsung-Dao Lee Institute, Shanghai, China
[61a]Kirchhoff-Institut für Physik, Ruprecht-Karls-Universität Heidelberg, Heidelberg, Germany
[61b]Physikalisches Institut, Ruprecht-Karls-Universität Heidelberg, Heidelberg, Germany
[62]Faculty of Applied Information Science, Hiroshima Institute of Technology, Hiroshima, Japan
[63a]Department of Physics, Chinese University of Hong Kong, Shatin, N.T., Hong Kong, China
[63b]Department of Physics, University of Hong Kong, Hong Kong, China
[63c]Department of Physics and Institute for Advanced Study, Hong Kong University of Science and Technology, Clear Water Bay, Kowloon, Hong Kong, China
[64]Department of Physics, National Tsing Hua University, Hsinchu, Taiwan
[65]IJCLab, Université Paris-Saclay, CNRS/IN2P3, 91405, Orsay, France
[66]Department of Physics, Indiana University, Bloomington, Indiana, USA
[67a]INFN Gruppo Collegato di Udine, Sezione di Trieste, Udine, Italy
[67b]ICTP, Trieste, Italy
[67c]Dipartimento Politecnico di Ingegneria e Architettura, Università di Udine, Udine, Italy
[68a]INFN Sezione di Lecce, Italy
[68b]Dipartimento di Matematica e Fisica, Università del Salento, Lecce, Italy
[69a]INFN Sezione di Milano, Italy
[69b]Dipartimento di Fisica, Università di Milano, Milano, Italy
[70a]INFN Sezione di Napoli, Italy
[70b]Dipartimento di Fisica, Università di Napoli, Napoli, Italy
[71a]INFN Sezione di Pavia, Italy
[71b]Dipartimento di Fisica, Università di Pavia, Pavia, Italy
[72a]INFN Sezione di Pisa, Italy
[72b]Dipartimento di Fisica E.Fermi, Università di Pisa, Pisa, Italy
[73a]INFN Sezione di Roma, Italy
[73b]Dipartimento di Fisica, Sapienza Università di Roma, Roma, Italy
[74a]INFN Sezione di Roma Tor Vergata, Italy
[74b]Dipartimento di Fisica, Università di Roma Tor Vergata, Roma, Italy
[75a]INFN Sezione di Roma Tre, Italy
[75b]Dipartimento di Matematica e Fisica, Università Roma Tre, Roma, Italy
[76a]INFN-TIFPA, Italy
[76b]Università degli Studi di Trento, Trento, Italy
[77]Institut für Astro- und Teilchenphysik, Leopold-Franzens-Universität, Innsbruck, Austria
[78]University of Iowa, Iowa City, Iowa, USA
[79]Department of Physics and Astronomy, Iowa State University, Ames, Iowa, USA
[80]Joint Institute for Nuclear Research, Dubna, Russia
[81a]Departamento de Engenharia Elétrica, Universidade Federal de Juiz de Fora (UFJF), Juiz de Fora, Brazil
[81b]Universidade Federal do Rio De Janeiro COPPE/EE/IF, Rio de Janeiro, Brazil
[81c]Instituto de Física, Universidade de São Paulo, São Paulo, Brazil
[82]KEK, High Energy Accelerator Research Organization, Tsukuba, Japan
[83]Graduate School of Science, Kobe University, Kobe, Japan
[84a]AGH University of Science and Technology, Faculty of Physics and Applied Computer Science, Krakow, Poland
[84b]Marian Smoluchowski Institute of Physics, Jagiellonian University, Krakow, Poland
[85]Institute of Nuclear Physics Polish Academy of Sciences, Krakow, Poland
[86]Faculty of Science, Kyoto University, Kyoto, Japan
[87]Kyoto University of Education, Kyoto, Japan
[88]Research Center for Advanced Particle Physics and Department of Physics, Kyushu University, Fukuoka, Japan
[89]Instituto de Física La Plata, Universidad Nacional de La Plata and CONICET, La Plata, Argentina
[90]Physics Department, Lancaster University, Lancaster, United Kingdom
[91]Oliver Lodge Laboratory, University of Liverpool, Liverpool, United Kingdom
[92]Department of Experimental Particle Physics, Jožef Stefan Institute and Department of Physics, University of Ljubljana, Ljubljana, Slovenia
[93]School of Physics and Astronomy, Queen Mary University of London, London, United Kingdom

[94]Department of Physics, Royal Holloway University of London, Egham, United Kingdom
[95]Department of Physics and Astronomy, University College London, London, United Kingdom
[96]Louisiana Tech University, Ruston, Louisiana, USA
[97]Fysiska institutionen, Lunds universitet, Lund, Sweden
[98]Centre de Calcul de l'Institut National de Physique Nucléaire et de Physique des Particules (IN2P3), Villeurbanne, France
[99]Departamento de Física Teorica C-15 and CIAFF, Universidad Autónoma de Madrid, Madrid, Spain
[100]Institut für Physik, Universität Mainz, Mainz, Germany
[101]School of Physics and Astronomy, University of Manchester, Manchester, United Kingdom
[102]CPPM, Aix-Marseille Université, CNRS/IN2P3, Marseille, France
[103]Department of Physics, University of Massachusetts, Amherst, Massachusetts, USA
[104]Department of Physics, McGill University, Montreal QC, Canada
[105]School of Physics, University of Melbourne, Victoria, Australia
[106]Department of Physics, University of Michigan, Ann Arbor, Michigan, USA
[107]Department of Physics and Astronomy, Michigan State University, East Lansing, Michigan, USA
[108]B.I. Stepanov Institute of Physics, National Academy of Sciences of Belarus, Minsk, Belarus
[109]Research Institute for Nuclear Problems of Byelorussian State University, Minsk, Belarus
[110]Group of Particle Physics, University of Montreal, Montreal QC, Canada
[111]P.N. Lebedev Physical Institute of the Russian Academy of Sciences, Moscow, Russia
[112]National Research Nuclear University MEPhI, Moscow, Russia
[113]D.V. Skobeltsyn Institute of Nuclear Physics, M.V. Lomonosov Moscow State University, Moscow, Russia
[114]Fakultät für Physik, Ludwig-Maximilians-Universität München, München, Germany
[115]Max-Planck-Institut für Physik (Werner-Heisenberg-Institut), München, Germany
[116]Nagasaki Institute of Applied Science, Nagasaki, Japan
[117]Graduate School of Science and Kobayashi-Maskawa Institute, Nagoya University, Nagoya, Japan
[118]Department of Physics and Astronomy, University of New Mexico, Albuquerque, New Mexico, USA
[119]Institute for Mathematics, Astrophysics and Particle Physics, Radboud University/Nikhef, Nijmegen, Netherlands
[120]Nikhef National Institute for Subatomic Physics and University of Amsterdam, Amsterdam, Netherlands
[121]Department of Physics, Northern Illinois University, DeKalb, Illinois, USA
[122a]Budker Institute of Nuclear Physics and NSU, SB RAS, Novosibirsk, Russia
[122b]Novosibirsk State University Novosibirsk, Russia
[123]Institute for High Energy Physics of the National Research Centre Kurchatov Institute, Protvino, Russia
[124]Institute for Theoretical and Experimental Physics named by A.I. Alikhanov of National Research Centre "Kurchatov Institute", Moscow, Russia
[125]Department of Physics, New York University, New York, New York, USA
[126]Ochanomizu University, Otsuka, Bunkyo-ku, Tokyo, Japan
[127]Ohio State University, Columbus, Ohio, USA
[128]Homer L. Dodge Department of Physics and Astronomy, University of Oklahoma, Norman, Oklahoma, USA
[129]Department of Physics, Oklahoma State University, Stillwater, Oklahoma, USA
[130]Palacký University, RCPTM, Joint Laboratory of Optics, Olomouc, Czech Republic
[131]Institute for Fundamental Science, University of Oregon, Eugene, Oregon, USA
[132]Graduate School of Science, Osaka University, Osaka, Japan
[133]Department of Physics, University of Oslo, Oslo, Norway
[134]Department of Physics, Oxford University, Oxford, United Kingdom
[135]LPNHE, Sorbonne Université, Université de Paris, CNRS/IN2P3, Paris, France
[136]Department of Physics, University of Pennsylvania, Philadelphia, Pennsylvania, USA
[137]Konstantinov Nuclear Physics Institute of National Research Centre "Kurchatov Institute", PNPI, St. Petersburg, Russia
[138]Department of Physics and Astronomy, University of Pittsburgh, Pittsburgh, Pennsylvania, USA
[139a]Laboratório de Instrumentação e Física Experimental de Partículas—LIP, Lisboa, Portugal
[139b]Departamento de Física, Faculdade de Ciências, Universidade de Lisboa, Lisboa, Portugal
[139c]Departamento de Física, Universidade de Coimbra, Coimbra, Portugal
[139d]Centro de Física Nuclear da Universidade de Lisboa, Lisboa, Portugal
[139e]Departamento de Física, Universidade do Minho, Braga, Portugal
[139f]Departamento de Física Teórica y del Cosmos, Universidad de Granada, Granada (Spain), Spain
[139g]Dep Física and CEFITEC of Faculdade de Ciências e Tecnologia, Universidade Nova de Lisboa, Caparica, Portugal

[139h]Instituto Superior Técnico, Universidade de Lisboa, Lisboa, Portugal
[140]Institute of Physics of the Czech Academy of Sciences, Prague, Czech Republic
[141]Czech Technical University in Prague, Prague, Czech Republic
[142]Charles University, Faculty of Mathematics and Physics, Prague, Czech Republic
[143]Particle Physics Department, Rutherford Appleton Laboratory, Didcot, United Kingdom
[144]IRFU, CEA, Université Paris-Saclay, Gif-sur-Yvette, France
[145]Santa Cruz Institute for Particle Physics, University of California Santa Cruz, Santa Cruz, California, USA
[146a]Departamento de Física, Pontificia Universidad Católica de Chile, Santiago, Chile
[146b]Universidad Andres Bello, Department of Physics, Santiago, Chile
[146c]Instituto de Alta Investigación, Universidad de Tarapacá, Arica, Chile
[146d]Departamento de Física, Universidad Técnica Federico Santa María, Valparaíso, Chile
[147]Universidade Federal de São João del Rei (UFSJ), São João del Rei, Brazil
[148]Department of Physics, University of Washington, Seattle, Washington, USA
[149]Department of Physics and Astronomy, University of Sheffield, Sheffield, United Kingdom
[150]Department of Physics, Shinshu University, Nagano, Japan
[151]Department Physik, Universität Siegen, Siegen, Germany
[152]Department of Physics, Simon Fraser University, Burnaby BC, Canada
[153]SLAC National Accelerator Laboratory, Stanford, California, USA
[154]Physics Department, Royal Institute of Technology, Stockholm, Sweden
[155]Departments of Physics and Astronomy, Stony Brook University, Stony Brook, New York, USA
[156]Department of Physics and Astronomy, University of Sussex, Brighton, United Kingdom
[157]School of Physics, University of Sydney, Sydney, Australia
[158]Institute of Physics, Academia Sinica, Taipei, Taiwan
[159a]E. Andronikashvili Institute of Physics, Iv. Javakhishvili Tbilisi State University, Tbilisi, Georgia
[159b]High Energy Physics Institute, Tbilisi State University, Tbilisi, Georgia
[160]Department of Physics, Technion, Israel Institute of Technology, Haifa, Israel
[161]Raymond and Beverly Sackler School of Physics and Astronomy, Tel Aviv University, Tel Aviv, Israel
[162]Department of Physics, Aristotle University of Thessaloniki, Thessaloniki, Greece
[163]International Center for Elementary Particle Physics and Department of Physics, University of Tokyo, Tokyo, Japan
[164]Graduate School of Science and Technology, Tokyo Metropolitan University, Tokyo, Japan
[165]Department of Physics, Tokyo Institute of Technology, Tokyo, Japan
[166]Tomsk State University, Tomsk, Russia
[167]Department of Physics, University of Toronto, Toronto ON, Canada
[168a]TRIUMF, Vancouver BC, Canada
[168b]Department of Physics and Astronomy, York University, Toronto ON, Canada
[169]Division of Physics and Tomonaga Center for the History of the Universe, Faculty of Pure and Applied Sciences, University of Tsukuba, Tsukuba, Japan
[170]Department of Physics and Astronomy, Tufts University, Medford, Massachusetts, USA
[171]Department of Physics and Astronomy, University of California Irvine, Irvine, California, USA
[172]Department of Physics and Astronomy, University of Uppsala, Uppsala, Sweden
[173]Department of Physics, University of Illinois, Urbana, Illinois, USA
[174]Instituto de Física Corpuscular (IFIC), Centro Mixto Universidad de Valencia—CSIC, Valencia, Spain
[175]Department of Physics, University of British Columbia, Vancouver BC, Canada
[176]Department of Physics and Astronomy, University of Victoria, Victoria BC, Canada
[177]Fakultät für Physik und Astronomie, Julius-Maximilians-Universität Würzburg, Würzburg, Germany
[178]Department of Physics, University of Warwick, Coventry, United Kingdom
[179]Waseda University, Tokyo, Japan
[180]Department of Particle Physics and Astrophysics, Weizmann Institute of Science, Rehovot, Israel
[181]Department of Physics, University of Wisconsin, Madison, Wisconsin, USA
[182]Fakultät für Mathematik und Naturwissenschaften, Fachgruppe Physik, Bergische Universität Wuppertal, Wuppertal, Germany
[183]Department of Physics, Yale University, New Haven, Connecticut, USA

[a]Deceased.
[b]Also at Department of Physics, King's College London, London, United Kingdom.
[c]Also at Istanbul University, Dept. of Physics, Istanbul, Turkey.
[d]Also at Instituto de Fisica Teorica, IFT-UAM/CSIC, Madrid, Spain.
[e]Also at TRIUMF, Vancouver BC, Canada.

[f]Also at Department of Physics and Astronomy, University of Louisville, Louisville, Kentucky, USA.
[g]Also at Physics Department, An-Najah National University, Nablus, Palestinian Authority.
[h]Also at Department of Physics, University of Fribourg, Fribourg, Switzerland.
[i]Also at Departament de Fisica de la Universitat Autonoma de Barcelona, Barcelona, Spain.
[j]Also at Moscow Institute of Physics and Technology State University, Dolgoprudny, Russia.
[k]Also at Department of Physics, Ben Gurion University of the Negev, Beer Sheva, Israel.
[l]Also at Universita di Napoli Parthenope, Napoli, Italy.
[m]Also at Institute of Particle Physics (IPP), Canada.
[n]Also at Department of Physics, St. Petersburg State Polytechnical University, St. Petersburg, Russia.
[o]Also at Borough of Manhattan Community College, City University of New York, New York, New York, USA.
[p]Also at Department of Physics, California State University, Fresno, USA.
[q]Also at Department of Financial and Management Engineering, University of the Aegean, Chios, Greece.
[r]Also at Centro Studi e Ricerche Enrico Fermi, Italy.
[s]Also at Department of Physics, California State University, East Bay, USA.
[t]Also at Institucio Catalana de Recerca i Estudis Avancats, ICREA, Barcelona, Spain.
[u]Also at Graduate School of Science, Osaka University, Osaka, Japan.
[v]Also at Physikalisches Institut, Albert-Ludwigs-Universität Freiburg, Freiburg, Germany.
[w]Also at University of Chinese Academy of Sciences (UCAS), Beijing, China.
[x]Also at Institute of Physics, Azerbaijan Academy of Sciences, Baku, Azerbaijan.
[y]Also at CERN, Geneva, Switzerland.
[z]Also at Joint Institute for Nuclear Research, Dubna, Russia.
[aa]Also at Hellenic Open University, Patras, Greece.
[bb]Also at Center for High Energy Physics, Peking University, China.
[cc]Also at The City College of New York, New York, New York, USA.
[dd]Also at Dipartimento di Matematica, Informatica e Fisica, Università di Udine, Udine, Italy.
[ee]Also at Department of Physics, California State University, Sacramento, USA.
[ff]Also at Département de Physique Nucléaire et Corpusculaire, Université de Genève, Genève, Switzerland.
[gg]Also at Institute for Nuclear Research and Nuclear Energy (INRNE) of the Bulgarian Academy of Sciences, Sofia, Bulgaria.
[hh]Also at Faculty of Physics, M.V. Lomonosov Moscow State University, Moscow, Russia.
[ii]Also at Institut für Experimentalphysik, Universität Hamburg, Hamburg, Germany.
[jj]Also at CPPM, Aix-Marseille Université, CNRS/IN2P3, Marseille, France.
[kk]Also at National Research Nuclear University MEPhI, Moscow, Russia.
[ll]Also at Institute for Particle and Nuclear Physics, Wigner Research Centre for Physics, Budapest, Hungary.
[mm]Also at Giresun University, Faculty of Engineering, Giresun, Turkey.
[nn]Also at Department of Physics and Astronomy, Michigan State University, East Lansing, Michigan, USA.